SEMMELWEIS EGYETEM

DOKTORI ISKOLA

Ph.D. értekezések

3046.

BARTI BENJÁMIN

Neuromorfológia és sejtbiológia
című program

Programvezető: Dr. Alpár Alán, egyetemi tanár

Témavezető: Dr. Katona István, tudományos tanácsadó

TONIC REGULATION OF HIPPOCAMPAL INHIBITION BY ENDOCANNABINOIDS

Ph. D thesis

Benjámin Barti

János Szentágothai PhD School of Neurosciences

Semmelweis University

Supervisor: István Katona, D. Sc

Official reviewers: Katalin Schlett, Ph. D
Zoltán Varga, Ph. D

Head of the Final Examination Committee:
Gábor Gerber, D.M.D, Ph. D

Members of the Final Examination Committee:
Márk Kozsurek, M.D, Ph. D
Lucia Wittner, D. Sc

Budapest
2024

Table of Contents

List of abbreviations

2-AG	2-arahydonoylglycerol
ABHD6/12	Alpha/beta-hydrolase domain containing 6 or 12
ACSF	Artificial Cerebrospinal Fluid
AEA	Anandamide or N-arachidonoylethanolamine
AF	Alexa Fluor (a family of fluorescent dye molecules)
AM251	N-(piperidin-1-yl)-5-(4-iodophenyl)-1-(2,4-dichlorophenyl)-4-methyl1H-pyrazole-3-carboxamide; a CB_1 receptor antagonist/ inverse agonist
AMPA receptor	α-amino-3-hydroxy-5-methyl-4-isoxazolepropionic acid receptor
AP	Action potential
AZ	Active zone
BDI	Bouton Distribution Index
CA	Cornu ammonis
CB_1 R	Cannabinoid type-1 receptor
CB_1BC	CB_1R expressing (perisomatic) basket cell
CCK	Cholecystokinin
CGE	Caudal ganglionic eminence
Cnr1	Cannabinoid type-1 receptor coding gene
COX-2	Cyclooxygenase-2
CV	Coefficient of Variation
DAG	Diacylglycerol
DAGLα/β	Diacylglycerol-lipase α or β

DMSO	Dimethyl sulfoxide
DSE	Depolarization-induced Suppression of Excitation
DSI	Depolarization-induced Suppression of Inhibition
eCB	Endocannabinoid
FAAH	Fatty acid amide hydrolase
GABA	γ (gamma)-aminobutyric acid
GPCR	G-protein coupled receptor
HCN channel	Hyperpolarization-activated cyclic nucleotide-gated channel
IP_3	Inositol trisphosphate
IPSC	Inhibitory Postsynaptic Current
JZL184	4-nitrophenyl 4-[bis(1,3-benzodioxol-5-yl)(hydroxy) methyl]piperidine-1-carboxylate; an MGL enzyme inhibitor
KO	Knock-out
LTD	Long-Term Depression
LTP	Long-Term Potentiation
MGE	Medial ganglionic eminence
MAGL	Monoacylglycerol Lipase
$mGluR_{1/5}$	Metabotropic glutamate receptor 1 and 5
NAE	N-acyl-ethanolamine
NAPE-PLD	N-acyl-phosphatidylethanolamine-hydrolyzing phospholipase D
NECAB1/2	N-terminal EF-hand calcium-binding protein 1 and 2
Nf	Number of functional release sites
NLP	Number of Localization Points
NMDA receptor	N-methyl-D-aspartate receptor

PB	Phosphate Buffer
PC	Pyramidal cell
PFA	Paraformaldehyde
PIP_2	Phosphatidylinositol biphosphate
PLC	Phospholipase C
Pr	Release probability
PSD	Postsynaptic density
PV	Parvalbumin
Q	Quantal size
Rab3	Ras-related protein-3
RIM	Rab3-interacting molecule
RIM-BP	RIM-binding protein
R_{in}	Input resistance
RMP	Resting membrane potential
ROI	Region of interest
SEM	Standard error of the mean
SNARE	Soluble NSF (N-ethylmaleimide-sensitive factor) attachment protein receptor
STORM	Stochastic Optical Reconstruction Microscopy
TBS	Tris-Buffered Saline
THC	Δ^9-tetrahydrocannabinol
VGCC	Voltage Gated Calcium Channel
VGPC	Voltage Gated Potassium Channel
WT	Wild type

1. Introduction

Stochasticity and variability are essential properties of the world as we know it. While these terms are often viewed as synonyms of chaos and disorder, they are elemental ingredients of life. The earliest example of this can be found around 10^{-36} seconds after the Big Bang, where the whole universe was just a small, extremely dense and hot sphere of energy. This energy bubble wasn't completely uniform though: due to quantum fluctuations minor inhomogeneities in density and temperature already existed, which were amplified during the expansion of the universe. Then, gravitational pull at the more densely packed regions led to the formation of galaxies and planets. Therefore, existence in general is built on random fluctuations in the first place.

Proteins, the fundamental building blocks of life on Earth, are often considered as precisely structured keys fitting into locks. However, many proteins have disordered regions and domains, thus lacking a fixed structure (Holehouse and Kragelund, 2024). This uncertainty and imprecision, however, is not due to sloppy design, but serves an essential function: as these proteins are able to quickly respond to intracellular changes and bind multiple different targets depending on the exact circumstances to assist cell survival. Thus, life is dependent on variability.

In nature, every complex living organism needs to collect, process, store and recall information from their environment in order to survive, adapt and respond to changes. These functions are fulfilled by neuronal cells, which arose already at the early stages of evolution. The assembly of individual neurons into functional networks has reached its complexity peak within the mammalian brain, where the development of the cerebral cortex enabled the coordination of extremely versatile processes. To achieve this, neurons are generating well-orchestrated rhythmic oscillation while communicating with each other via electro-chemical signals. Interestingly, in this context as well, stochasticity forms the basis of these processes: the nature of synaptic transmission between neurons is inherently probabilistic. Hence, synaptic fluctuations are essential ingredients for complex brain functions.

To study synaptic variability, this thesis focuses on synapses between specific neurons in the mammalian hippocampus and describes a retrograde signaling modality that can regulate and influence synaptic variability and stochasticity.

In the hippocampus, there is a perplexing anatomical and electrophysiological diversity of cells (Klausberger and Somogyi, 2008; Pelkey et al., 2017; Poulin et al., 2016; Usoskin et al., 2015; Zeisel et al., 2015). Each cell receives tens of thousands of synaptic inputs (Andersen et al., 2007) and each synaptic input has distinct molecular and physiological characteristics, making it a unique entity (Nusser, 2018). Due to this remarkable level of complexity and the relatively small size of synaptic profiles, we utilized and combined various methodologies to enable cell type-, and nanodomain-specific investigations of individual synapses.

Throughout the following chapters of the introduction, I will briefly present some crucial features and molecular components of the anterograde synaptic neurotransmission and the role of the retrograde endocannabinoid system as a fine regulator of neurotransmitter release and synaptic strength. A concise overview of the neuroanatomy and primary connections within the hippocampal region of the brain will also be given, along with an in-depth introduction to the cell types under investigation.

1.1. Anterograde synaptic transmission

1.1.1. Basic principles of anterograde neuronal communication

The first direct observations that led to the elucidation of the principles of anterograde synaptic transmission were conducted by Bernard Katz and his colleagues in the early 1950s. They were studying the electrical properties of the neuromuscular junction and observed randomly occurring electrical events in the preparation (Fatt and Katz, 1952). They also noticed that although these detected membrane potentials showed substantial amplitude fluctuations, large events were precisely two, three or multiple times larger than the amplitude of the smallest recorded miniature potential (Del Castillo and Katz, 1954). In the same year, the first image of an earthworm nerve terminal was taken via electron microscopy, that showed an accumulation of vesicles in the anatomical apposition between two cells (De Robertis and Bennett, 1955). These seminal observations solidified the fundamentals of quantal synaptic neurotransmission theory, that synaptic vesicular exocytosis transfers electro-chemical signals to the receiver cell in a quantal manner.

Synapses are extremely complex, precisely organized structures. Information arrives at the presynaptic axon terminal in the form of membrane depolarization after an action potential (AP) is generated at the axon-initial segment and is transmitted to the postsynaptic cell via chemical neurotransmitter molecules. These molecules then interact with ionotropic receptors, which upon opening, allows ion flux in- and out from the postsynaptic cell, therefore changing its membrane potential, that can lead to AP generation. Neurotransmission happens in an extremely fast time scale: the latency between calcium entry in the axon terminal during AP propagation and secretion of neurotransmitters occurs in less than 200 μs (Sabatini and Regehr, 1996). Such precision is achieved via specific molecular complexes, which construct the synapse itself.

1.1.2. Anatomical structure and molecular composition of the synapse

The term ‘synapse’ refers to the anatomical specialization between two cells which serves as the location for fast chemical information transfer via neurotransmitter molecules. In the cortex, these structures are usually formed between the axon terminals or boutons of the presynaptic neuron and the somato-dendritic compartment of the postsynaptic neuron (Figure 1/a). As the diameter of an average cortical synaptic complex is about 200-300 nm, small sized inherent molecular assemblies fall beneath the diffraction limit of light, which makes conventional microscopical investigations challenging. Therefore, the precise examination of synapses relied exclusively on electron microscopy for a long time. Their characteristic ultrastructure carries multiple information about their function. There are two types of synapses which can be easily differentiated at the level of electron microscopy (Gray, 1959). Excitatory, asymmetric, or type-I synapses have notable electron-dense postsynaptic site and round synaptic vesicles (Figure 1/b). Symmetrical or type-II synapses are usually inhibitory, have less prominent postsynaptic density and oval vesicles – as they are more susceptible to shape changes during aldehyde fixation (Figure 2/b). Excitatory synapses are found mainly on dendrites and dendritic spines, whereas inhibitory synapses are abundant on the soma and axonal initial segment, with a sparse distribution along the dendritic shafts (Harris and Weinberg, 2012). Within the synaptic specialization, the membranes of the two cells are closely opposed to each other in a parallel manner, forming a 20 ± 2.8 nm thick synaptic cleft between the pre- and the postsynaptic compartment. The presynaptic site of the

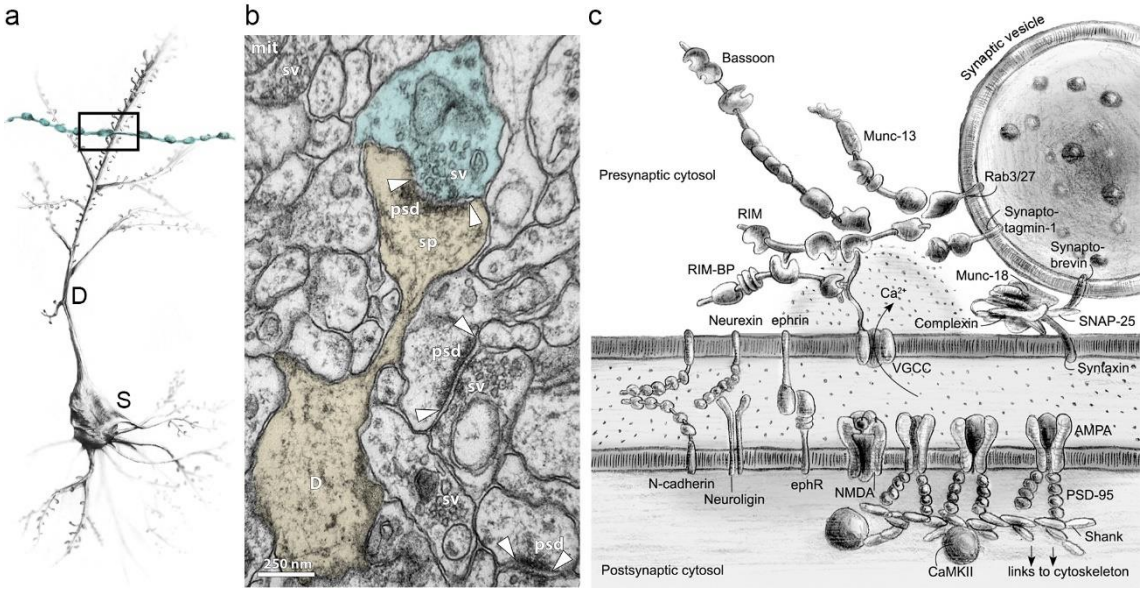

Figure 1. ***Morphological and molecular composition of a cortical synapse.*** **a)** Illustration shows a presynaptic axon string with terminals (cyan) which forms a synaptic contact on a postsynaptic dendritic spine of a PC. D: dendrite, S: soma. **b)** Ultrastructure of an excitatory synapse: an axon terminal (cyan) terminating on a dendritic spine (yellow) of a hippocampal CA1 PC in the mouse brain. Synaptic specializations labeled with arrowheads. mit: mitochondria, psd: postsynaptic density, sp: dendritic spine, sv: synaptic vesicles. (Electron microscopical sample and image prepared by the author) **c)** Schematic of the molecular machinery regulating Ca^{2+} mediated synaptic transmission. Membrane depolarization evoked Ca^{2+} entry from the extracellular space through voltage-gated channels (VGCCs) triggers the fusion of a docked synaptic vesicle via activation of Synaptotagmins and the vesicle fusion complex (Synaptobrevin, SNAP-25, Complexin, Munc-18, Syntaxin) Vesicle docking to the active zone and to VGCCs regulated by a second molecular complex composed of Rab3/27, RIM, RIM-BP, Munc-13 and bassoon proteins. Neurotransmitters released in the synaptic cleft can activate ionotropic AMPA, NMDA (at inhibitory synapses: $GABA_A$) and metabotropic mGluR receptors to regulate postsynaptic ion concentrations or to initiate secondary messenger mediated actions (e.g.: via Ca^{2+}/calmodulin-dependent protein kinase II (CaMKII) dependent pathways). The synaptic cleft is also crowded with proteins linking the two synaptic sites together allowing the stabilization of the synapse and further communication between the two cells (drawings based on: Biederer et al., 2017; Südhof, 2013).

synapse is filled with synaptic vesicles (with a diameter of 35 ± 0.3 nm), that contain neurotransmitter molecules. This specific region of the axon terminal in which vesicles are clustered near the plasma membrane surface called the synaptic active zone (AZ), and can span at 300 ± 150 nm in its diameter (Ribrault et al., 2011). Active zones are composed of an insoluble protein matrix that is heterogeneous in size and composition

(Figure 1/c). Over the past decades, six major evolutionarily conserved protein families have emerged as key organizers of the AZ (Südhof, 2012). In the AZ core, RIM proteins interact with vesicular Rab3 proteins and form scaffolds at the fusion sites. They organize the priming and docking of synaptic vesicles (Kaeser et al., 2011) and are essential for most forms of short- and long-term synaptic plasticity (Castillo et al., 2002; Schoch et al., 2002). RIM proteins together with RIM-BPs, tether presynaptic voltage-gated Ca^{2+} channels (VGCCs) to the AZ, close to vesicle fusion sites (Kaeser et al., 2011). This is crucial as calcium rapidly equilibrates intracellularly, thus, to establish high-enough concentration VGCCs have to be at maximum 50-100 nm apart from the release machinery (Dittman and Ryan, 2019). RIMs also anchor and activate Munc-13 proteins, which are also essential for synaptic vesicle priming (Augustin et al., 1999). ELKS and α-liprin molecules both form scaffolds and are important for AZ formation, however their roles still remain enigmatic (Südhof, 2012). Bassoon and Piccolo are two large homologous proteins, which are highly enriched at the AZ. They contribute indirectly to VGCC targeting and play important role in synaptic vesicle guidance (Dani et al., 2010; Davydova et al., 2014; Hallermann et al., 2010).

When an AP induced membrane potential change propagates through the axon and invades the axon terminals, it opens presynaptic VGCCs, which initiate neurotransmission. In the AZ, vesicles dock and fuse to the membrane and release the neurotransmitters in the synaptic clefts by Ca^{2+}-triggered exocytosis. The calcium ions entering the cell subsequently interact with a calcium sensor located at the synaptic vesicles (namely: Synatotagmin-1/ 2/ 7) and trigger the fusion of one or more vesicles with the presynaptic plasma membrane (Bacaj et al., 2013; Chen et al., 2017; Fernández-Chacón et al., 2001). After the closing of the calcium channels, the diffusion of free Ca^{2+} within the cytosol and their binding to Ca^{2+} sensors are tightly regulated by various Ca^{2+} buffering proteins such as parvalbumin (PV), calbindin and calretinin (Schwaller, 2020). Intracellular Ca^{2+} buffering limits the spread of Ca^{2+} at the AZs and thus provides specific locus to its action in the close vicinity of Ca^{2+} channels (Eggermann et al., 2012). Therefore, endogenous Ca^{2+} buffers have important role in the modulation of synaptic release (Eggermann and Jonas, 2012; Rozov et al., 2001).

In basal conditions, the energy cost of fusing synaptic vesicle membranes with the lipid bilayer of the plasma membrane is high enough to prevent vast majority of random release

events (Dittman and Ryan, 2019). Synaptic fusion proteins (or SNARE proteins) play a crucial role in aiding the vesicles to overcome this barrier and fuse with the plasma membranes. The plasma membrane SNARE protein complex, composed of Syntaxin, SNAP-25, Complexin, Munc-18 and Synaptobrevin molecules provides energy and physically modulates the fusion with the plasma membrane (Südhof and Rothman, 2009). The precise place of where the release happens termed as release site. Depending on the exact type of the synapse, from one to several release sites can be found within the AZ area (Pulido and Marty, 2017). While AZ regions can be labeled using multiple proteins, precise anatomical detection of the individual release sites is still challenging. Although it is possible that VGCCs are clustered in close vicinity to the vesicle release locations (Miki et al., 2017) and would serve as an optimal target, antibodies that reliably label VGCCs on basic immunohistochemical experiments are lacking. The other participant protein which forms discrete supramolecular self-assemblies around release sites is Munc-13-1 (Sakamoto et al., 2018), therefore visualizing these clusters would help to estimate anatomical transmitter-releasing regions inside the AZs. In the absence of anatomical markers, the number of functional release sites in a given connection can be estimated using electrophysiological and optical methods (Clements and Silver, 2000; Pulido et al., 2015; Silver et al., 1998; Wall and Usowicz, 1998).

Upon release, neurotransmitter molecules diffuse across the synaptic cleft. Rather than just an extracellular gap, the synaptic cleft is a protein-rich environment crowded with multiple synapse-organizing and cell adhesion molecules (Figure 1/c). On the postsynaptic site, neurotransmitters bind to various receptors on the membrane surface which can lead to postsynaptic depolarization and subsequent initiation of postsynaptic molecular cascades. As we look through these precisely arranged molecules, we can easily get a false intention that synapses are rigid, hard-wired elements. However, on the contrary, nearly all of the synaptic molecules express dynamic movements in space and time. Receptors and intramembrane proteins are driven by Brownian movement within membranes and can alternately switch between mobile and immobile states. These transitions are regulated by reversible binding to stable elements such as scaffold molecules or other cytoskeletal anchoring slots in a process called diffusion trapping (Choquet and Triller, 2013). The number, state and position of these aligned postsynaptic

receptors in the AZ determines the properties of the postsynaptic response, therefore, regulation of the molecular dynamics can shape the synaptic strength.

Electron microscopy still represents an inimitable resolution in the investigation of small diffraction-limited structures, however, recent developments achieved in light-microscopy techniques extended our understanding of synapses as well. Using super-resolution microscopy, many observations highlighted a previously unexpected level of fine-organization in classical synaptic transmission (Biederer et al., 2017; Sigal et al., 2018). Allowing the measurements of individual synaptic proteins with nanometer precision provided high-resolution spatial and quantitative data about their distribution at both excitatory and inhibitory synapses (Dani et al., 2010; Nair et al., 2013; Specht et al., 2013). One of the most interesting, recently recognized features of the synaptic organization is the existence of trans-synaptic nanocolumns. Localization of presynaptic vesicle fusion sites within the AZ precisely correlates with the position of α-Amino-3-hydroxy-5-methyl-4-isoxazolepropionic acid (AMPA) receptor clusters and scaffolding PSD-95 proteins in the postsynaptic density (Tang et al., 2016). Furthermore, activation of N-methyl-D-aspartate (NMDA) receptors triggers various plasticity events which are supplemented with the respective trans-synaptic realignment of the nano-organization. The specific columnal alignment also spans through the synaptic cleft region (Trotter et al., 2019). The discrete mechanisms by which the proteins are anchored to synaptic membrane compartments are not yet known, although regarding the principles of this organization, direct transsynaptic interactions between pre- and postsynaptic proteins can provide a potential explanation (Biederer et al., 2017). It was also revealed that presynaptic matrix proteins have distinct roles besides providing a scaffold for the release machinery itself. Via molecular crowding, the clustered presynaptic bassoon molecules can restrict the recruitment of release machinery to the AZ (Glebov et al., 2017). This process can be controlled bidirectionally by neuronal activity; therefore, AZ matrix also controls presynaptic function. Glial cells are also fundamental and indispensable players of synaptic transmission regulation (Allen and Lyons, 2018; Durkee and Araque, 2019; Stogsdill and Eroglu, 2017; Wilton et al., 2019), however, introducing their detailed function lies outside the scope of this study.

1.1.3. Synaptic strength and the role of variability

One of the most surprising features of such a precisely constructed and orchestrated complex as a synapse is stochasticity. Both neurotransmitter exocytosis, neurotransmitter diffusion and the magnitude of the postsynaptic response to neurotransmitter release has probabilistic factors (Ribrault et al., 2011). However, this stochasticity itself can carry multiple information about the network and cellular states. The strength of a connection is dependent on three main factors: the number of functional release sites (Nf), the quantal size (Q), which is the size of the postsynaptic depolarization caused by neurotransmitter release from a single synaptic vesicle and the probability of neurotransmitter release (Pr). Changing the number of synapses or the postsynaptic receptor distribution at the synapse are important mechanisms of strength regulation (Diering and Huganir, 2018; Fauth and Tetzlaff, 2016). However, the dynamic control over the likelihood of neurotransmitter release is a process that can be influenced in the widest range with high spatio-temporal precision. Therefore, Pr is an essential parameter in determining synaptic strength. When the Pr is high (or close to 100%), it implies that each presynaptic AP will result in transmitter release from the functional release sites, that can activate subsequent postsynaptic receptors. However, when Pr is low (or close to 0%) a presynaptic depolarization event will not have postsynaptic effects since no transmitter release occurs. Precise control of Pr can be achieved through regulation of multiple variable factors, including the size of the readily releasable vesicle pool, modulation of release machinery proteins, Ca^{2+} sensor composition of the vesicles, intracellular Ca^{2+} concentration, Ca^{2+} buffering capacities or the specifically expressed metabotropic receptors (Branco and Staras, 2009). Moreover, Pr shows correlation with the size of the AZ and the number of docked vesicles, which can further affect synaptic strength (Holderith et al., 2012; Malagon et al., 2020; Maus et al., 2020).

What can be the functional implication of this synaptic uncertainty? One important outcome of having variable Pr is flexible filtering. An adjustable Pr provides a broad dynamic range to the synapse, that is sensitive to the activity pattern of the given pre- and postsynaptic cell (Branco and Staras, 2009). Low levels of baseline Pr support the continuous facilitation of the connection throughout repetitive stimulation, therefore can serve as a high-pass filter. Similarly, moderate Pr works as a band-pass-, while high Pr represents low-pass filters, as synapses with high initial neurotransmitter release are likely

to deplete their releasable vesicle pool and become depressed upon sustained presynaptic activity. Each dendritic branch, on which a given input signal arrives acts as an electrotonically independent compartment due to its unique conductance set. Therefore, a neuron is more like a multiple-unit network, than a single linear system. Information arriving from a single axon can be filtered differently from one dendritic compartment to another, while different axonal branches synapsing on the same dendritic compartment have more similar Prs (Branco et al., 2008). Variability in synaptic strength can therefore also resemble the importance of information carried by the synapse. Moreover, fluctuations in synaptic transmission can enhance the sensitivity to the temporal pattern of stimulation via stochastic resonance (Hänggi, 2002). This effect appears when a weak signal needs to be detected in a non-linear system. In this case, an optimal amount of synaptic noise (arising from the fluctuations) that is correlated with the signal enhances the probability of the signal to be detected and transmitted (Ribrault et al., 2011). Variability in synaptic signaling can also play a role in synaptic learning via a phenomenon called Bayesian inference (Aitchison et al., 2021). At certain synapses, the ability for fast, energy efficient learning is crucial for effectively participate in memory related tasks. There, variability sets a high dynamic range of synaptic strengths, which increases learning rates (Aitchison et al., 2021; Schug et al., 2021).

1.2. Retrograde synaptic signaling: the endocannabinoid system

1.2.1. General overview of the endocannabinoid molecular machinery

As previously introduced, variability and fluctuations of postsynaptic responses are important features in the fine regulation of synaptic information transfer. Although it was discussed that both pre- and postsynaptic neurons can participate in the generation of the optimal stochasticity of transmission, significant adjustments of neurotransmitter Pr also rely on feedback mechanisms from the postsynaptic target cell. The retrograde endocannabinoid (eCB) signaling is one of the most extensively studied and most widespread molecular feedback pathways at the level of individual synapses in the brain. One of the most interesting features of this signaling modality is the use of lipid messengers, instead of classical vesicle-packed neurotransmitters. In the brain, 2-arachidonoyl-glycerol (2-AG) and N-arachidonoyl-ethanolamine or anandamide (AEA)

are the two main endocannabinoid ligands present. These lipid molecules are released from the postsynaptic cell membrane in activity-dependent manner and activate CB_1Rs at the presynaptic cell surface (Katona and Freund, 2012). Although it has multiple distinct functions, the main role of the eCB signaling from the perspective of this study is to dampen the synaptic transmission between cells. Therefore, it acts as a negative regulator and a synaptic circuit breaker (Katona and Freund, 2008). Interestingly, compared to anterograde synaptic transmission, much less is known about the nanoscale molecular principles that determine retrograde endocannabinoid signaling.

1.2.1.1. Molecular composition of 2-AG-mediated endocannabinoid signaling

2-AG stands as the primary eCB messenger, as it acts as a full-agonist of the CB_1R and can be found at high concentrations in brain tissue (Mechoulam et al., 1995; Stella et al., 1997). Under physiologically relevant conditions, there are three molecular routes which can led to the postsynaptic generation of 2-AG (Figure 2/c): depolarization of the postsynaptic cell, which elicit large Ca^{2+} influx; activation of $G_{q/11}$ coupled metabotropic receptors (e.g.: $mGluR_{1/5}$) by spillover-glutamate or with the combination of the beforementioned two processes (Katona and Freund, 2012). The initiation steps converge to the activation of phospholipase C-β (PLC-β) (Fukaya et al., 2008), which cleaves the membrane lipid phosphatidylinositol biphosphate (PIP_2) into inositol trisphosphate (IP_3) and diacylglycerol (DAG) (Hashimotodani et al., 2005; Stella et al., 1997). Located in the perisynaptic site of the postsynaptic cell (Katona et al., 2006; Yoshida et al., 2006), diacylglycerol-lipase α (DAGLα) is the main enzyme that converts DAG to 2-AG (Bisogno et al., 2003; Gao et al., 2010). DAGLβ can serve as an alternative enzyme of 2-AG biosynthesis, although, in the brain it mainly produces a separate 2-AG pool only in microglia (Hsu et al., 2012; Viader et al., 2016). Therefore, DAGLα is potentially responsible for the generation of the major neuronal eCB ligand messenger. As lipids cannot be stored, they usually synthetized on demand at locations where they are needed (Alger and Kim, 2011). After synthesis, 2-AG molecules travel back to the presynaptic site, where they activate CB_1Rs. The process with which these lipids are reaching the presynaptic membranes more than 20 nm away from their genesis remains much of an enigma. Recent evidences highlight the role of fatty-acid–binding protein-5 and 7 (FABP-5, 7) in the retrograde transport of 2-AG (Haj-Dahmane et al., 2018), however, the process of simple diffusion is also a possibility.

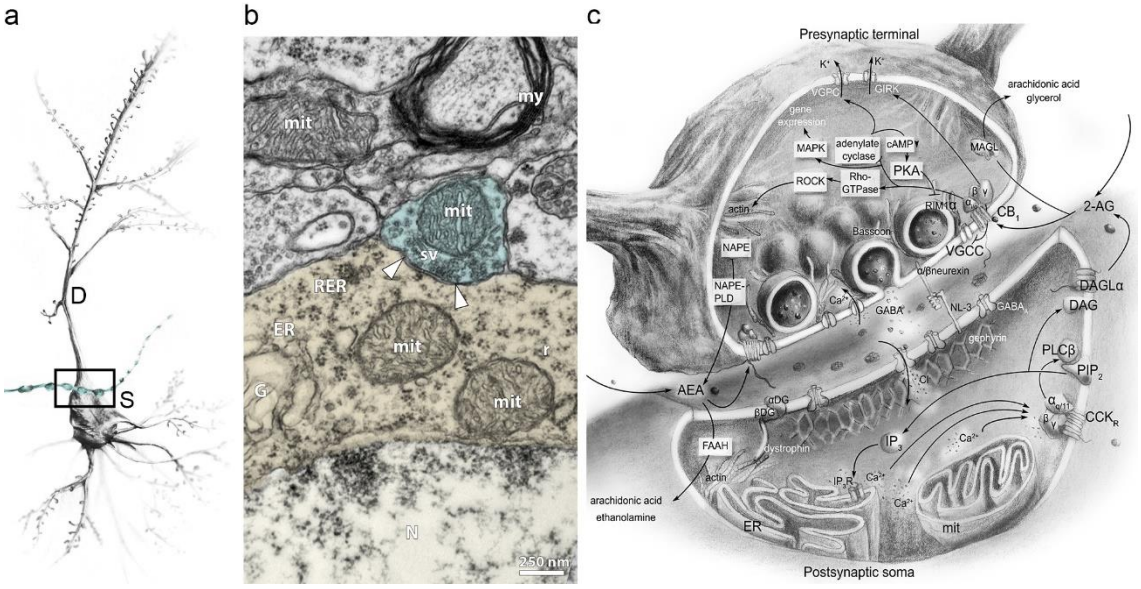

Figure 2. E*ndocannabinoid signaling at perisomatic inhibitory synapse.* **a)** Illustration shows a presynaptic axon string with terminals (cyan) which forms perisomatic inhibitory synaptic contact on the somata of a PC. D: dendrite, S: soma. **b)** Ultrastructure of an inhibitory synapse: axonal bouton (cyan) terminating on the soma (yellow) of a hippocampal CA1 PC in the mouse brain. Synaptic specialization labeled with arrowheads. ER: endoplasmic reticulum, G: Golgi body, mit: mitochondria, my: myelinated fiber, N: nucleus, r: ribosomes, RER: rough endoplasmic reticulum, sv: synaptic vesicles. (Electron microscopical sample and image prepared by the author) **c)** Schematic of the molecular machinery underlying eCB signaling. Increased levels of postsynaptic intracellular Ca^{2+}, or activation of GPCRs (such as: cholecystokinin (CCK) receptor or $mGluR_{1/5}$ at excitatory synapses) can initiate the synthesis of 2-AG or AEA. After metabotropic receptor activation, the $G_{q/11}$ complex activates phospholipase C-β (PLC-β) which splits phosphatidylinositol biphosphate (PIP_2) into inositol trisphosphate (IP_3) and diacylglycerol (DAG). Diacylglycerol-lipase α (DAGLα) then converts DAG to 2-AG which travels backwards through the synapse and activates CB_1Rs. Parallelly, N-arachidonoyl phosphatidylethanolamine (NAPE) can be converted into AEA via NAPE-specific phospholipase-D (NAPE-PLD), which can partially bind to CB_1R. Activation of the presynaptic CB_1R triggers multiple molecular cascades via $G_{i/o}$ complex activity, resulting in the inhibition of presynaptic transmitter release. CB_1Rs are also able to couple $G_{12/13}$ protein complexes, through which they can also regulate the organization of the actin cytoskeleton. The signaling process is terminated by inactivation and hydrolysis of 2-AG or AEA via monoacylglycerol lipase (MAGL) and fatty acid amide hydrolase (FAAH), respectively. α/βDG: α/β-dystroglycan, MAPK: Mitogen-activated protein kinase, NL-3: Neuroligin-3, PKA: Protein kinase A, ROCK: Rho-associated protein kinase.

CB_1Rs and CB_2Rs are G-protein coupled receptors (GPCRs) of the rhodopsin family and serves as the major target for endo- and exocannabinoids (Howlett et al., 1990; Matsuda

et al., 1990; Munro et al., 1993; Pertwee, 1997). These receptors exert several similarities, but also marked differences, not only in crystal structure and conformational states (Hua et al., 2016, 2017; Li et al., 2019), but also in cellular expression patterns. CB_2Rs were generally considered as mainly expressed by cells of the peripheral immune system and microglia (Benito et al., 2008; Munro et al., 1993; Núñez et al., 2004), however, recent evidences suggest cell type-specific postsynaptic neuronal expression in certain hippocampal subregions (Stempel et al., 2016). CB_1R expressed mainly on axons and boutons by both inhibitory and excitatory cells (Katona et al., 2006; Katona et al., 1999) with a remarkably high level of expression on inhibitory axon terminals. It is the most abundant GPCR in the brain with expression levels comparable to the major postsynaptic receptors such as AMPA, NMDA and γ (gamma)-aminobutyric acid type-A ($GABA_A$) receptors (Zhang et al., 2014). Alongside neurons, glial cells also express CB_1Rs throughout the central nervous system (Hu and Mackie, 2015; Navarrete and Araque, 2008; Stella, 2010). Since the major behavioral effects of cannabinoids, as well as the direct regulation of synapses by endocannabinoids are mediated by CB_1Rs (Kawamura et al., 2006; Wilson et al., 2001; Zimmer et al., 1999), I will mainly focus on this receptor while neglect the role of CB_2R from this study. Activation of CB_1Rs via endogenous ligands initiate a signaling cascade in the presynaptic terminal which consist of multiple molecular routes and will supplement the decrease of neurotransmission both short- and long-term (Figure 2/c). As the final step, the signaling is terminated by the main 2-AG degrading enzyme, monoacylglycerol lipase (MAGL). MAGL hydrolyses the vast majority of brain 2-AG (~85%) to arachidonic acid and glycerol, while the rest being catalyzed by alpha/beta-hydrolase domain containing 6 and 12 enzymes (ABHD6, ABHD12) (Blankman et al., 2007).

1.2.1.2. Molecular composition of AEA-mediated endocannabinoid signaling

Although, AEA was the first endocannabinoid to be isolated from the brain (Devane et al., 1992), the lipid tissue levels are two orders of magnitude lower than the concentration of 2-AG and acts only as a partial agonist on CB_1R (Ahn et al., 2008; Di Marzo, 2018; Pertwee et al., 2010). Beside the ability to partially activate CB_1R, AEA is also a full agonist of transient receptor potential cation channel subfamily V member 1 vanilloid receptor (TRPV1) and thus, in some studies it is referred more as an endovanilloid (Di Marzo, 2018; Katona and Freund, 2012). The precise synthesis

pathways of AEA are still not clarified. There are multiple different enzymatic pathways on which generation of AEA can be achieved (Maccarrone, 2017). Among these routes the most relevant biosynthetic pathway includes N-arachidonoyl phosphatidyl-ethanolamine (NAPE), as a precursor, which can be found in the plasma membrane as well as in intracellular membrane compartments such as mitochondria or endoplasmic reticulum. After cleavage, NAPE is hydrolyzed to AEA by an enzyme called NAPE-specific phospholipase-D (NAPE-PLD) (Okamoto et al., 2004). Regarding the subcellular localization of this enzyme, NAPE-PLD can be found in various compartment, including intracellular membrane cisternae in both pre- and postsynaptic locations as well (Cristino et al., 2008; Nyilas et al., 2008; Zou and Kumar, 2018). The inactivation of AEA is carried out by a serine hydrolase called fatty acid amide hydrolase (FAAH) (Cravatt et al., 1996), which cleaves AEA to arachidonic acid and ethanolamine. Interestingly, contrary to MAGL, FAAH localized postsynaptically and associated with membranes of cytoplasmic organelles (Gulyas et al., 2004). Besides the degradation by FAAH, minor oxidative pathways catalyzed by cyclooxygenase-2 (COX-2), and other oxidases have also been described (Maccarrone et al., 2010).

1.2.2. Effect of endocannabinoids on synaptic transmission

Given its remarkable abundance in the brain, CB_1Rs and eCB signaling plays pivotal role in multiple functions of the whole nervous system throughout development. Despite its importance, early developmental aspects of the eCB signaling, including its role in proliferation, differentiation, axonal growth, guidance, and cell motility (Gaffuri et al., 2012; Harkany et al., 2007) falls out from the scope of this study. Therefore, in this chapter, I will briefly focus on their function in regulating neuronal activity and synaptic transmission (Alger, 2012; Busquets-Garcia et al., 2015; Kano et al., 2009; Katona and Freund, 2012).

Endocannabinoids function as retrograde messengers and contribute to both short-term and long-term synaptic plasticity. A classic form of eCB-mediated short-term depression (STD) also called depolarization induced suppression of inhibition or excitation (DSI or DSE). This plasticity can be induced experimentally by substantial depolarization of the postsynaptic neuron. After phasic release of eCBs, presynaptic CB_1Rs are activated which decrease the inhibitory or the excitatory synaptic transmission (Kreitzer and Regehr, 2001; Pitler and Alger, 1992; Wilson et al., 2001; Wilson and Nicoll, 2001). When

activated, CB_1R can initiate multiple molecular cascades via various downstream effectors (Figure 2/c). The phenomenon of DSI and DSE are mediated by the fast βγ subunits of the $G_{i/o}$ protein to which the CB_1R are coupled. These βγ subunits directly blocks N-type VGCCs, therefore decreasing intracellular Ca^{2+} levels and thus reducing Pr (Herlitze et al., 1996; Szabó et al., 2014). The suppression lasts for several seconds after DSI/DSE induction. Evidences from genetically modified animals showed that DAGLα is indispensable for all forms of endocannabinoid-mediated short-term synaptic plasticity (Gao et al., 2010; Tanimura et al., 2010; Yoshino et al., 2011), while lacking MAGL results in a prolonged eCB plasticity (Pan et al., 2011). These observations together suggest pivotal role of 2-AG in regulating synaptic plasticity and highlighting the role of the canonical DAGLα – 2-AG – CB_1R molecular route. Recent advancements in eCB visualization techniques also enabled the *in vivo* investigation of eCB signaling in physiologically relevant time scales, which also suggests that 2-AG is the main activity-dependent eCB in the hippocampus (Farrell et al., 2021). The exact role of AEA in synaptic plasticity is still debated (Ohno-Shosaku and Kano, 2014). AEA and endovanilloid signaling could influence and counteract 2-AG-mediated endocannabinoid signaling and thus regulate GABA release probability (Lee et al., 2015).

Long-term depression (LTD) of synaptic transmission dependent on endocannabinoids has been also found in several areas of the brain (Chevaleyre et al., 2006; Heifets and Castillo, 2009; Kano, 2014). The induction of eCB-LTD is similar to the eCB-STD events: it usually begins with a transient increase in the activity of glutamatergic afferents and the consequent release of eCBs from postsynaptic neurons which then travel retrogradely to activate CB_1Rs. The precise induction protocol by which this phenomenon can be evoked varies from tetanic afferent stimulation at 1 Hz to 100 Hz, to the more patterned theta burst stimulation. An important feature of the eCB signaling that it can activate CB_1R in the surface of the afferent from which the stimulus arrived (homosynaptically) (Marsicano et al., 2002) and also can have effect on receptors located on nearby boutons (heterosynaptically) (Chevaleyre and Castillo, 2003). However, eCB release from the postsynaptic pyramidal cell (PC) and CB_1R activation alone does not enough to induce LTD (Ronesi et al., 2004). Another induction signal is also needed to evoke this phenomenon. Initiation of eCB-LTD is only successful if the presynaptic neuron is activated at a relatively high frequency. Together with various experiments

utilizing NMDA-blockers, these results suggested that presynaptic activation of NMDA receptors are required (Sjöström et al., 2003). Long-term effects in synaptic transmission typically last from minutes to hours. Regarding molecular changes, eCB-LTD achieved via modulation of the slow α_i subunit of $G_{i/o}$ protein which blocks the activity of adenylate-cyclase enzyme. Reduction of cAMP levels will result in blocking neurotransmitter release in a long-term through RIM-1α-dependent manner (Chevaleyre et al., 2007). CB_1R directly stimulates protein synthesis in axon terminals during eCB-LTD in the hippocampus via the mTOR pathway (Younts et al., 2016). The molecular machinery regulating this process is precisely coupled and organized in a complex, since a ~100 nm shift in the localization of DAGLα completely disrupts eCB-LTD in a mouse model of autism (Jung et al., 2012).

The application of exogenous CB_1R ligands impact a broad range of physiological processes from homeostatic control of feeding to memory formation. Although, describing the specific roles of eCBs in these complex behaviors can be challenging. Functional relevance of both short- and long-term plasticity mediated by eCBs have been shown to expand through multiple forms of cortical plasticity. Endocannabinoid-mediated STD and LTD can both play leading role in synaptic weakening that occurs at cortical synapses, which is an essential prerequisite for novel memory formation (Heifets and Castillo, 2009). Long-term changes in synaptic strength are also believed to underlie associative memory formation and incidental association learning in a CB_1R-dependent manner (Busquets-Garcia et al., 2018).

Activation of CB_1R will also affect numerous other signaling pathways, from which all support the dampening of synaptic transmission of the given cell or synapse (Figure 2/c). Besides shaping neuronal morphology and axonal pathfinding during development, CB_1R-mediated signaling can rapidly transform the neuronal cytoskeleton. Cannabinoid receptors can be coupled to heterotrimeric $G_{12/13}$ proteins. Through this complex, activation of the receptors can trigger rapid and reversible non-muscle myosin II-dependent contraction of the actomyosin cytoskeleton via Rho-GTPase and Rho-associated kinase (ROCK) (Roland et al., 2014). This contractility mechanism can be a major underlying mechanism responsible for eCB-LTD, since it can lead to redistribution and depletion of synaptic vesicles from the presynaptic active zone (McFadden et al., 2018). Recently it was also shown that beside receptors localized on axon terminals,

CB_1R which are present at axonal segments also have an important signaling role in mature neurons. In neural axons and dendrites actin, spectrin and they interacting molecules create a scaffold called membrane-associated periodic skeleton (MPS). Through this MPS, CB_1Rs are localized together with transmembrane proteins, ion channels and adhesion molecules in periodic signaling platforms, created precisely 190 nm apart from each other (Zhou et al., 2019). These platforms play a major role in receptor tyrosine kinases (RTK) – extracellular signal–regulated kinase (ERK) signaling and initiate several intracellular signal transduction cascades to alter gene expression in cells. Postsynaptic CB_1Rs located on dendritic compartments can also influence the somatodendritic excitability of neurons via hyperpolarization–activated cyclic nucleotide–gated (HCN) channels in slice preparations (Maroso et al., 2016) and also via direct somatodendritic inhibition of cAMP-PKA pathway in cell cultures (Ladarre et al., 2015). Therefore, contrary to the most popular view, CB_1R can have physiological effects not only on presynaptic boutonal sites, but also at dendritic or axonal cell compartments.

1.2.3. Tonic cannabinoid signaling

There are two main forms of eCB signaling through which it can affect synaptic strength. Phasic or *"on demand"* signaling introduced in the previous paragraphs occurs via transient release of eCB molecules and depresses neurotransmission in a prompt manner. This form of signaling is extensively investigated and plays a considerable role in nearly all the aforementioned processes regulated by the eCB system. The second, much less-studied form is tonic or persistent eCB signaling. While using paired recordings to detect postsynaptic currents on PCs after presynaptic stimulation of an interneuron, it was shown that there are functional synapses in the hippocampus, which exhibit low Pr under general baseline conditions unless CB_1R antagonist/inverse-agonist AM251 is applied to the slice. After pharmacological blockade of CB_1R however, the amplitude of inhibitory postsynaptic currents (IPSC) and the number of successful events were significantly increased (Losonczy et al., 2004). This observation highlighted the presence of a baseline, ongoing tonic eCB signaling, which can continuously regulate the synapses.

While there are multiple features of this signaling modality which makes it a promising target of interest, many questions regarding tonic cannabinoid signaling are still unanswered. Importantly, tonic, but not phasic cannabinoid signaling is selectively

disrupted in mouse models of autism (Földy et al., 2013; Speed et al., 2015) raising the possibility that mechanistically distinct principles underlie the phasic forms of eCB-mediated synaptic plasticity and the synaptic cannabinoid tone. The main molecular players, however, that set the magnitude of the later one are still debated. Both AEA and 2-AG have been reported to mediate tonic cannabinoid signaling in *ex vivo* experimental assays (Haj-Dahmane et al., 2018; Hashimotodani et al., 2007; Huang and Woolley, 2012; Kim and Alger, 2010; Lee et al., 2015). Likewise, NAPE-PLD-synthesized AEA and DAGLα-synthesized 2-AG have been both proposed as tonic endocannabinoid mediators *in vivo* (Marcus et al., 2020; Petrie et al., 2023). It is also suggested that at certain synapses in the hippocampus, tonic cannabinoid signaling can also modulate information transmission via constitutively active CB_1Rs (Jensen et al., 2021; Lee et al., 2015). Moreover, even the involvement of CB_1Rs in tonic cannabinoid signaling has been questioned due to potential pharmacological off-target effects of CB_1R antagonist/inverse agonists on $GABA_A$ receptors (Baur et al., 2012).

Contrary to phasic eCB modulation, which can be effective heterosynaptically at multiple neighboring synapses in the close vicinity of the eCB release (Chevaleyre and Castillo, 2003), experiments with calcium chelator infusion into the postsynaptic cell revealed that tonic cannabinoid signaling functions homosynaptically and necessitates intact postsynaptic Ca^{2+} signaling (Neu et al., 2007). Besides its feature of being synapse-specific, tonic cannabinoid signaling is also cell-type specific: it selectively regulates perisomatically-targeting, but not dendritically-targeting GABAergic interneuron synapses in the hippocampus brain region (Lee et al., 2010, 2015).

Altogether, despite its considerable pathological importance, the detailed underlying mechanisms that regulate tonic cannabinoid signaling are still elusive.

1.2.4. Cannabinoid signaling during pathophysiological conditions

Endocannabinoids have an important role in regulating synaptic transmission, therefore, it is not surprising that impairment of the eCB signaling can lead to serious neurological disorders. Also, from the opposite perspective: the eCB system is a promising potential therapeutic target for several pathophysiological conditions.

Given their role as a neural circuit breaker, eCBs play a key role in the resolution of multiple pain states (Alkaitis et al., 2010). While acute pain is an evolutionary adaptive

phenomenon, chronic neuropathic pain is a pathological condition. Expression levels of eCB proteins are altered at various sites in nociceptive pathways in chronic pain (Sagar et al., 2012). Therefore, many components of the eCB signaling machinery were targeted experimentally to achieve analgesia including acute or chronic inhibition of eCB degrading enzymes, utilization of positive allosteric modulators or exogen agonists of CB_1R, (Jhaveri et al., 2006; Laprairie et al., 2017; Pamplona et al., 2012; Schlosburg et al., 2009).

Occurrence of imbalances in excitation and inhibition among cortical neurons are one of the most prominent prerequisites in the pathogenesis of seizure disorders, such as epilepsy. Epilepsy is one of most common neurological disorders and can be characterized by appearing episodic seizures. The main cause of common epilepsies is likely to be complex, comprised of multiple factors. Broadly they can be classified in two main groups including the genetic-type, which can arise from mutations in genes coding, for example ion channels and the acquired-type, which develops after severe head injury. Endocannabinoid control of glutamatergic and GABAergic synapses plays a crucial role in setting physiological ratio of excitatory-inhibitory balance. This property is making them excellent therapeutic target for treating this pathophysiological condition (Soltesz et al., 2015). Cell type-specific changes of the eCB system during epileptic conditions, which could mechanistically contribute to seizures are well-documented. CB_1R and DAGLα expression on excitatory axon terminals within the inner molecular layer of the dentate gyrus was found to be downregulated (Ludanyi et al., 2008), while CB_1R expression on inhibitory axon terminals was upregulated (Maglóczky et al., 2010). Temporal changes of receptor expression also occur as the disease propagates. In the acute phase, CB_1Rs are markedly downregulated throughout the hippocampus but upregulated in the chronic phase of the disorder (Falenski et al., 2009).

Specific disruption of the tonic cannabinoid signaling pathway is also associated with neurological disorders. Besides its specific impairment in autism models (Földy et al., 2013), in experimental fever-induced (febrile) seizures, which are the most common form of childhood seizures, an increase of the eCB-mediated tonic inhibition of GABA release was detected (Chen et al., 2003). In a mouse model of Huntington's Disease, output neurons of the striatum displayed higher excitability and more depolarized membranes compared to wild-type littermates. The underlying mechanism involved a retrograde eCB

signaling by which synaptic GABA release is persistently suppressed. Enhancement of this tonic eCB pathway during diseased conditions led to the disinhibition of striatal output activity (Dvorzhak et al., 2013).

Marijuana, a derivative of the plant *Cannabis sativa*, has been used for recreational and therapeutic purposes since antiquity. Out of the few hundred cannabinoid molecules which can be found in the plant, Δ^9-tetrahydrocannabinol (THC) is the most potent exogen agonist of CB_1R. Even nowadays, this compound is a highly promising candidate for the treatment of both above-mentioned conditions. However, till recently, every trial resulted in major setbacks which prevented the methods from translating into the clinic (Woodhams et al., 2017). In the case of pain treatment, the beneficial effects are often accompanied by mood disorders, loss of appetite or disturbed sleep, not to mention psychoactive side-effects, tolerance, and potential appearance of physical dependence. These symptoms probably arise due to the abundant expression of the eCB molecules in various cell- and synapse types along generally every neuronal pathway. While these results are not completely satisfying, targeting the endogenous cannabinoids as potential analgesic still holds many promises which can be fulfilled after detailed understanding of the eCB system. CB_1R agonists can also act as anticonvulsants in epileptic patients (Gaston and Friedman, 2017). Exogenously applied THC or endogenously released 2-AG, after binding to CB_1R on glutamatergic axon terminals, can suppress glutamate release and thus prevents over-excited circuits from undergoing uncontrolled hyperexcitability. Albeit, due to the versatile expression of CB_1Rs in the brain, potentially cell-type- and likely even cell-nanodomain specific targeting of drugs are required.

Potential beneficial effects of THC application can also increase negative consequences. While the legalization of recreational or medical marijuana is continuously spreading worldwide, one should not exaggerate the hazards of use. There is a constantly increasing trend among pregnant women in the western countries to use cannabis in order to treat morning sickness. However, multiple studies showed that prenatal cannabis exposure predisposes individuals to a wide array of behavioral and cognitive deficits. In the cellular level for example, it induces extensive molecular and synaptic alterations in dopaminergic neurons of the ventral tegmental area (Frau et al., 2019). Therefore, together with beneficial possibilities, interacting with the eCB system during development or through adulthood should be handled with caution.

1.3. Organization of the hippocampus

A prerequisite of the effective complex computations that the brain can perform is the division of labor between different brain regions and cell-types. Amongst many cortical areas, one important hub of learning and memory storage is the hippocampal formation (Buzsáki and Moser, 2013; Lisman et al., 2017; Voss et al., 2017). The hippocampus has an indispensable role in processing incoming data and comparing it with previous experiences. Since this study is mainly focusing on a specific synapse type within the hippocampus, the description of main anatomical characteristics and cellular components of this brain region should not be avoided.

1.3.1. Anatomical organization of the hippocampal formation

The hippocampus is a cortical brain structure, that developmentally originates from the medial edge of the telencephalic pallium. It is part of the limbic system and receives highly processed multimodal sensory input from cortical and subcortical brain regions as well. Although it has multiple functions, the hippocampus is best known for its crucial role in information coding, memory storage and recall. This brain area is evolutionally well preserved and structurally similar throughout multiple species. Together with its relatively simple organization and its remarkable functions, it is not surprising that the rodent hippocampus became one of the most widespread model systems of neuroscience (Andersen et al., 2007).

The appellation of “the hippocampal formation” comprises of multiple distinct brain regions which are the entorhinal cortex, the dentate gyrus, the hippocampus proper and the subicular regions (subiculum, presubiculum, parasubiculum). The hippocampus proper can be further differentiated by three subdivisions of the Ammon's horn (or Cornu Ammonis): CA1, CA2 and CA3 (Figure 3). Each of these structures have unique functions in information processing which will be briefly discussed in this chapter.

One key feature of the hippocampal formation is its extraordinary organization. While neocortical principal cells usually make reciprocal connections to each other, neuroanatomy of the hippocampus supplements a unidirectional information flow. The main entry point of the sensory inputs is the entorhinal cortex. This region is also the end point before the information is relayed back to the neocortex, therefore the whole hippocampal information transfer forms a complex loop.

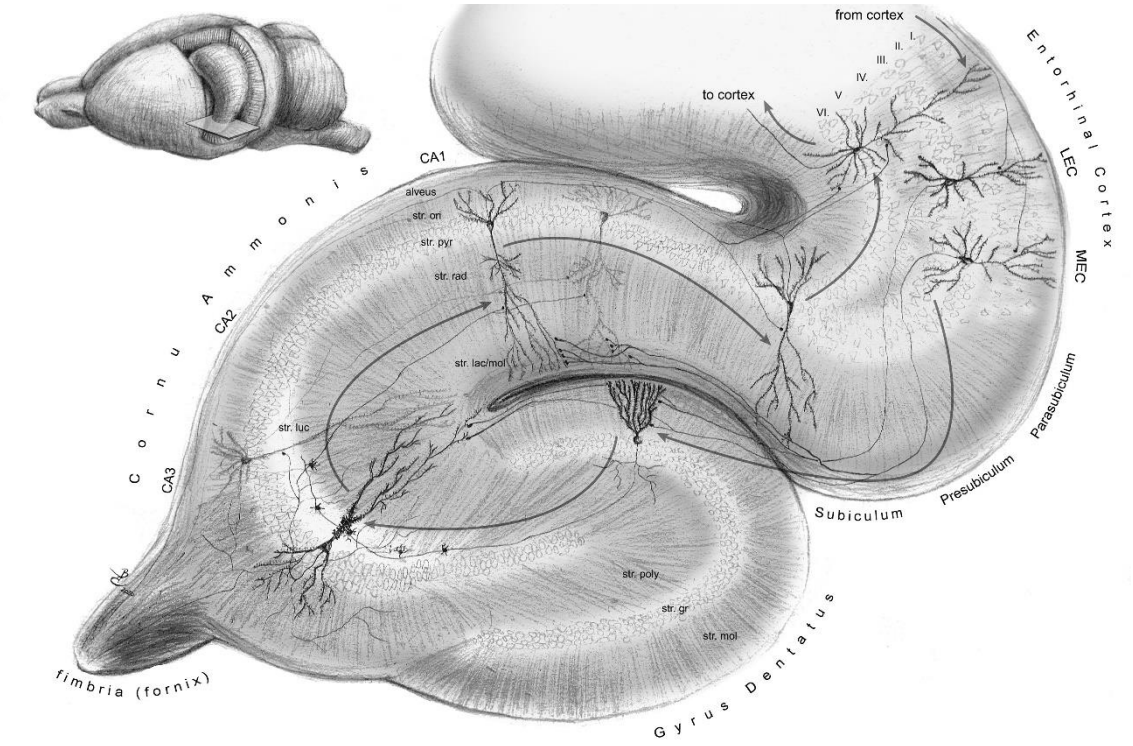

Figure 3. ***Anatomical organization and major connections of the hippocampus.*** Inset in the upper left corner shows subcortical localization of the hippocampal formation in the mouse brain (left hemisphere of the cortex was partially removed in a window to allow visualization of the structure). Schematic representation of the main hippocampal local excitatory pathways drawn from the plane depicted on the inset (entorhinal regions were compressed to the same plane for clarity). Synaptic input from the entorhinal cortex propagates through the perforant path and reaches the granule cells of the dentate gyrus (or Gyrus Dentatus). Granule cells project to the CA3 area via their so-called mossy fibers and target thorny CA3 pyramidal cells with their large mossy terminals. CA3 pyramidal cells send their Schaffer collaterals to the dendrites of principal cells located in the CA1 area. These cells send information to the subicular pyramidal cells, but also directly back to the deep layers of the entorhinal cortex together with the pyramidal cells of the subiculum. The entorhinal cortex also sends direct inputs to the CA1 region in multiple parallel pathways; fibers from the lateral entorhinal cortex (LEC) mainly targets superficial pyramidal cells, while cells in the medial entorhinal cortex (MEC) prefer deep pyramidal cells. str. ori: stratum oriens; str. pyr: stratum pyramidale; str. rad: stratum radiatum; str. lac/mol: stratum lacunosum/moleculare; strl luc: stratum lucidum; str. poly: polymorphic layer; str. gr: stratum granulosum; str. mol: stratum moleculare.

Principal cells located in the superficial layers of the entorhinal cortex (in layers I-II) send their axons to the dentate gyrus through the major hippocampal input pathway called the perforant path. These axons terminate on granule cells which are the principal excitatory

cells of the dentate gyrus. Axons originating from the lateral entorhinal cortex project to the upper part of the dentate molecular layer, while the medial entorhinal projections terminate on the medial part of the molecular layer. The continuous neurogenesis (also throughout adulthood) and the large number of granule cells in this region support a very specific function to this area. Based on our current knowledge, cortical sensory information from the outside world are stored and represented in the brain as memory engram complexes (Josselyn and Tonegawa, 2020). These complexes consist of multiple cells that are activated and tuned together during learning or experiencing, also referred to as engram cells. Each individual memory is therefore coded as the combined activity of an individual group of cells. As it operates with an enormous number of granule cells, the dentate gyrus is able to process and separate these individual memory prints to unique cell-activity patterns before it gets transmitted to the hippocampus proper (Acsády and Káli, 2007). This process is called pattern-separation. Granule cells give rise to axons called mossy fibers that project to thorny PCs of the CA3 field (also to CA2, see: Kohara et al., 2013). These connections formed via characteristic mossy boutons onto the apical dendrite of PCs enable reliable neurotransmission even during high-frequency activity (Evstratova and Tóth, 2014). Given their exceptionally large size, mossy terminals have multiple release sites with high number of readily releasable vesicles which allows the granule cells to conduct highly reliable information transmission with those PCs which will contribute to coding of a memory print. It is also worth to mention that mossy boutons not only innervate PCs, but also connect to many inhibitory neurons via their filopodia and small *en passant* boutons (Acsády et al., 1998), therefore granule cells are able to drive both excitation and inhibition of the whole network. In the CA3 region, one specific feature of the principal cells is that they have long axons (~0.5 m in total length) and make extensive local collaterals. PCs of this region are able to preserve those activity patterns which represent a given memory engram by the strength of synaptic connections between each other, therefore playing a pivotal role in memory generation and recall. Beside the large number of local connections, CA3 PCs innervate PCs in the CA1 via their Schaffer collaterals, as the next important station in the hippocampal loop. While the other parts of the CA area have received extensive attention, the CA2 region has been largely neglected, due to its small size and uncertain borders. Recent recognition of those novel marker proteins whose expression pattern highlights its borders unfolded specific role of

CA2 in social recognition memory, and also opened new opportunities to study this subregion (Tzakis and Holahan, 2019). CA1 region plays an important role in novelty detection and enrichment of hippocampal output information. Precise organization and function of this area will be discussed more extensively in the forthcoming chapter. Finally, as the last part of the loop, CA1 PCs project to the subiculum and back to deep layers of the entorhinal cortex.

This description is a simplified view of the main information processing route in the hippocampal formation. Multiple other pathways and molecular factors contribute to the complexity of this brain structure. Regarding subdomains of the whole hippocampus, the ventral hippocampus has been shown to be involved in anxiety-related behaviors and influences the characteristic fear memory processing of the amygdala, given that the ventral hippocampus projects directly to the amygdala (Fanselow and Dong, 2010; Moser and Moser, 1998). The dorsal part of the hippocampus is implicated in working memory and spatial navigation. Lesion of this specific field have been shown to be just as effective in disrupting spatial working memory as complete hippocampal lesions (Moser et al., 1995; Pothuizen et al., 2004). Although this view already depicts functional differences between regions, the real picture is much more sophisticated. The whole structure expresses a transcriptomic gradient along the dorso-ventral axis overlaid onto the discrete borders, which could further enhance the computational power of the hippocampus (Strange et al., 2014).

Beside local circuits, the hippocampal formation receives important subcortical, divergent, mostly modulatory input from the septum, supramamillary nucleus, locus coeruleus, ventral tegmental area, nucleus reuniens of the thalamus and raphe nuclei.

1.3.2. Structure and function of the CA1 region

As the hippocampus proper (including CA1) is part of the archicortex, it consists of three cortical layers in strict laminar arrangement (Figure 3). Somata of the excitatory PCs are concentrated in a single layer (stratum pyramidale), while their basal dendrites and apical dendrites are located in the oriens and radiatum layers, respectively. The most distal dendrites of PCs can be found in the lacunosum-moleculare layer, to where a subdivision of the entorhinal perforant path projects and forms direct contact with CA1. PCs in this region do not innervate other PCs with axon collaterals. Their axons leave the

hippocampus through the alveus and target mainly the subiculum and the entorhinal cortex. I will mostly focus on local connections, however, CA1 PCs also innervate the retrosplenial cortex, the amygdala and the septum.

The general view for a long-time regarding principal neurons was that they form homogeneous populations in each hippocampal area (Kesner and Rolls, 2015; Marr, 1971). Albeit recent evidence highlighted that different excitatory cell-subpopulations are present in the hippocampus. Superficial PCs located closer to the radiatum layer express multiple differences compared to deep-layer PCs in CA1. They not only differ in the timing of neurogenesis and thus their genetic programs, but they express different molecules, morphology, innervation and exhibit different activity during various brain states (Cembrowski et al., 2016; Lee et al., 2014; Li et al., 2017; Masurkar et al., 2017; Mizuseki et al., 2011). The complexity also extends to the connectivity formed with local inhibitory cells: Parvalbumin (PV) expressing perisomatically-targeting basket cells receive more excitation from superficial PCs but deliver stronger inhibition to deep PCs (Lee et al., 2014). Beside layer specific differences of principal cells, transcriptional gradients along the radial hippocampal axis were also demonstrated (Cembrowski et al., 2016). Together these results strongly suggest the existence of intra-hippocampal nonuniform subnetworks that allow parallel information processing (Soltesz and Losonczy, 2018). The heterogenous population of PCs and potential micro-circuits in the CA1 region is therefore the basis of a highly complex architecture in this brain area.

It is also noteworthy to mention the role of hippocampal PCs in spatial memory. There are certain cells whose activity is determined by the spatial location of the animal itself. These are the so called “place cells”, which fire bursts of action potentials in specific places of the environment (O’Keefe et al., 1971). All subfields of the hippocampus contain place cells including granule cells of the dentate gyrus, but the most distinct firing fields are found in the CA areas. These place fields generated by PCs produce a cognitive map which can help the animal to navigate and orient its own position in space (Moser et al., 2008). While the exact origin of the information which code the receptive fields in the CA1 are still not clarified yet, major role of the entorhinal cortex is certain (Mallory and Giocomo, 2018). Therefore, entorhinal cells are crucial elements of the brain’s metric system for spatial navigation. These entorhinal “grid cells” derive their name from the fact that the centers of their firing fields form a grid with hexagonal symmetry. “Border

cells" (Solstad et al., 2008), "head-direction cells" (Taube et al., 1990) and "object-vector cells" (Høydal et al., 2019) are also specific subgroups of neurons which code various important spatial information in the hippocampal formation. Through these cell groups, the entire environment of the animal can be represented.

1.3.3. Diversity of inhibitory neurons in the CA1 region

Amongst multiple types of excitatory principal cells, cortical networks are also supplemented with inhibitory neurons, which constitute ~10–15% of the total hippocampal neuron population. Inhibition serves an important role in keeping the excitatory-inhibitory balance via tuning the firing of PCs, filtering dendritic integration, and therefore modulating rhythmic activity. Given the immense complexity of the cortical circuits in which GABAergic interneurons are embedded, it is not surprising that despite their importance, there are still gaps in our understanding regarding their diverse role in network computations.

Interneuron somata can be found in each layer of the CA1 area. Compared to the PCs, these neurons exhibit remarkable variability in developmental origin, morphology, innervation, firing pattern and expressed molecules (Freund and Buzsáki, 1996; Pelkey et al., 2017). These factors gave the main frame for the classification of inhibitory cells for a long time leading to the separation of at least 21 different interneuron classes (Figure 4). Novel techniques implementing transcriptomic profile analysis of the cells widened the phylogenetic systematization and identified 49 potential cell-clusters (Harris et al., 2018; Tasic et al., 2016; Zeisel et al., 2015). Although, direct classification is mainly dependent on how finely and firmly the borders of cell-clusters are set (as continuous variations also exist within certain cellular transcriptomic profiles (Harris et al., 2018)), these datasets nicely illustrate notable specialization amongst inhibitory cells.

Inhibitory synapses cover the entire somato-dendritic membrane surface of PCs (including the axon initial segment). An important key feature which arises from the diverse morphology of interneurons is that they can specifically innervate distinct domains of the PCs (Figure 4). With this fine-tuned division of labor, these highly specialized interneuron groups can precisely keep a dynamic, spatio-temporal GABAergic control over the PCs, regulating their synchrony and discharge (Somogyi and Klausberger, 2005). The diversity of interneurons directly relates to their developmental

origins in the embryonic brain. Contrary to cortical PCs, which are generated at the ventricular zones of dorsal telencephalon and reach their final position through radial migration, GABAergic progenitor pools are located far from their destined location. The vast majority of interneurons originate from the two main germinative zones of the ventral subcortical telencephalon: the medial ganglionic eminence (MGE) and the caudal ganglionic eminence (CGE). Neurons generated here reaches their final location via tangential migration (Pelkey et al., 2017).

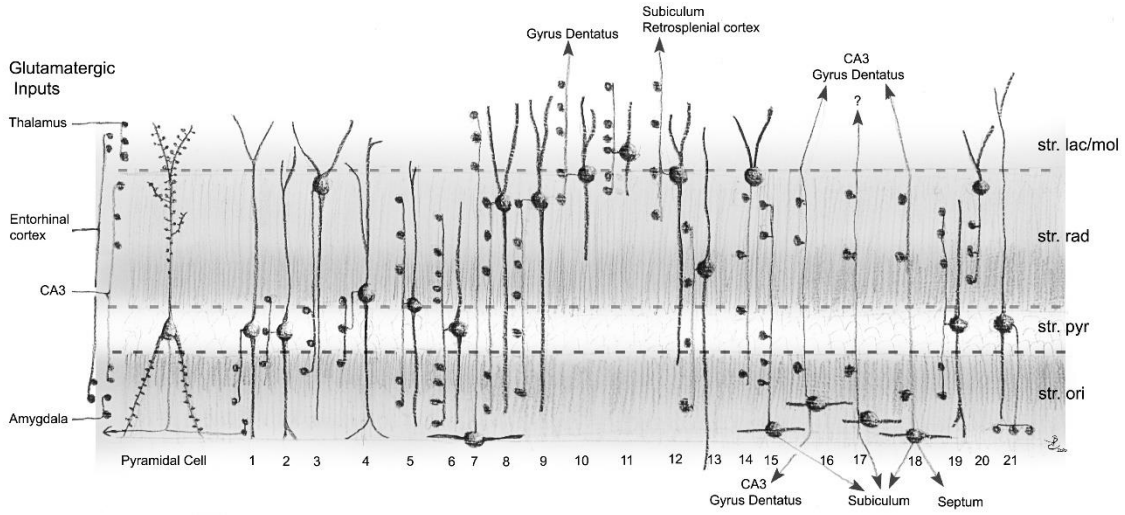

Figure 4. ***Variability of interneurons in the hippocampal CA1 region.*** Schematic representation of average somatic localization, dendritic arborization and characteristic axonal target region of inhibitory cells. Based on cellular morphology and expression of major neurochemical markers, the classical view depicts at least 21 different interneuron classes in the hippocampal CA1 area: 1) Axo-axonic, 2) PV Basket, 3) CCK/VIP Basket, 4) CCK/vGluT3 Basket, 5) Bistratified, 6) Ivy, 7) Oriens-Lacunosum/moleculare (O-LM), 8) Schaffer collateral-associated, 9) Apical dendritic innervating, 10) Perforant path-associated, 11) Neurogliaform, 12) Radiatum-retrohippocampal projection, 13) Large calbindin, 14) Cholinergic, 15) Trilaminar, 16) Back-projection, 17) Oriens-retrohippocampal projection, 18) Double projection, 19) Interneuron specific (IN)-1, 20) IN-2, 21) IN-3. PV: parvalbumin, CCK: cholecystokinin; VIP: vasoactive intestinal polypeptide; vGluT3: vesicular glutamate transporter 3 (drawing based on: Klausberger and Somogyi, 2008).

1.3.3.1. Perisomatically-targeting interneurons

A specific group of interneurons exclusively target the somata and the close somatodendritic compartments of PCs. The axons of these perisomatic interneurons are

located in an optimal position to effectively control the timing and frequency of action potential generation and synchronization of principal cell assemblies (Cobb et al., 1995). There are three main classes of inhibitory neurons in the CA1 region which target the pyramidal perisomatic region: axo-axonic cells, PV-expressing basket cells (PVBCs) and CB_1R/CCK-expressing basket cells (CB_1BCs). Although axo-axonic cells are classified as perisomatic region-targeting cells, as they name also indicates, they specifically target the axon-initial segments of PCs (Somogyi et al., 1983). Interestingly, this group has the ability to not just inhibit the AP generation in the most efficient way but can also excite PCs in certain conditions and brain states (Szabadics et al., 2006).

Basket cells got their names from their characteristic axonal arborization, which wraps around the soma and soma-equivalent close proximal dendrites of PCs with axon terminals, forming "basket"-like structures. PVBCs are estimated to comprise ~14% (~5,530 cells) of CA1 interneurons and individual neurons innervate up to 2500 PCs, while CB_1BCs constitute only 9% of CA1 neuronal population (Pelkey et al., 2017). The CB_1BC group contacts roughly half as many PCs as PVBCs does. Distinct molecular expression profiles of the two different basket cell populations are derived from the distinct developmental origins of the cells. All hippocampal and cortical CB_1BC are generated in the CGE (Morozov et al., 2009; Tricoire et al., 2011), while PVBCs originate from the MGE (Tricoire et al., 2011). These differences are accompanied by distinct cellular orientation, physiology, and function. While somata of PVBCs can be found mainly in the oriens and pyramidal layers of the hippocampal CA1 region, CB_1BCs are accumulated in the radiatum layer. Both groups have their dendritic trees spanning from the alveus to the lacunosum-moleculare layer. Albeit this positioning allows both to receive input from all excitatory afferents innervating the hippocampal CA1 region, they receive distinct innervations. PVBCs have at least three times more glutamatergic synaptic inputs than CB_1BCs, whereas the latter receive subcortical, mostly serotonergic input from the median raphe (Freund and Katona, 2007). They also express $GABA_B$ receptors with different surface density (Booker et al., 2017) which can influence their inhibitory function.

1.3.3.2. CB_1BCs in network oscillations

Both groups of basket cells can effectively control the synchrony of principal cell output due to their perisomatic innervation schemes. However, they regulate PC activity

in a fundamentally distinct manner due to their different physiological properties. PVBCs can fire repetitively without any frequency changes or adaptations, thus reliably translate rapid excitatory inputs into fast, short-latency inhibitory outputs (Doischer et al., 2008; Jonas et al., 2004). This properties allow them to regulate general network oscillations in a clockwork-like precision (Freund and Katona, 2007). In contrast, CB_1BCs show regular, non-fast spiking or accommodating firing pattern (Wierenga et al., 2010) and can have large jitter, as the neurotransmitter release from these cells are largely asynchronous. CB_1BCs express N-type (Cav 2.2) calcium channels, which are loosely coupled to the vesicle release sites (Hefft and Jonas, 2005), therefore, these cells respond less reliably to afferent signals. Due to this property, they can produce prolonged inhibition on PCs in a larger time window (Glickfeld and Scanziani, 2006). Asynchronous release can be further enhanced in these cells via CB_1R-mediated eCB signaling (Ali and Todorova, 2010).

For a substantial time, there was no reliable genetic strategy that allowed for selective, precise targeting and manipulation of CB_1BCs, or even CCK interneurons in general (as PCs also express CCK protein). Therefore, the precise *in vivo* role of CB_1BCs is still lagging compared to PV-expressing ones. First recordings from anesthetized rats showed that these cells discharge with highest frequency during the ascending phase of theta oscillations (Klausberger et al., 2005). Recently, a transgenic mouse line was generated which allowed the restricted *in vivo* investigation of CB_1BCs. Calcium imaging experiments performed in awake behaving mouse showed opposing activity pattern for CB_1BCs and PVBSc during certain behavioral states: while PVBCs activity scales with CA1 network activity, CB_1BC activity is inversely correlated, thus these cells are mostly activated when the PCs are silent (Dudok et al., 2021). Moreover, CB_1BCs exhibit unique behavioral state-dependent activity patterns and play pivotal roles in neuronal ensemble formation that underlie spatial coding and memory engrams formation (Bloodgood et al., 2013; Bugeon et al., 2022; del Pino et al., 2017; Hartzell et al., 2018; Sun et al., 2020; Tomé et al., 2024; Vancura et al., 2023; Yap et al., 2021). Endocannabinoid-mediated short term plasticity expressed by these cells is also indispensable for proper spatial memory formation, as it was shown that DSI, a phenomenon well described in slice preparations is also present *in vivo* in physiologically relevant behavioral states and contribute to spatial memory-related place cell tuning (Dudok et al., 2024).

2. Objectives

Precise examination of cell type- and synapse specific regulatory mechanisms are indispensable prerequisites for detailed understanding of how individual neurons can affect network dynamics and information processing in the brain. Motivated by the physiological and pathophysiological significance, but limited mechanistic understanding of the cannabinoid tone, in this study our specific aims are the following:

1) Detailed anatomical and physiological investigation of CB_1BCs and inhibitory synapses specifically present between CB_1BCs and PCs in the hippocampal CA1 region.

- Identification of calcium-binding molecules which can determine unique physiological properties of CB_1BCs.
- Perform electrophysiological and anatomical experiments to study synaptic variability between identified cells.

2) Study the potential role of main molecular components of the endocannabinoid system in tonic cannabinoid signaling at CB_1BC – PC synapses.

- Utilization of multiple transgenic mouse lines in electrophysiological experiments to determine the role of CB_1Rs, together with the major 2-AG and AEA synthesizing enzymes, DAGLα and NAPE-PLD respectively in tonic cannabinoid signaling.

3) Develop a methodological workflow that can address nanoscale molecular principles of tonic cannabinoid signaling in complex brain tissue at CB_1BC – PC synapses.

- Application of *in vitro* paired patch-clamp recordings together with correlated confocal- and super-resolution microscopy to collect electrophysiological, anatomical and nanoscale molecular data from the very same synapse in acute brain slice preparations.
- Test the hypothesis with multiple *in vivo* perturbation models including modest genetic ablation of CB_1Rs and chronic administration of THC.

3. Methods

3.1. Animals

Animal experiments conducted in Hungary were approved by the Hungarian Committee of the Scientific Ethics of Animal Research (license number: MÁB-2018/1), and all animal experiments were performed according to the Hungarian Act of Animal Care and Experimentation (1998, XXVIII, Section 243/1998, renewed in 40/2013), which are in accordance with the European Communities Council Directive of November 24, 1986 (86/609/EEC; Section 243/1998). Animal experiments conducted in the U.S.A. were approved by the Institutional Animal Care and Use Committee of Indiana University and conform to the National Institutes of Health Guidelines on the Care and Use of Animals. Mice were kept under approved, specific-pathogen-free laboratory conditions (12-h light/12-h dark cycle, 22–24 °C, 40 – 70% humidity), and all efforts were made to minimize pain, suffering and to reduce the number of animals used. Both in electrophysiological, anatomical, and analytical experiments C57Bl/6J male mice (postnatal day 27 - 45) were used, together with strains containing genetic deletion of specific protein coding genes: CB_1R knockout (KO) (kindly provided by A. Zimmer, University of Bonn), DAGLα KO (kindly provided by K. Sakimura, Niigata University), NAPE-PLD KO (kindly provided by B. Cravatt, The Skaggs Institute for Chemical Biology and Department of Chemical Physiology and The Scripps Research Institute, La Jolla, California, USA). In cases where genetically modified mice were used, their wild-type littermates were utilized for control measurements.

3.2. Chronic drug treatment model in mice

All procedures were performed in accordance with the European legislation EU Directive 2010/63 and the National Institute of Health Guide for the Care and Use of Laboratory Animals and were approved by the Animal Ethics Committees of the University of Cagliari and by Italian Ministry of Health (auth. n. 659/2015-PR). Male C57BL/6J mice (Envigo, Italy), 22–31 days of age at the beginning of the treatments, were housed (ten per cage) in a controlled environment at constant temperature (21 ± 1°C) and humidity (60%) on a 12-h light–dark cycle (lights on at 7.00 a.m.) with free access to food and water. Procedures for chronic Δ^9-tetrahydrocannabinol (THC) treatment are described below.

3.3. Acute slice preparation

Mice were decapitated under deep isoflurane anesthesia. The brains were carefully removed from the skull and transferred rapidly to ice-cold sucrose containing artificial cerebrospinal fluid (Sucrose-ACSF; containing in mM: 75 NaCl, 75 sucrose, 2.5 KCl, 25 glucose, 1.25 NaH_2PO_4, 4 $MgCl_2$, 0.5 CaCl and 24 $NaHCO_3$, Sigma-Aldrich, St. Louis, MO, USA), equilibrated with 95% O_2 and 5% CO_2 (all chemicals were obtained from Sigma-Aldrich unless otherwise mentioned). 300 µm thick coronal hippocampal acute slices were cut with a VT-1200S Vibratome (Leica, Nussloch, Germany) (anteroposterior -1.8 mm to -2.8 mm from bregma) and were incubated in sucrose-ACSF for 1 h at 34˚C. Afterwards, the oxygenated incubation chamber was kept at room temperature and slices were subjected to subsequent electrophysiological, two-photon or lipid measurements.

3.4. *In vitro* slice electrophysiology

All electrophysiological recordings were made in a submerged recording chamber at 33 °C constantly perfused with oxygenated ACSF solution (in mM: 126 NaCl, 2.5 KCl, 10 glucose, 1.25 $NaH2PO_4$, 2 $MgCl_2$, 2 $CaCl_2$ and 26 $NaHCO_3$). Slices were visualized with an upright Nikon Eclipse FN1 microscope equipped with infrared differential interference contrast (DIC) optics (Nikon, Tokyo, Japan).

Whole-cell patch-camp recordings were obtained from interneurons in the CA1 region of the hippocampus after visual inspection of their somatic location in the radiatum layer and their multipolar morphology under DIC microscope. All selected cells displayed accommodating firing pattern implicating a CB_1R-positive interneuron phenotype. Recordings were carried out with borosilicate glass pipettes (0.86 mm inner diameter and 1.5 mm outer diameter with 3–5 MΩ resistance) filled with internal solution (containing in mM: 126 K-gluconate, 4 KCl, 10 HEPES, 4 Mg-ATP, 0.3 Na_2-GTP, 10 phosphocreatine and 8 biocytin; pH 7.2; 290 mOsm/kg). Pipettes were pulled with a P-1000 horizontal micropipette puller (Sutter Instrument, Novato, CA, USA). Recordings were performed using MultiClamp 700B amplifiers (Molecular Devices, San José, CA, USA). Signals were filtered at 3 kHz using a Bessel filter and digitized at 10 kHz with Digidata 1440a and 1550 analog-to-digital interface (Molecular Devices). The recorded traces were analyzed using the Clampfit 10 software (Molecular Devices). Interneuron firing patterns were studied in current-clamp configuration using current steps of 1 s duration, which ranged from −200 to +200 pA with 50 pA increments. For paired

recordings, pyramidal cells were selected in the pyramidal layer of the hippocampal CA1 region and were recorded in whole-cell voltage-clamp configuration (holding potential was set to –70 mV) with internal solution containing the following (in mM): 40 CsCl, 90 K-gluconate, 1.8 NaCl, 1.7 $MgCl_2$, 3.5 KCl, 0.05 EGTA, 10 HEPES, 2 Mg-ATP, 0.4 Na_2-GTP, 10 phosphocreatine; pH 7.2; 290 mOsm/kg). In a set of experiments, *post-hoc* visualization of pyramidal cells was required for detailed investigation of synaptic connection between the cell pairs. Therefore, in sequential-paired experiments, in variance-mean experiments and in correlated electrophysiological and super-resolution imaging experiments the postsynaptic internal solution also contained 1 mg/ml Cascade Blue hydrazide, trisodium salt (Molecular probes, Oregon, USA). Throughout paired recordings series resistances were carefully monitored, and recordings were discarded if the series resistance changed ≥ 20% or reached 25 MΩ. Action potentials in presynaptic interneurons were elicited in current-clamp mode by injecting 2 ms long 2 nA square pulses at 10 Hz frequency. Trains of 50 action potentials were evoked once in every minute and effective unitary inhibitory postsynaptic current (IPSC; average amplitudes include both successful events and failures) were monitored together with the number of successful events (Successes). Coefficient of variation (CV) for postsynaptic responses were calculated from the standard deviation of IPSC amplitudes after noise subtraction (3-3 minutes in control conditions and in the presence of the applied drug, when present) divided by the mean IPSC amplitude. Depolarization-induced suppression of inhibition (DSI) was induced by using a 1 s long depolarization pulse on the pyramidal cell from –70 mV to 0 mV. IPSCs were then compared between the pre-DSI period (2.5 s before DSI induction) and the post-DSI period (2.5 s after the end of the depolarization step). In case of sequential recording of multiple postsynaptic cells, the experimental procedure was similar to the paired recording protocol. After successfully finding a pyramidal cell which was synaptically connected to the interneuron, baseline values of synaptic transmission were recorded. After 10 - 15 minutes of recording the capillary was carefully removed from the pyramidal cell and recordings were repeated with a subsequent postsynaptic cell. Analysis of baseline electrophysiological properties of interneurons was conducted from data recorded in whole-cell current-clamp configuration. Resting membrane potential (RMP) was determined with zero holding current. Membrane input resistance (R_{in}) was measured using multiple current steps (from -200 to +200 pA at a

duration of 1 s). Action potential amplitude was calculated as the amplitude difference between the threshold of AP initiation and the peak of the AP. The magnitude of afterhyperpolarization (AHP) was also calculated from the inflexion point of AP initiation. AP width (full-width at half- maximal amplitude, FWHM) was measured at half-maximal AP amplitude. In order to measurement "sag" peak amplitude, membrane potential responses were analyzed at two time points: 60 ms after the start, and 60 ms before the end of a 1 s long -200 pA hyperpolarizing square current step and were derived from the difference between the two values. Rebound values were quantified as the difference in baseline membrane potential levels before and after hyperpolarizing and depolarizing current steps. Frequency adaptation ratio was determined as the ratio of appearing single APs during the first and last 200 ms of a 1 s long +200 pA depolarizing current step.

In pharmacological experiments, AM251 [(N-(piperidin-1-yl)-5-(4-iodophenyl)-1-(2,4-dichlorophenyl)-4-methyl1H-pyrazole-3-carboxamide)] (Tocris Bioscience, Bristol, UK, Cat# 1117) was used as a CB_1R antagonist/inverse-agonist, to block CB_1R activity. To examine acute drug effects bath ACSF was changed to drug-ACSF solution (containing 10 μM AM251) after the baseline was recorded for at least 5-10 minutes. To study the effect of MAGL blockade on synaptic transmission bath application of the MAGL inhibitor JZL184 [(4-nitrophenyl 4-[bis(1,3-benzodioxol-5-yl)(hydroxy) methyl]piperidine-1-carboxylate)] (Tocris Bioscience, Bristol, UK, Cat# 3836) was used. In these experiments, brain slices were incubated in a drug-ACSF solution (containing 100 nM JZL184) for 40 minutes before recording. In each experiment drug equivalent dimethyl sulfoxide (DMSO) concentration was used as a vehicle control. Acute drug effects were quantified by averaging the postsynaptic responses to three series of 50 induced action potential trials before and 10 minutes after the start of drug application. In non-acute experiments baseline values were compared between vehicle control DMSO and drug incubated samples.

Variance-mean analysis experiments were performed and interpreted using a simple binomial model (Clements and Silver, 2000). Briefly, 15 action potentials were evoked in the presynaptic cell with 0.3 Hz frequency in every 2 minutes and postsynaptic potentials were measured at the pyramidal cell soma. In order to block CB_1R activation 1 μM AM251 was included in all bathing ACSF solutions (except during baseline

recordings). After measuring baseline transmission properties on a cell pair, extracellular levels of Ca^{2+} and Mg^{2+} were changed to alter release probability (Pr) conditions. A minimum of 45 traces were required in each epoch of different Pr conditions to include a cell in the analysis. The stability of peak amplitudes in time throughout an epoch was determined by fitting a regression line to the scatter plot of IPSC amplitudes versus time. The mean Rs for the first analyzed epochs during the recordings was 18.7 ± 2.3 MΩ. Due to longer recording times (40-90 minutes), if the Rs changed >45% the recording was discarded. All recordings were rejected when the Rs became >25 MΩ. From the total of 5 Pr conditions per recording, stable data collection from at least 4 conditions were required to include a pair in the analysis. Control measurements without altering extracellular Ca^{2+} and Mg^{2+} concentrations were also conducted in parallel for similar length, to test potential time-induced changes. Comparing traces, obtained during the first and the last 10 minutes of these experiments revealed no significant change neither in variance nor in mean amplitudes (n = 3 experiments). The peak amplitudes of the IPSCs and the successes were measured in a 3 ms time window after the peak of presynaptic action potential and the mean amplitude of postsynaptic responses (I) and the variances (σ^2) were calculated. Background variance (σ^2_{noise}) was measured 5 ms before the onset of the averaged postsynaptic response and was subtracted. Quantal parameters, such as quantal size (Q) and number of functional release sites (Nf) were estimated from a parabolic function fit on the variance – mean amplitude plot: $\sigma^2 = QI - I^2/Nf$, where Q can be estimated from the initial slope and NfQ can be estimated from the larger X intercept of the parabola. Pr was then calculated from the mean current using the following equation: $Pr = I/NfQ$.

After each electrophysiological recording, the sections were transferred into 4% Paraformaldehyde (PFA, TAAB Ltd., Aldermaston, UK) in 0.1 M Phosphate Buffer (PB, pH 7.4), and fixed for 24 hours at 4 °C. After fixation, slices were stored in 0.1 M PB containing 0.05% Na-azide until further use.

3.5. Liquid chromatography, tandem mass spectrometry

Acute hippocampal slices were prepared and treated as described before for electrophysiological experiments. Animals were housed, and brain slices were prepared in the same manner and at the same time of the day, to reduce biological variability in endocannabinoid levels. After the 1h regenerating incubation in sucrose-ACSF,

hippocampal sections were transferred to treatment chambers at room temperature, containing oxygenated ACSF supplemented with 100 nM JZL184 or DMSO. In each chamber five 300 µm thick dorsal and ventral hippocampal sections of an individual animal were treated for 40 minutes. To further reduce potential variability slices were collected in an alternate manner from the left and right hemispheres and were pooled into a single measured sample after pharmacological treatment. Thus, endocannabinoid levels were always compared between two hippocampal tissue samples derived from an individual animal, with the tissue being treated by either an enzyme inhibitor or its corresponding vehicle control. After pharmacological treatment, the hippocampal samples were frozen in liquid nitrogen and stored at –70°C until the measurement of endocannabinoid levels by liquid chromatography tandem mass spectrometry (LC-MS/MS).

Sample preparation for chromatography started with tissue incubation on ice for 30 minutes in 1 ml of methanol (HPLC-grade, Merck, Darmstadt, Germany) containing the deuterated internal standards 2-arachidonoyl-glycerol-d5 (100 ng/ml; Cayman Chemicals) and arachidonoyl-ethanolamide-d4 (1 ng/ml, Cayman Chemicals). After ultrasonic homogenization, samples were centrifuged on an Eppendorf miniSpin microtube centrifuge at 13,400 rpm for 15 minutes. The supernatant was transferred into a plastic tube and was diluted with 3ml of ultrapure water. The samples were subjected to solid-phase extraction (SPE) sample clean-up according to the following protocol. First, the SPE cartridges (SUPELCO Discovery DSC-18 1 ml tubes, 100 mg, Sigma-Aldrich) were conditioned with 2 ml of methanol and 2 ml of ultrapure water. Diluted samples were loaded onto the SPE columns (~0.5 ml/min flow rate) and consecutive washing steps were carried out by percolating 2 ml of ultrapure water and 2 ml of methanol/water (50:50 v/v%) through the sorbent material. Elution was performed with 0.7 ml of methanol. Eluates were diluted to initial HPLC eluent composition with 10 mM ammonium formate solution (Riedel-de Haën, Seelze, Germany).

To measure endocannabinoid levels, we used a PerkinElmer Life and Analytical Sciences HPLC Series 200 system (PerkinElmer, Waltham, MA, USA), which was coupled to an Applied Biosystems/Sciex 4000 QTRAP triple quadrupole/linear ion trap tandem mass spectrometer (Applied Biosystems, Foster City, CA, USA) operated in positive electrospray ionization mode. The ESI+ ion source parameters were set as follows:

curtain gas: 10; ionspray voltage: 5000 V; temperature: 500°C; collisionally activated dissociation (CAD) gas: medium; gas-1: 50; gas-2: 40. Chromatographic separation was achieved with a Phenomenex Kinetex C18 column (50 mm x 3.00 mm, 2.6 µm, 100 Å, Phenomenex, Torrance, CA, USA) using methanol and 10 mM ammonium formate as elution solvents at a flow rate of 500 µL/min. The injection volume was 50 µl. The initial eluent condition was 80% methanol – 20% buffer that was increased to 85% organic phase for 3 minutes and then further elevated to 95% during 2 minutes and was kept at this condition for 2 minutes. Afterwards, the column was equilibrated to the initial condition. Analytes were detected in multiple reaction monitoring (MRM) mode at the following ion transitions and parameter settings: (1) 2-AG, MRM transition [mass/charge ratio (m/z) 379.4→287.2, m/z 379.4→91.1], declustering potential (81 V), collision energy (23 V, 81 V), cell exit potential (10 V, 8 V); (2) 2-arachidonoylglycerol-d5, MRM transition (m/z 384.4→287.2, 384.4→91.1), declustering potential (81 V), collision energy (23 V, 81 V), cell exit potential (10 V, 8 V); (3) arachidonoylethanolamide, MRM transition (m/z 348.4→62.1, 348.4→90.9), declustering potential (51 V), collision energy (43 V, 63 V), cell exit potential (4 V, 8 V); and (4) arachidonoylethanolamide-d4, MRM transition (m/z 352.4→66.0, 352.4→91.2), declustering potential (81 V), collision energy (41 V, 77 V), cell exit potential (6 V). The peak areas were determined with Analyst 1.4.2. software. The quantity of the analytes was calculated by comparing their peak areas with those of the deuterated internal standards and normalized to the sample weight.

3.6. Immunolabeling

Fluorescent immunolabeling was used throughout the study to visualize single- or multiple labeled individual cells and protein distributions in brain slices. All samples were stained in a free-floating manner in 24-well tissue culture plates (Greiner Bio-One, Mosonmagyaróvár, Hungary) in 500 µl volume on an orbital shaker (Biosan, Riga, Latvia). Protocols were fine-tuned to each experiment to provide the best quality of labeling compared to the individual antibodies and utilized methods.

After electrophysiological recordings single-labeled interneuron-containing 300 µm-thick slices were washed three times in 0.1 M PB for 10 minutes and treated with 0.5% Triton-X100 in 0.1 M PB together with 10% normal donkey serum (NDS) in 0.1 M PB for 30 minutes for permeabilization and blocking of non-specific sites. Slices were incubated with streptavidin conjugated to DyLight-488 (Table 2) for 2 hours to visualize

biocytin. After washing the slices three times with 0.1 M PB for 10 minutes, samples were mounted on glass slides in Vectashield (H-1000, Vector Laboratories, Burlingame, CA, USA), coverslipped, and sealed with nail polish.

In order to visualize pyramidal cells labeled with Cascade blue along with biocytin filled interneurons, 300 μm-thick slices were washed (3 × 10 minutes in 0.1 M PB) and blocked with 10% NDS in 0.1 M PB for 30 minutes. Then, samples were incubated with a mixture of 0.5% Triton X-100, 2% NDS and anti-Cascade blue antibody (Table 1) in 0.1 M PB, which was previously incubated with one leftover non-used slice for 1 day at 4°C, to reduce background staining. After 48 hours of incubation in primary antibody at 4°C, brain slices were washed (3 × 10 minutes in 0.1 M PB) and treated with a solution containing 2% NDS and fluorescent secondary antibodies (Table 2) for 2 hours at room temperature. Slices were washed in 0.1 M PB for 3-times for 10 minutes, and were mounted on glass slides in Vectashield, coverslipped, and sealed with nail polish.

After confocal imaging of cellular morphology, 300 μm-thick sections were first returned to PB and then embedded in 2% agarose in distilled water for resectioning. 10 - 20 μm-thick sections were cut with a Leica VT-1000S Vibratome in 0.1 M PB. Wells were pre-blocked with 5% NDS in 0.1 M PB or with 1% Bovine Serum Albumin (BSA) in 0.05 M Tris-buffered Saline (TBS, pH=7.4) to prevent the slices from sticking to the walls. After extensive washing (3 × 10 minutes in 0.1 M PB and 3 × 15 mins in 0.05 M TBS), slices were treated with a solution containing 5% NDS and 0.1% Triton X-100 in TBS for 45 minutes to further enhance antibody penetration. Then samples were incubated in the TBS-solution of the primary antibodies overnight at room temperature (Table 1). On the following day samples were thoroughly washed (3 × 15 minutes in 0.05 M TBS) and incubated in the TBS-solution of the fluorescently labeled secondary antibodies (Table 2) for 4 hours. Finally, samples were washed in TBS and PB, and mounted in Vectashield for confocal imaging and sealed with nail polish.

Table 1. Primary antibodies utilized in the study

Antigen	Host species	Dilution	Catalogue number or reference
Bassoon	Mouse	1:2000	Ab82958, Abcam (Cambridge, UK)
AF-405/Cascade Blue	Rabbit	1:1000	A-5760, Thermo Fisher Scientific (Waltham, USA)
CB_1*	Guinea pig	1:2000	Gift of M. Watanabe (Hokkaido, Japan) (Fukudome et al., 2004)
CB_1	Rabbit	1:2000	IMG-pAB001, ImmunoGenes (Budapest, Hungary)
NECAB1	Rabbit	1:300	HPA023629, Atlas Antibodies (Bromma, Sweden)
NECAB2	Rabbit	1:500	HPA013998, Atlas Antibodies
Parvalbumin	Goat	1:4000	PVG-214, Swant (Marly, Switzerland)

* Primary antibody used only in the variance-mean experiments.

Table 2. Fluorescent secondary antibodies utilized in the study

Target species	Host species	Dilution	Catalogue number
- (anti-biotin DyLight-488)	- (Streptavidin)	1:1000	016-540-084, Jackson ImmunoResearch (West Grove, USA)
anti-goat AF-647	Donkey	1:400	705-605-147, Jackson
anti-guinea pig CF-568*	Donkey	1:1000	20377, Biotium (Fremont, USA)
anti-mouse AF-647	Donkey	1:400	715-005-150, Jackson
anti-rabbit AF-597	Goat	1:400	711-585-152, Jackson
anti-rabbit AF-647	Donkey	1:400	711-605-152, Jackson
anti-rabbit Cy3 + AF-647#	Donkey	2 μg/ml	711-005-152, Jackson
anti-rabbit DyLight-405	Donkey	1:200	711-475-152, Jackson

* Secondary antibody used only in the Variance-mean experiments. # Secondary antibody used only in STORM experiments.

A subset of resectioned slices were immunostained for Stochastic optical reconstruction microscopy (STORM) imaging of CB_1 receptors, to assess receptor density and receptor numbers at axon terminals of biocytin filled interneurons. The staining protocol was as described above, however an activator-reporter STORM secondary immunolabel was used (Table 2). For detailed description see: (Barna et al., 2016). Samples were incubated for 4 hours with the prepared Cy3 + AF-647 STROM-secondary antibody in 0.05 M TBS to enable super-resolution acquisition of CB_1 receptors. After thorough washing in TBS and PB, STORM samples were mounted and dried on coverslips. Before imaging, samples were covered with 25 µl of freshly prepared imaging medium containing 5% glucose, 0.1 M mercaptoethylamine, 1 mg/ml glucose oxidase, and catalase (2.5 µl/ml of aqueous solution from Sigma, approximately 1500 U/ml final concentration) in Dulbecco's Phosphate buffered saline (PBS) and sealed with nail polish.

3.7. Confocal microscopy

To assess interneuron morphology, 20x-magnification z-stacks (with 1 µm step size in z direction) and maximal intensity z-projections of recorded cells were collected from 300 µm-thick sections on a Nikon A1R confocal scan head coupled to a Nikon Ti-E inverted microscope (Nikon Instruments, Japan) using a CFI Plan Apo VC 20x objective (NA: 0.75 NA). In order to visually identify close anatomical appositions of those paired recordings in which the pyramidal cells were also labeled, 60x-magnification objectives were used (CFI Plan Apo VC 60X Oil; NA: 1.4) together with appropriate Nyquist-sampling (pixel size = 0.14 µm/px, z-step = 0.125 µm) to capture high-resolution z-stacks. The same microscope and objectives were used to obtain high-resolution z-stacks of fluorescent immunostainings in hippocampus.

3.8. STORM sample preparation and imaging

Sections were stained (see Immunolabeling) and mounted on borosilicate glass coverslips and imaged (see Confocal microscopy) following a previously described protocol (Barna et al., 2016). Confocal images of Cascade Blue, biocytin, bassoon and CB_1R, and STORM images of CB_1R, were captured on a Nikon N-STORM system. Biocytin-filled boutons impinging on Cascade Blue-filled postsynaptic targets, identified during previous steps, were located in widefield mode. In confocal mode, z-stacks of 15 sections, with 150 nm step size were captured. Then, in STORM mode, z-stacks of 7 3D-STORM movies, 1000 cycles each, were captured using an interleaved sampling strategy,

centered on the middle section of the confocal z-stack (reference plane). That is, 4 movies were captured with increasing distance from the coverslip, and then 3 movies were captured in between the planes of the first 4 movies. The N-STORM z-stack module was used to control TIRF angle and z-position using the optical 'perfect focus system' for each step. This recording strategy allowed highly homogenous sampling of the volume over 1000 nm thickness, as determined from inspecting the histograms of z coordinates in assembled STORM z-stack datasets (see below). Before setting the STORM acquisition range, confocal z-stacks of the bouton were inspected to ensure that the bouton is included in the recorded volume and the volume is centered (±150 nm) on the largest bassoon cluster inside the bouton, and the reference plane was adjusted as necessary. In case of multiple boutons in a section, images were captured in an order that prevented bleaching of the additional boutons, by using a rectangular field stop set tightly around the center of the imaged field of view and progressing through boutons in a direction opposite to the angle of the oblique TIRF illumination. In cases where multiple boutons were too close to be recorded in consecutive STORM z-stacks, the pair was excluded from further analysis.

Boutons from WT and CB_1R HET mice were imaged similarly as described above, with the exception that multiple CB_1R-positive boutons, selected in widefield mode at random, were imaged from each section. Boutons in the str. pyramidale, located at ~1500 nm from the coverslip, were selected, and the field of view was centered on the selected bouton. Additional inclusion criteria were applied after inspecting the confocal z-stack: no contact with neighboring CB_1R-positive boutons (to avoid the ambiguity of detecting bouton surface), and at least one bassoon cluster within the bouton visible on the confocal image. Then, correlated confocal and 3D-STORM z stacks were recorded as described above. In the case of imaging boutons from THC- and vehicle-treated mice 3D STORM images were taken only from a single plane in the CA3 region of the hippocampus. In those experiments, the z coordinates were filtered to a 600 nm wide range (+/- 300 nm from the focal plane) to match the extent of the middle 3 confocal slices of the stack that were used for thresholding the bassoon channel.

3.9. STORM data processing and analysis

Confocal volume images were deconvolved using Huygens (SVI) using theoretical PSF and the CMLE algorithm with default settings. STORM image molecule

localization was performed separately on each movie of the z-stacks, using NIS Elements N-STORM (Nikon), including corrections for spherical and chromatic aberration and sample drift, and fitting z positions based on a calibration curve (Barna et al., 2016). Because NIS Elements returns z coordinates as distance from the coverslip, to align volumetric 3D-STORM and confocal data, it is necessary to transform z coordinates to distance from the reference plane, i.e., the initial focal plane and the center plane of the confocal stack. The molecule lists from the 7 (partially overlapping) STORM imaging planes were merged, and the z coordinates of localization points (LPs) were clustered into 7 clusters using k-means. The mean of the resulting 7 centroids was used as the reference z position. The centroids and the mean were plotted against the z histogram of the merged molecule list and inspected for each file to exclude any STORM z-stacks with anomalous coordinate distribution. Finally, the reference z position was subtracted from all z coordinate values.

For each imaged bouton, the confocal and STORM images of CB_1R were first aligned manually, and CB_1R LPs belonging to the bouton were selected in 2D using VividSTORM (Barna et al., 2016). The selected molecule list and the values of the x-y offsets for fitting the confocal and STORM datasets were saved, and all following steps were carried out using custom Python scripts. Next, the overlaid confocal and STORM volumes were plotted in three orthogonal maximum intensity projections, and the selection was further refined to exclude LPs located below or above the bouton. Then, the bassoon channel of the confocal z-stack was converted to a list of positive voxel coordinates. The stack was binarized using one third of the Otsu threshold of a region centered on the bouton (128 by 128 pixels), and positive voxels inside the bouton were selected in 3D on the orthogonal views. The included bassoon confocal voxels were density-filtered using DBSCAN (minimum 3 neighbors within 200 nm). Finally, a 3D convex hull was fit on density-filtered (DBSCAN, 3 neighbors within 100 nm) CB_1R LPs (Barna et al., 2016), and the distance of each CB_1R LP from the convex hull and the nearest bassoon voxel was measured. CB_1R/bassoon ratios in either cumulative or non-overlapping distance bins were measured using the pre-processed CB_1R STORM molecule lists and confocal bassoon voxel lists. For consistency between analyses, 200 nm perisynaptic threshold distance was used for plotting Figures 16, 17 and 18. Importantly, however, the results of statistical analysis did not critically depend on the

choice of distance threshold between 100-200 nm. Despite the nanoscale localization accuracy of CB_1Rs, due to the localization uncertainty of bassoon-positive active zones determined from confocal imaging (60 nm lateral and 150 nm axial voxel size) on one hand, and the lack of information on the exact distance-dependence of CB_1R downstream signaling on the other, setting a lower perisynaptic distance threshold is not expected to further improve the accuracy of the analysis. For determining correlations with Pr, we used the following formula, assuming 3 release sites per boutons with a single confocal bassoon cluster: Pr = 1 - (1 - s) ^ (1 / (n * 3)), where 's' is the ratio of successes over all trials, and 'n' is the number of boutons in the connection.

3.10. Cell-type identification

Perisomatically targeting interneurons (CB_1BCs) were separated from dendritic targeting interneurons (dendritic cells) based on their axonal arborization: the laminar distribution of boutons within the different hippocampal layers was quantified as a bouton distribution index (BDI) (see detailed method in: Dudok et al., 2015). Briefly, axon terminals of the interneuron were identified in the maximal intensity z-projections (using ImageJ software). After specifying the pyramidal layer, the relative distance of each bouton from this layer was measured and the overall values were expressed as a bouton distribution index (BDI). High BDI (>1) means that the boutons of the cell mainly accumulated in the pyramidal layer. When the BDI value was <0.5, the cells were classified as dendritically-targeting. Cells with intermediate BDI value (between 0.5 and 1) were excluded from the study. Based on these BDI criteria, 9% of the cells were excluded and 21% of the cells were classified as dendritically-targeting ones, which were not analyzed here. This feature of the cells together with their electrophysiological characteristics and immunohistochemical expression patterns of specific proteins were used for unequivocal identification of CB_1BCs.

3.11. Western blot experiments

25-30 days-old male CB_1R wild-type (WT), heterozygous (HET) and knockout (KO) mice were euthanized by cervical dislocation and decapitated. 3 mice were used for each genotype. After sectioning, 300 μm thick slices containing hippocampi were collected. From these slices, 3 pairs of hippocampi (including the cortex) were isolated for further experiments during constant cooling with dry ice. Then the tissue was homogenized in homogenization buffer (HB: 10 mM HEPES, 10 mM KCl, 1 mM MgCl2,

1 mM DTT, 1 Roche complete protease inhibitor pill/10 ml). After spinning at 3500 rpm for 5 minutes at 4 ˚C, the pellets were discarded as the nuclear fraction. The supernatants were collected and span at 15000 rpm for 1 hour at 4 ˚C, then the new supernatants were gathered as cytoplasmic and the pellets as membrane fractions. The pellets were resuspended in 150 µl HB, then 1% (v/v) Triton X-100 was added to both the cytoplasmic and membrane fractions. The samples were vortexed and left on ice for 30 minutes, then span at 15000 rpm for 10 minutes at 4°C. The fractions were aliquoted and the concentrations were analyzed by Coomassie Plus protein assay reagent (Thermo). 40 µg purified membrane protein were denaturated with 4x Laemmli Sample Buffer (Bio-Rad) for 10 minutes at 37˚ C. Samples were run on 13.5% polyacrylamide gel at 60 V for 30 min, then at 200 V for 2 hours at 4˚ C and transferred onto nitrocellulose membranes (Bio-Rad) at 300 mA for 2 hours at 4 ˚C. The transfer was verified with Ponceau S stain (Amresco) and the membranes were washed twice with Tris Buffered Saline containing 0.05% Tween-20 (TBST), then blocked with 5% skimmed milk powder (TUTTI Élelmiszeripari Kft.) in TBST for 1 hour at room temperature. After the membranes were washed twice in TBST, the blots were incubated in primary antibodies (rabbit polyclonal CB1R antibody, 1/4000 diluted in blocking solution overnight at 4˚ C. Then the membranes were washed twice in TBST and incubated in HRP-linked anti-rabbit secondary antibody solution (Cell Signaling, 1/1000) for 1 hour at room temperature. The blots were washed twice with TBST and Tris Buffer (TB), then incubated in enhanced chemiluminescent substrate solution (Thermo Scientific SuperSignal West Dura Extended Duration Substrate) according to the manufacturer's instructions. The luminescence was imaged with Chemi Genius 2 Bio Imaging System (Syngene). The blot was then reexposed with another antibody, mouse Na^+/K^+-ATPase (Merck Millipore, 1/4000) and the incubation steps were repeated with HRP-linked anti-mouse secondary antibody solution (Cell Signaling, 1/1000). Grey value calculation and western visualization were done using Adobe Photoshop.

3.12. *In vivo* chronic drug treatment of mice

Animals were grouped in a randomized manner and treated either with THC or its vehicle (1% ethanol, 2% Tween 80 and saline) intraperitoneally at a dose of 10 mg/kg (i.p. injection volume of 10 ml/kg) twice a day for 6.5 days. THC (THC-Pharm GmbH, Germany) was dissolved in a solution containing 1% ethanol, 2% Tween 80 and saline.

The chronic treatment regimen with a dose of 10 mg/kg was shown to induce behavioral tolerance in mice (Bass and Martin, 2000; Mckinney et al., 2008). From all the experimental groups, twenty-four hours after the last THC or vehicle injection, mice were anesthetized with isoflurane and acute slices were cut to perform electrophysiological recordings as described above. For the duration of the experiment and analysis samples were processed by experimenters blinded to treatment.

3.13. Quantification, statistical analysis and figure preparation

The obtained data from the different experiments were statistically analyzed using Prism 10 (GraphPad Software, San Diego, CA, USA). Sample sizes were estimated based on previous experience and are similar to those generally applied in the field. Normality of the data was checked by Shapiro–Wilk test or Kolmogorov–Smirnov normality test (depending on sample numbers). If data showed normal distribution, paired or unpaired t-test was used for analysis, when the data did not show normal distribution, nonparametric Wilcoxon's signed-rank or Mann–Whitney U tests were used for paired and unpaired data, respectively. Data was analyzed via two-way ANOVA with repeated measures at electrophysiological experiments where pharmacological treatment of samples derived from multiple genotypes were studied. Statistical tests among groups in western blot experiments were performed with one-way ANOVA with Dunnett`s multiple comparisons test. Data are presented as mean ± standard error of the mean (SEM), unless otherwise mentioned. Throughout the study, differences were considered statistically significant when: $p \leq 0.05$ (*), $p \leq 0.01$ (**), $p \leq 0.001$ (***). In case of calcium imaging measurements where one experiment consisted of 25 boutons per cell, boutons from different animals were pooled if there was no significant difference between the baseline values of animals or cells of any group (Kruskal–Wallis test, $p > 0.05$).

Graphs were generated using GraphPad Prism-10 software (San Diego, CA, USA). Neurolucida software (MBF Bioscience, Delft, The Netherlands) was used to create reconstructions from individually labeled cells. For figure preparation Adobe Photoshop and Illustrator (Adobe Inc., San Jose, CA, USA) were used, where all images were treated in the same manner for all groups or genotypes.

3.14. Personal contribution to the results

Multiple scientists from various laboratories contributed to the results presented in this study, mainly my colleagues from the Laboratory of Molecular Neurobiology (Institute of Experimental Medicine, Budapest, Hungary) and from the Laboratory of Addiction and Neuroplasticity (Indiana University, Bloomington, Indiana, USA).

My own contribution was to perform the majority of the electrophysiological experiments presented (including slice preparations, single cell, paired- and sequential paired recordings with variance-mean recordings). I also analyzed the subsequent data, performed statistical analysis and interpreted the results. Kata Kenesei and Marco Ledri also contributed to the paired recordings on samples from CB_1R WT, KO and DAGLα WT, KO mice. Single cell-labeling for NECAB1-2 protein immunostainings were carried out together with Kata Kenesei and Máté Kisfali. Major part of the immunostaining was done by Vivien Miczán together with Miklós Zöldi and me. Confocal imaging of filled neurons and identification of synaptic connections between pairs was done by Vivien Miczán and me. Endocannabinoid lipid measurements were performed by Kata Kenesei and Blanka Tóth (from Budapest University of Technology, Budapest, Hungary). Correlated confocal and STORM microscopy was performed by Barna Dudok, Miklós Zöldi and László Barna, who also analyzed subsequent data. Chronic drug treatment of mice was done by Petra Aradi and Claudia Sagheddu (from University of Cagliari, Cagliari, Italy). Western blot experiments were performed by Gyula Balla. I have prepared the samples and acquired electron microscopical images for the Introduction chapter. I have done all Neurolucida reconstructions from cells and have prepared all the figures including the hand-drawn- and vector-based illustrations in the thesis. I have written this thesis. Technical assistance with the experiments was provided by Balázs Pintér, Bence Kókay, Joseph Leffel and Erika Tischler. All experiments were supervised by István Katona.

4. Results

4.1. Properties of CB_1BC – PC perisomatic synapses in the CA1 region

4.1.1. Characterization of CB_1BCs and their synaptic targets

CB_1BCs in an acute brain slice were found under Differential Interference Contrast (DIC) illumination based on the position of the multipolar soma in str. radiatum. Upon detection and successful patching of the cell, electrophysiological parameters were inspected. Hyperpolarizing and depolarizing current steps were injected into the cell to record the membrane potential responses and firing profile. The firing pattern can be used as a footprint to recognize unlabeled cells of interest. Only those cells were included in the analysis that showed accommodating firing pattern upon depolarization, which is typical to CB_1BCs (Figure 5/b). The average input resistance of CB_1BCs was 169.2 ± 3.12 MΩ and the resting membrane potential was -65.3 ± 0.36 mV (n = 123 cells). During the experiments, cells were labeled with biocytin to allow morphological reconstruction and further investigations (Figure 5/a). Besides electrophysiological and morphological parameters, *post-hoc* CB_1R immunostaining was performed to verify cell type.

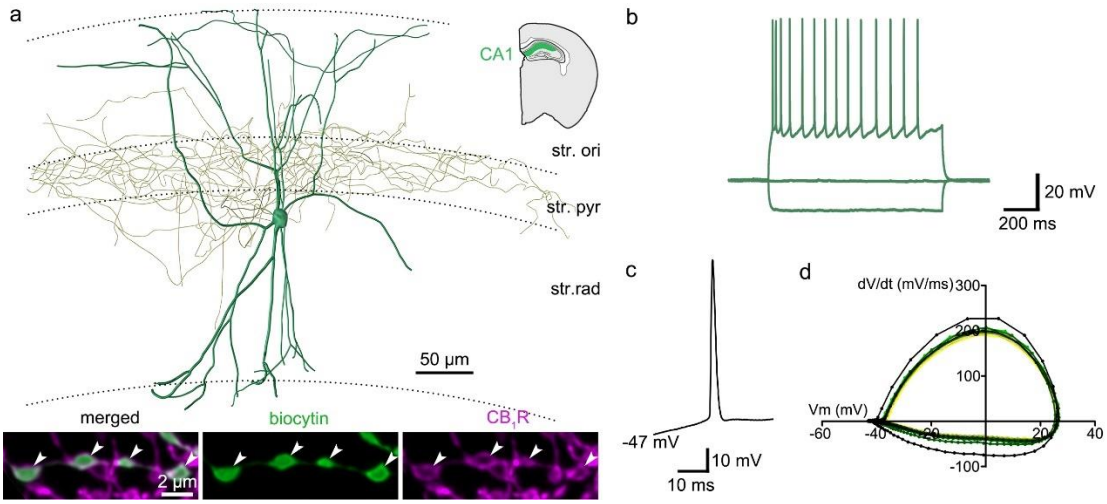

Figure 5. ***Morphological and physiological properties of CB_1BCs.*** **a)** Neurolucida reconstruction of a representative biocytin-labeled CB_1BC. The dens axonal projections are characteristically mainly distributed in the pyramidal layer. *Post-hoc* immunolabeling reveals expression of CB_1Rs on biocytin positive boutons. **b)** Voltage traces in response to indicated -200, 0 and +300 pA hyperpolarizing and depolarizing current steps respectively, from resting membrane potential recorded in whole-cell current-clamp configuration. Accommodating firing pattern is a characteristic physiological property of this cell type. **c)** Shape of a single AP fired by the interneuron. **d)** Phase plot representation of the Aps and their accommodation shown on **b**. APs colored from first to last as progressing colors from darker to lighter tones.

To investigate synapses in a cell-type specific manner, a postsynaptic PC was also patched in the preparation with a second electrode (Figure 6/a). The presence of functional synaptic connections between cells were addressed using injection of brief depolarizing currents into the interneuron to evoke AP generation. Upon successful pairing, postsynaptic responses were detected at the PC soma (Figure 6/b). Evaluation of IPSCs can be instantly used to differentiate CB_1BC – PC synapses from PVBC – PC synapses due to the different electrophysiological properties of the interneurons (see introduction). Moreover, induction of DSI via brief depolarization of the PC can reveal eCB mediated short-term plasticity (Figure 6/c). These electrophysiological properties were checked at the beginning of each recording and were utilized to select CB_1BC – PC cell pairs and differentiate them from dendritically-targeting CB_1R-positive interneuron – PC pairs, that usually produce smaller IPSCs with different kinetics and do not express profound DSI (Lee et al., 2010).

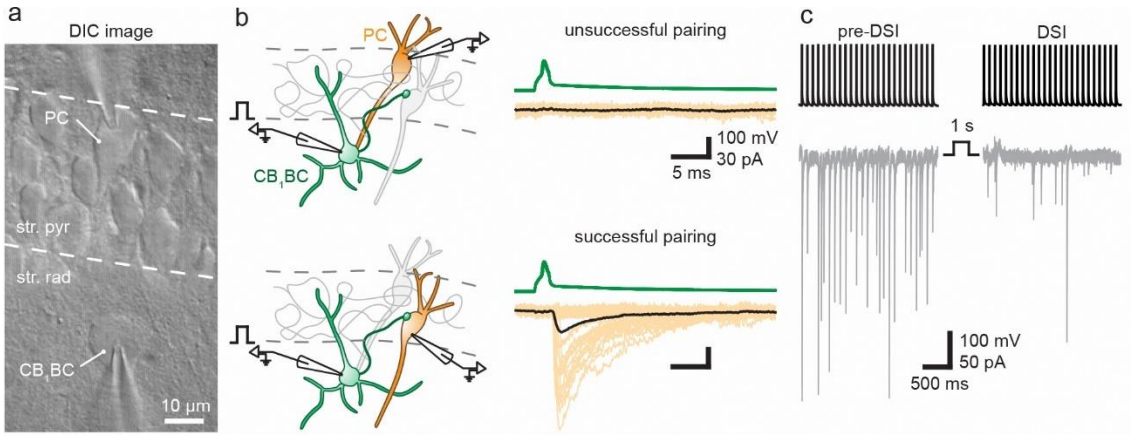

Figure 6. ***Investigation of CB_1BC – PC synaptic connection using paired electrophysiological recordings.*** **a)** DIC image of a patched CB_1BC (bottom) and a PC (top). **b)** Schematic representation of experimental design in two scenarios: the upper case shows an unsuccessful pairing when the patched PC is not innervated by the presynaptic CB_1BC; the lower case shows successful pairing. Representative traces are also presented for each case. Presynaptic APs evoked on CB_1BC (top green traces) and respective postsynaptic responses (bottom traces) recorded on the PC soma. Fifty consecutive unitary inhibitory postsynaptic currents (orange) and their average euIPSC (black) are presented. Note the large variability in the amplitude of detected events in case of successful pairing. **c)** Postsynaptic depolarization of PC (from -70 mV to 0 mV) induces DSI via activation of presynaptic CB_1Rs.

4.1.2. Different subcellular distribution of NECAB1 and NECAB2 calcium-buffering proteins in CB_1BCs

As it was highlighted in the introduction, interneurons are routinely classified and differentiated based on the various Ca^{2+}-buffer proteins that they express. Identification of cell-group specifically expressed proteins can greatly accelerate the experiments that aim to study the network functions of defined cell groups. While cytosolic Ca^{2+}-buffers, such as PV or calbindin have been used as neurochemical markers of GABAergic interneuron types for decades, surprisingly, to date no typifying calcium-binding proteins have been found in CB_1R-positive interneurons. Moreover, while electrophysiological and calcium imaging experiments demonstrated that calcium-binding proteins play important physiological roles in establishing interneuron-specific temporal dynamics (Eggermann and Jonas, 2012), it has remained largely elusive, that how the kinetic properties of Ca^{2+}-signaling determine the activity of CB_1R-positive interneurons (Freund and Katona, 2007).

In order to identify unique molecular markers defining CB_1R-expressing interneurons, we used an *in silico* single-cell mRNA sequencing database (Zeisel et al., 2015). We found that the most frequently used calcium-binding protein marker genes (Calb1 /calbindin, Calb2 /calretinin, Pvalb /parvalbumin, Scgn /secretagogin) were missing from the majority of CB_1-positive cells, however, the expression of N-terminal EF-hand Calcium Binding Protein 1 and 2 genes (Necab1 and Necab2) showed strong correlation with exclusively Cnr1 and Cck gene levels in both the somatosensory cortex and the hippocampus (Miczán et al., 2021).

These observations pose the interesting question of why a single interneuron needs two phylogenetically closely related calcium-binding proteins. In light of the different kinetic properties of boutonal and somatodendritic Ca^{2+}-transients in regular-spiking CB_1R-expressing interneurons in the CA1 area (Kisfali et al., 2013), we tested the hypothesis that the two NECAB proteins bear distinct subcellular compartmentalization and thereby regulate different Ca^{2+}-mediated physiological processes in CB_1BCs.

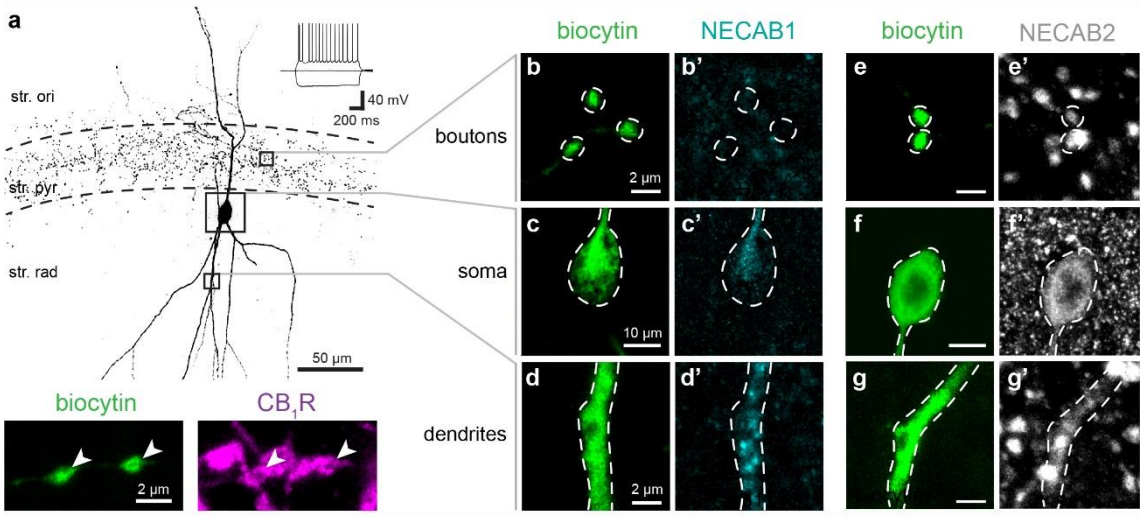

Figure 7. ***Cell compartment-specific identification of NECAB1 and NECAB2 proteins.*** **a)** Example maximum intensity projection confocal image of a single-labeled CB_1BC. Characteristic hyperpolarization and firing pattern of the cell can be seen in the inset as responses to -200 pA, 0 pA and +100 pA current steps. CB_1R expression was verified at the axon terminals of the cell (arrowheads). **b-d')** NECAB1 expression is absent from boutons (**b, b'**), but can be observed in the perisomatic region (**c-c'**) and in dendritic compartments (**d-d'**). **e-g')** NECAB2 immunostaining is present in boutons (**e, e'**), in perisomatic compartments (**f, f'**) and in dendritic processes as well (**g, g'**) in CB_1BCs. (modified from Miczán et al., 2021).

To directly investigate subcellular distribution of the proteins in cellular compartments, individual CB_1BCs were filled with biocytin during electrophysiological measurements in the CA1 region, and the cell morphology was then explored (Figure 7/a). First, we validated the CB_1R expression of the cells via immunostaining of axon terminals (Figure 7/a). Every recorded interneuron (n = 6 CB_1BCs) displayed high CB_1R levels in its axon terminals. Next, we stained the remaining sections for NECAB1 (Figure 7/b-d') or for NECAB2 proteins (Figure 7/e-g'). In the case of the NECAB1-immunostaining, we found that this calcium-binding protein is present throughout interneuron somata and dendrites (Figure 7/c-d'). In contrast, NECAB1 levels remained under the detection threshold of confocal microscopy in the boutons of CB_1BCs (Figure 7/b, b'). On the other hand, NECAB2- immunostaining was highly concentrated in the axon terminals (Figure 7/e, e') and was also found in the cell bodies and dendrites of CB_1BCs (Figure 7/f-g').

Taken together, the subcellular compartment-specific differences between NECAB1 and NECAB2 proteins indicate that these calcium-binding proteins could fulfill multiple functionally different roles in the regulation of Ca^{2+}-signaling dynamics in CB_1BCs. Furthermore, these two NECAB proteins could serve as a novel cell-type identifying markers of CB_1R-positive interneurons.

4.1.3. Target cell-dependent variability of CB_1BC – PC synapses

CB_1BC – PC connections exhibit large variability in terms of synaptic strength measured via the number of putative anatomical connections, the amplitude and the number of successful IPSCs (Figure 8). The average connection number between pairs was 2.7 ± 1.5, although, there were pairs that contained only 1 or 9 close anatomical appositions as well (Figure 8/a). Surprisingly, the number of anatomical connections only showed weak correlation with the IPSC amplitudes and successes (Figure 8/b, c).

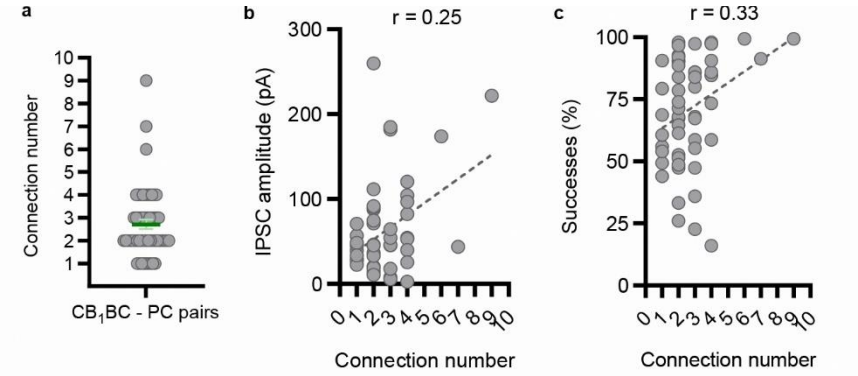

Figure 8. ***Main anatomical and electrophysiological characteristics of CB_1BC – PC pairs.*** **a)** Summary graph shows the number of connections identified between recorded pairs. **b, c)** Correlation between the number of identified anatomical connections and baseline electrophysiological parameters such as IPSC amplitude (**b**) and successes (**c**) at recorded pairs (n = 55 pairs, IPSC: $p_{ns} = 0.06$, successes: *p = 0.01, Spearman's rank-order correlation).

These results arise from the variations of these properties which are profound even when there are similar numbers of connections between cells. At PVBCs, it was shown that interneurons inhibit close and distant target cells differently relative to their position: synaptic strength continuously decreases at connections which are further away from the presynaptic interneuron (Strüber et al., 2015). It is also known that in case of CB_1BCs, the intense variations in transmission levels can be altered and set by the firing history of

the presynaptic interneuron (Földy et al., 2006). To determine whether the synapse-specific fine-tuning of the synaptic weights of CB_1BC synapses is primarily driven by the presynaptic or the postsynaptic neuron, we performed sequential paired whole-cell patch-clamp recordings (Figure 9). In these experiments, for a single presynaptic interneuron multiple postsynaptic PC pairs were investigated. When APs were triggered in a single presynaptic CB_1BC, we observed a wide dynamic range of the amplitudes of IPSCs in the distinct postsynaptic PCs (Figure 9/a, b). The presynaptic interneuron and its postsynaptic PCs were filled with biocytin and Cascade Blue dye, respectively, to perform *post-hoc* reconstruction of cellular and synaptic morphological features (Figure 9/c). All potential synaptic connections from CB_1BCs were validated by immunolabeling for bassoon protein. Out of 40 appositions as putative synaptic connections, 39 contained bassoon concentrated in the side of the axon terminal facing the postsynaptic neuron (Figure 9/d). One single CB_1BC can establish various numbers of synaptic contacts with different postsynaptic targets: certain PC receives one, while its neighbor could have up to 6 synaptic connections (Figure 9/c). Similarly to the previous observations based on individual cell pairs, quantitative analysis confirmed that the large postsynaptic target cell-dependent variability in IPSC amplitudes and in successful synaptic events was not due to the variable number (2.6 ± 0.3) of synaptic connections (Figure 9/e-i). The coefficient of variation (CV) of IPSC peak amplitudes between postsynaptic targets of the same CB_1BC was comparable to all pairs pooled (Figure 9/g) These observations suggest that the efferent synapses of a single CB_1BC exhibit large differences in their synaptic weights in a postsynaptic target cell-dependent manner.

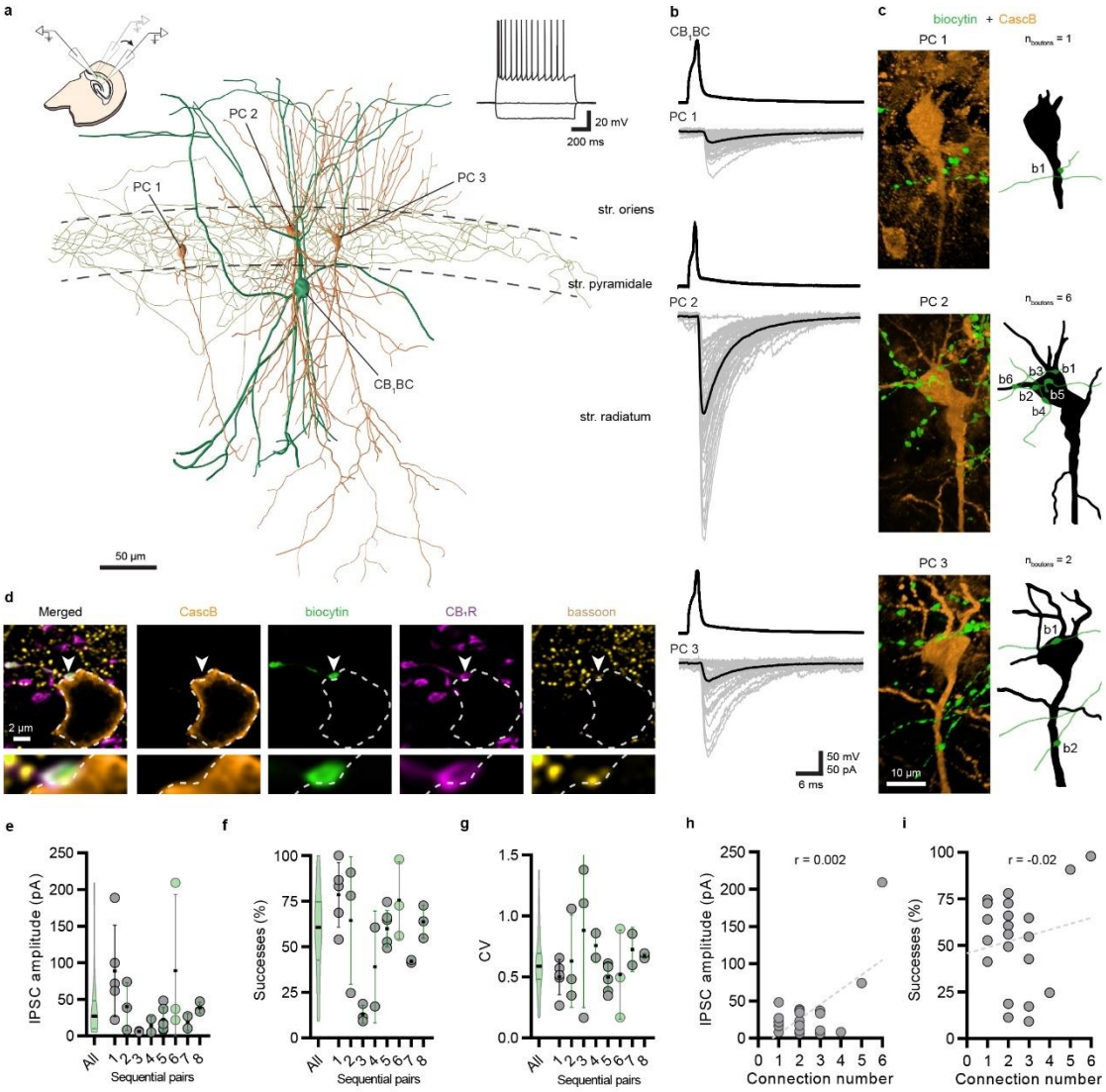

Figure 9. ***Target cell-dependent variability of CB_1BC efferent synapses*** **a)** Schematic illustration of experimental design. Inset traces show firing pattern of CB_1BC in response to -200, 0 and +300 pA current steps. Reconstruction of a CB_1BC (green) that is synaptically coupled to three postsynaptic PCs (orange). **b)** Example traces of patch-clamp recordings from the three pairs. **c)** Confocal 3D maximum intensity projection images and reconstructions of CB_1BC axons and PCs reveal the number and location of perisomatic connections (b1-b6) between pairs. **d)** Confocal images of quadruple staining demonstrate the presence of CB_1R expression in the biocytin-labeled bouton (arrowhead) and show the accumulation of bassoon protein. Bottom insets show enlarged images of the synaptic connection. **e-g)** Summary graphs show large variability in peak IPSC amplitude (**e**), number of successful events (**f**) and coefficient of variation (CV) of IPSCs (**g**) in sequential paired recordings. Green data points depict the representative experiment presented on a-d. Violin plots of pooled data show median ± IQR. Data presented as mean ± SD. **h-i)** The number of synaptic connections between pairs does not correlate with IPSC amplitude (**h**) or successes (**i**) (n = 22 pairs, IPSC amplitude: p_{ns} = 0.99, successes: p_{ns} = 0.91, Spearman's rank-order correlation). (Barti et al., 2024)

4.1.4. Quantal features of CB_1BC – PC synapses

Variations at the level of synaptic transmission can arise as a consequence of multiple factors. Besides cellular morphology and anatomy, intrasynaptic factors can also add to this variance. Therefore, with the next set of experiments we wanted to study the individual synapses and their quantal parameters to assess how they account for this variability. Due to the small and compact size of synaptic active zones, which are under the diffraction limit of light, we utilized electrophysiological methods to determine quantal parameters. As it was discussed in the introduction, synaptic strength is determined by three major factors: Pr, Nf and Q (Del Castillo and Katz, 1954). Amplitude fluctuations in postsynaptic responses from trial-to-trial contain information about these parameters which can be calculated using a method called variance-mean analysis (or multiple probability fluctuation analysis) (Silver, 2003). In these recordings, Pr was continuously modified in a high dynamic range via alteration of extracellular Ca^{2+} and Mg^{2+} concentrations in the ACSF (Figure 10/a). After acquiring a sufficient number of IPSCs, their variance can be calculated for each subsequent Pr condition (Figure 10/d). Fitting a parabolic function to the variance – mean plot generated by this dataset can be utilized to estimate the quantal parameters within cell pairs (Figure 10/e-g). Quantal analysis showed a relatively low baseline Pr value (0.2 ± 0.04) with a quantal size of 45 ± 6.4 (n = 10 pairs). The average number of release sites per pairs determined by the variance-mean analysis was 7.5 ± 1.7, which potentially suggests the presence of multiple release sites even in bouton with a single active zone as shown previously for a wider group of CCK-expressing interneurons in the CA3 region (Biro et al., 2006). In order to also associate anatomical features to the quantal physiological data, both cells were reconstructed and every individual connection between cells were identified (Figure 10/b, c). After identification of the anatomical connection sites between pairs, the average number of release sites within boutons were also calculated, which indeed showed 3.07 ± 0.57 release sites per single bouton (Figure 10/i). Given the relatively low measured Pr and N values, Pr can also be estimated from success values obtained via regular paired recordings in pairs, where there are only 1 or 2 connections present between cells (Figure 10/j).

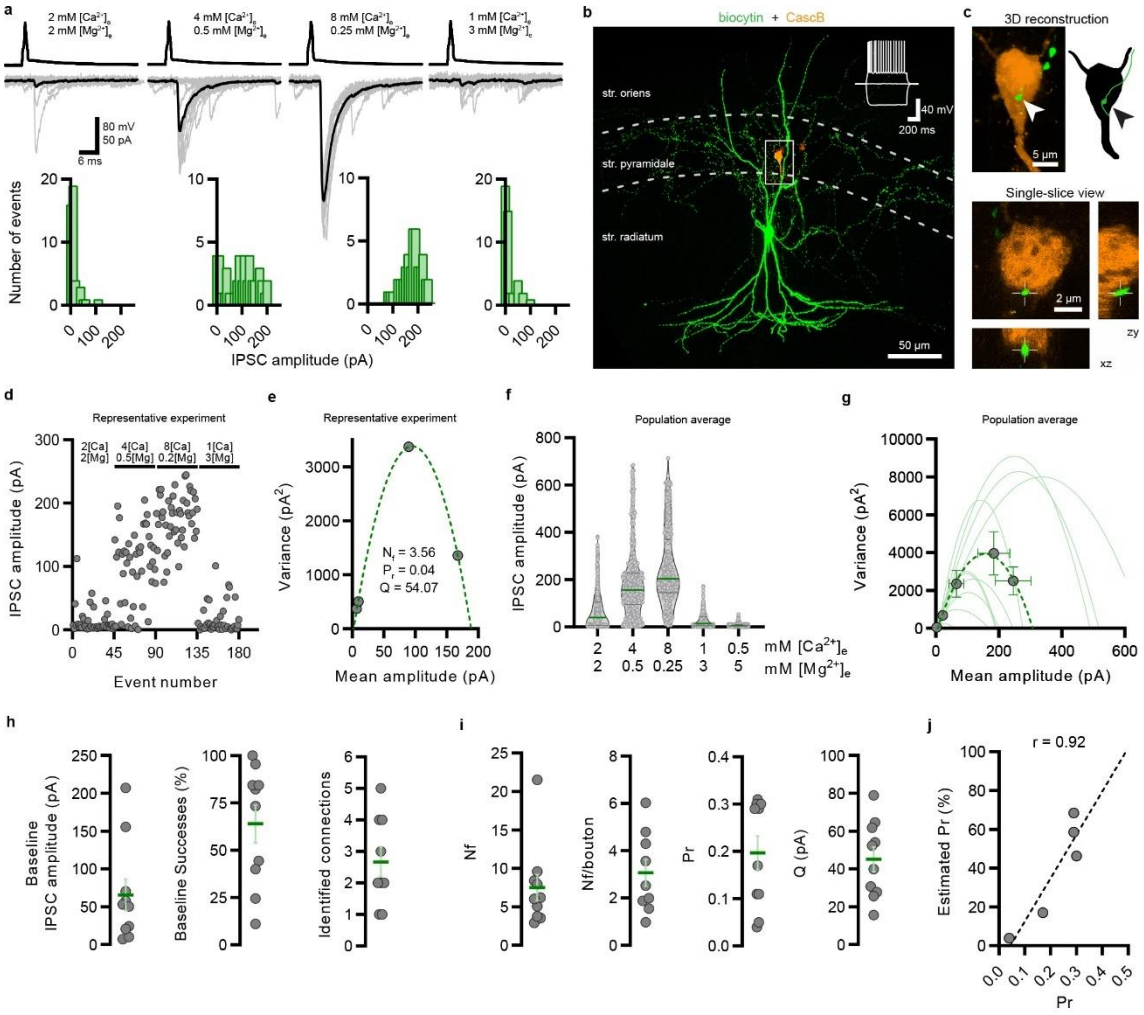

Figure 10. ***Variance-mean analysis determines quantal properties of CB$_1$BC – PC synapses.*** **a)** Example traces of different Pr conditions with histograms showing the distribution of IPSCs at each epoch. **b)** Confocal maximum intensity projection image of the same pair. Inset traces show CB$_1$BC responses to -200, 0 and +100 pA current injections. **c)** High magnification confocal images and reconstructions of boxed region in b. Arrowhead shows single synaptic connection between cells. **d)** Peak IPSC amplitude in analyzed epochs for the representative experiment. **e)** Parabolic function fitted on the variance–mean amplitude plot reveals quantal parameters such as the number of functional release sites (Nf), the baseline release probability (Pr) and quantal size (Q) obtained during the experiment. **f)** Plot of peak IPSC amplitude in analyzed epochs for all measured pairs. Violin plots show median ± IQR values with individual data points. **g)** Summary variance–mean amplitude plot of all experiments (n = 10 pairs). **h)** Main baseline electrophysiological and anatomical parameters of pairs analyzed in variance-mean recordings. **i)** Quantal parameters of CB$_1$BC – PC synapses obtained. Data presented as mean ± SEM with individual values. **j)** Correlation between measured Pr and estimated Pr in variance-mean analysis pairs connected with only 1 (n = 2) or 2 (n = 3) boutons (n = 5 pairs, *p = 0.027, Pearson`s correlation). (Barti et al., 2024)

4.2. Tonic endocannabinoid signaling fine-tunes synaptic transmission

4.2.1. The presynaptic cannabinoid tone is a major factor in synaptic variability

In physiological conditions baseline tonic cannabinoid signaling consistently fine-tunes CB_1BC-PC synapses (Lee et al., 2015; Losonczy et al., 2004; Neu et al., 2007). This retrograde modification of presynaptic Pr can influence synaptic variability. However, pharmacological drugs utilized to study tonic eCB signaling can also have nonspecific off-target effects (Baur et al., 2012; Porcu et al., 2018; Raffa and Ward, 2012), thus direct potentiation of postsynaptic $GABA_A$ receptors or involvement of $GABA_B$ receptors in pharmacological experiments cannot be excluded.

To determine whether tonic suppression of GABA release is solely mediated by CB_1Rs, and to study how this signaling contributes to previously observed synaptic variability, we performed paired whole-cell patch-clamp recordings on acute brain slices between CB_1BC and PC pairs in wild-type (WT) and littermate CB_1R knock-out (KO) mice. CB_1BC morphology and firing pattern were similar between genotypes (Figure 11/a, b). In case of CB_1R KO animals, interneurons were identified as the lack of PV immunostaining in the boutons (Figure 11/b) Bath application of the CB_1R antagonist/inverse agonist AM251 (10 μM) readily increased IPSC amplitudes and successful events in WT, but not in KO mice (Figure 11/c-f). Importantly, both the genetic inactivation and the pharmacological antagonism of CB_1Rs strongly reduced the variability (coefficient of variation, CV) of IPSCs (Figure 11/g). Furthermore, AM251 application did not affect CV values in KO mice (Figure 11/g). Comparing the CV values, we estimated that the CB_1R-dependent synaptic cannabinoid tone is responsible for about one-third of synaptic variability (33.6 ± 10.7%) at perisomatic GABAergic synapses. These results demonstrate that CB_1Rs are solely required for tonic cannabinoid signaling and support a specific site of action for AM251 in this experimental paradigm. Moreover, these experiments provide direct evidence that presynaptic CB_1R activity tonically controls GABA release thereby substantially influencing target cell-dependent synaptic variability.

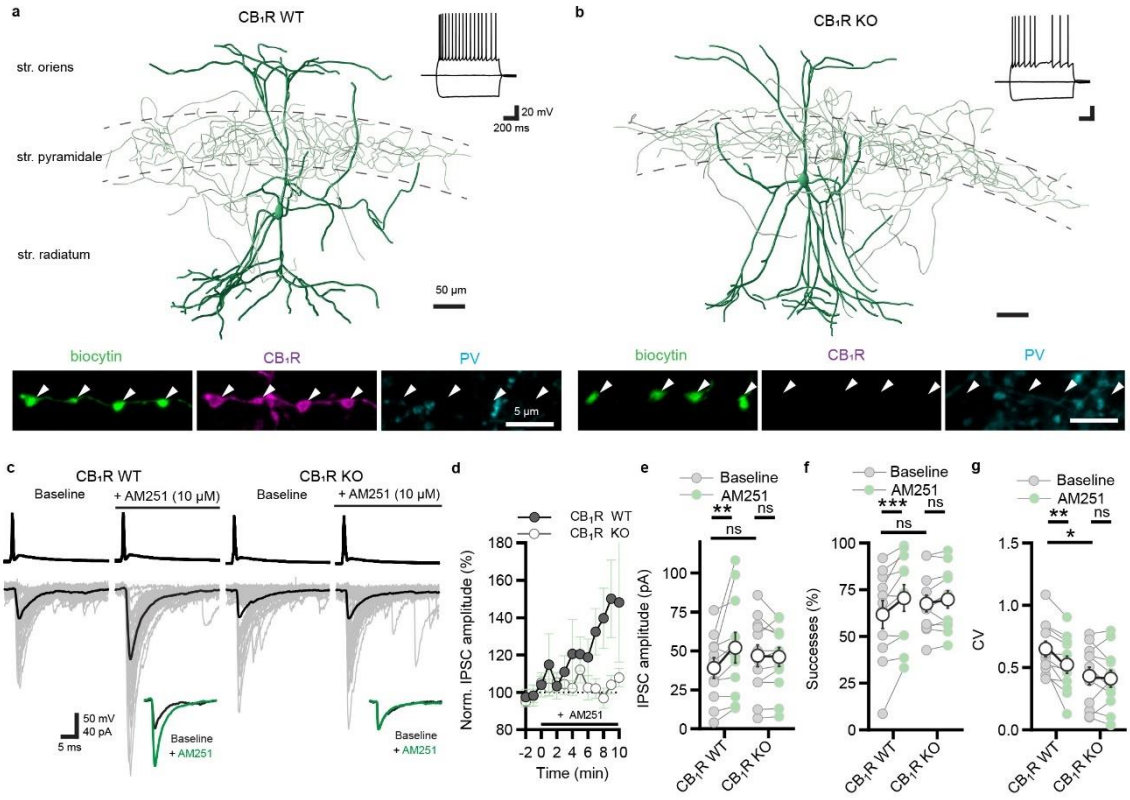

Figure 11. ***Tonic cannabinoid signaling is a major contributor to synaptic variability.*** **a, b)** Morphological reconstruction of CB_1BC recorded from CB_1R WT or KO mice. Inset traces show firing pattern in response to -200 pA, 0 pA, and +150 pA current steps. Both cells axon arbor is largely confined to the str. pyramidale. Inset confocal microscopical images show immunostainings for CB_1R and PV of labeled boutons (arrowheads). **c)** Representative traces of CB_1BC – PC paired recording obtained from CB_1R WT and KO mice under baseline condition and after the application of the CB_1R antagonist/inverse agonist AM251. Average IPSCs are highlighted as separate inset for easier comparison. **d)** Summary plots of whole experiments show increase of IPSC amplitudes in CB_1R WT, but not in KO after AM251 application. **e)** Graph of IPSC amplitudes before (baseline) and after application of AM251 in CB_1R WT (n = 11 pairs, **p = 0.006) and KO samples (n = 12 pairs, p_{ns} = 0.86). **f)** Graph of successes before and after application of AM251 in CB_1R WT (***p=0.0003) and KO samples (p_{ns} = 0.25). **g)** Graph of relative variability of postsynaptic events measured by the coefficient of variation (CV) of IPSCs before and after AM251 application in CB_1R WT (**p = 0.001), and KO samples (p_{ns} = 0.53). Baseline CV differs between genotypes (*p = 0.03). Two-way ANOVA with repeated measures, graphs show mean ± SEM with individual values. (Barti et al., 2024)

4.2.2. DAGLα-dependent tonic 2-AG production is constrained by persistent MAGL activity

Observed similarities between tonic and phasic eCB signaling in the presynaptic side through CB_1Rs shifted our focus to the underlying regulatory mechanisms and ligands by which persistent receptor activation occurs. Since 2-AG is the most abundant endogenous cannabinoid ligand in the brain (Stella et al., 1997) and plays pivotal role in phasic mode of retrograde signaling (Gao et al., 2010; Tanimura et al., 2010; Yoshino et al., 2011) we aimed to study its contribution in persistent cannabinoid regulation. In order to achieve this, we used a mouse model in which DAGLα, the main enzyme responsible for synthetizing 2-AG was deleted (Bisogno et al., 2003).

Previously, our group has shown that in acute living slices incubated in ACSF, 2-AG levels increased continuously under basal conditions in the absence of any pharmacological perturbation (Lee et al., 2015). These results indicated that 2-AG can be mobilized constitutively in acute hippocampal slice preparations. To investigate the potential role of ligand-mediated eCB signaling in the generation of persistent eCB blockade of GABA release, we used pharmacological blockade of 2-AG degradation pathway. Lipidomic experiments in combination with MAGL inhibition via preincubating WT slices with JZL184 unmasked a remarkable increase of 2-AG levels in the samples compared to DMSO treated slices (Figure 12/a). The increase was completely absent from DAGLα KO brain tissue. This indicates a continuous production of 2-AG in the presence of DAGLα. When we used MAGL inhibitors during paired recordings, the results were similar to the lipidomic measurements. While a robust decrease of IPSCs and successes in WT animals was detected due to continuously generated 2-AG, MAGL inhibition does not changed synaptic transmission in the absence of DAGLα in KO samples (Figure 12/b-d).

Altogether, our observations indicate the presence of an ongoing 2-AG production in the slice preparations mediated solely by DAGLα. The effect of the continuously generated 2-AG is kept under the tight control of MAGL.

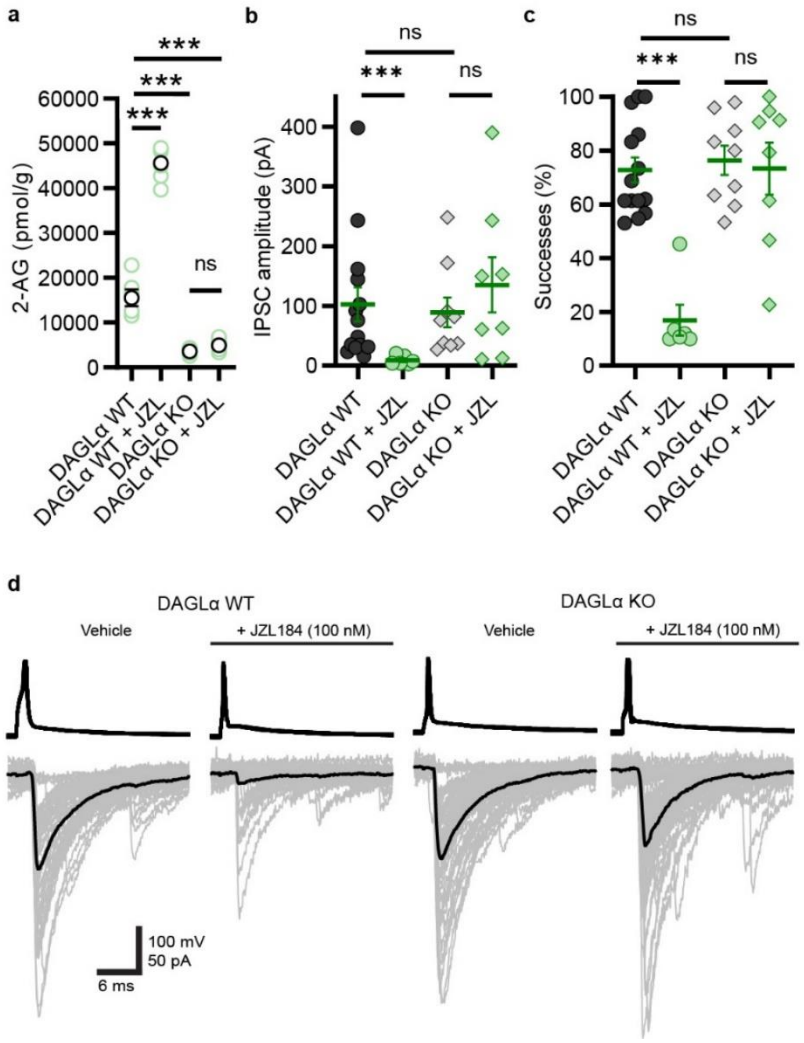

Figure 12. ***DAGLα-dependent tonic 2-AG production and synaptic effects are constrained by constitutive MAGL activity.*** **a)** 2-AG lipid measurements of DAGLα WT and KO hippocampal slices after pretreatment with either DMSO (vehicle) or with the irreversible MAGL inhibitor JZL184 (100 nM) for 40 minutes (n = 6 animals/ group, 6 samples/ treatment, ***p < 0.0001, p_{ns} = 0.057, Unpaired t-test). **b, c)** Summary graphs of electrophysiological experiments obtained from acute slices after 40 min incubation in each condition showed on panel a, and effect on IPSC amplitude (b) and successes (c) in DAGLα KO pairs (WT: n = 14 pairs, WT+JZL184: n = 6 pairs, KO: n = 9 pairs, KO+JZL184: n = 8 pairs, IPSC amplitude: ***p = 0.0002, p_{ns} = 0.81, WT-KO difference: p_{ns} = 0.8, successes: ***p < 0.0001, p_{ns} > 0.99, WT-KO difference: p_{ns} = 0.7, Mann-Whitney U test). **d)** Example traces of paired recordings from slices incubated in each condition shown above. Graphs show median ± IQR with individual values except on panel A, where it shows mean ± SEM with individual values. (Barti et al., 2024)

4.2.3. DAGLα-independent tonic cannabinoid signaling fine-tunes synaptic transmission

Interestingly, despite the absence of phasic eCB regulation and lacking persistent 2-AG signaling, baseline synaptic transmission properties measured via paired-recordings were unaltered in DAGLα KO (Figure 12/b, c). Therefore, we hypothesized the existence of another regulatory mechanism, which can adjust the magnitude of synaptic transmission. As a first step, the involvement of the non-canonical eCB system was studied. We performed AM251 treatment in paired recordings to test other possibly CB_1R-mediated mechanisms in DAGLα WT and KO slices. Interestingly, in the absence of DAGLα, the principal 2-AG-synthesizing enzyme, there was no change in the synaptic cannabinoid tone compared to WT. Blockade of CB_1Rs via AM251 application significantly increased IPSC amplitudes and successes in both genotypes (Figure 13/a-d), while also induced similar changes in CV values (Figure 13/e).

Overall, our results support the notion that beside the continuously released 2-AG, another mode of tonic cannabinoid signaling is present at the hippocampal CB_1BC GABAergic synapses. This form of persistent synaptic modulation is independent from DAGLα, the main 2-AG synthetizing enzyme, however, it is mediated by presynaptic CB_1Rs, suggesting potential contribution of non-canonical participants of eCB signaling.

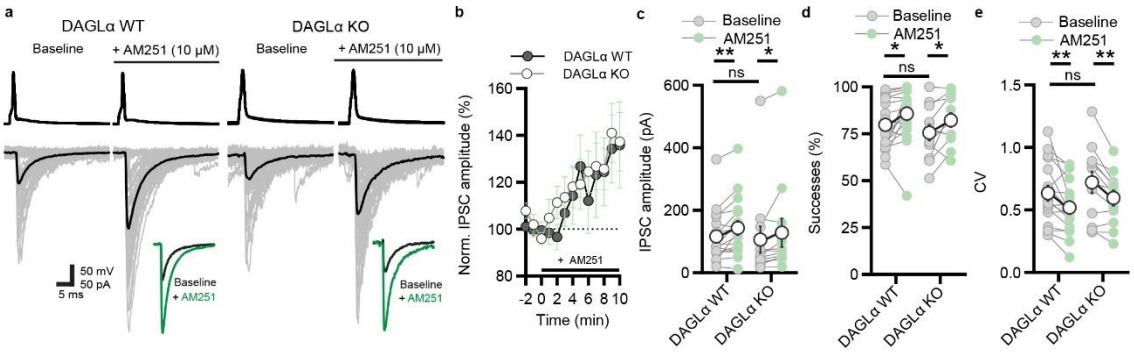

Figure 13. ***DAGLα independent tonic cannabinoid signaling is unmasked by CB_1R blockade.*** **a)** Representative traces of CB_1BC–PC paired recording obtained from DAGLα WT and KO mice during baseline and after AM251 application. Inset shows average IPSCs for easier comparison. **b)** Summary plots of IPSC amplitudes during whole experiment. **c)** Graph of IPSC amplitudes in DAGLα WT (n = 17 pairs, **p = 0.003) and KO (n = 12 pairs, *p = 0.03). **d)** Graph of successes in DAGLα WT (*p=0.003) and KO (*p = 0.004). **e)** Graph of CV values in DAGLα WT (**p = 0.02), and KO (**p = 0.05). Two-way ANOVA with repeated measures, graphs show mean ± SEM with individual values. (Barti et al., 2024)

4.2.4. NAPE-PLD does not contribute to tonic cannabinoid signaling

As based on our results, synaptic 2-AG independent tonic cannabinoid signaling is still present in DAGLα KO slices, an obvious explanation would be that this process is mediated by AEA, the second major endogenous cannabinoid lipid messenger in the brain (Devane et al., 1992). AEA can also be a key player in the regulation of tonic eCB signaling in various brain regions including the hippocampus (Hill et al., 2009; Kim and Alger, 2010; Lee et al., 2015; Morena et al., 2016). However, compared to 2-AG, AEA can be synthesized through multiple enzymatic pathways (Katona and Freund, 2012; Piomelli, 2003) which makes its contribution in certain mechanisms challenging to unfold. NAPE-PLD is described as the primary enzyme responsible for the synthesis of AEA (Okamoto et al., 2004; Ueda et al., 2013). Moreover, recent evidence also suggests that this enzyme generates an endogenous anandamide tone (Mock et al., 2020). Therefore, we studied the contribution of this persistent AEA generation in tonic cannabinoid signaling present at CB_1BC – PC synapses.

For this purpose, we utilized NAPE-PLD KO mice strains. We performed paired recordings in mice lacking NAPE-PLD and used pharmacological blockade of CB_1Rs by AM251. Notably, inhibition of CB_1R again influenced both amplitude, successes and CV values of NAPE-PLD WT and KO similarly (Figure 14/a-e).

These observations demonstrated that AEA, generated by the major NAPE-PLD synthesis pathways does not play a role in this form of tonic, CB_1R-dependent cannabinoid signaling. These findings demonstrate that there are mechanistically different forms of tonic cannabinoid signaling even at the same synapse type.

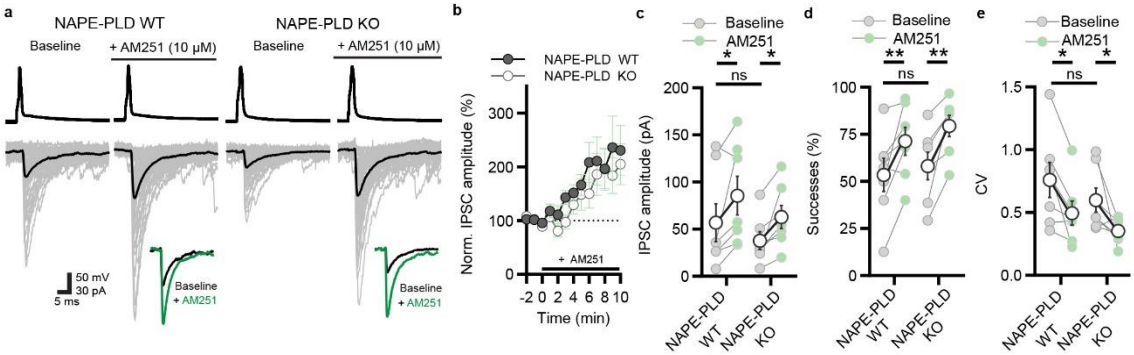

Figure 14. ***Reduced anandamide levels in NAPE-PLD KO mice does not influence tonic cannabinoid signaling.*** **a)** Representative traces of CB_1BC–PC paired recording obtained from NAPE-PLD WT and KO mice during baseline and after AM251 application. Inset shows average IPSCs for easier comparison. **b)** Summary plots of IPSC amplitudes during whole experiment. **c)** Graph of IPSC amplitudes in NAPE-PLD WT (n = 7 pairs, *p = 0.02) and KO (n = 7 pairs, *p = 0.04). **d)** Graph of successes in NAPE-PLD WT (**p=0.009) and KO (**p = 0.003). **e)** Graph of CV values in NAPE-PLD WT (*p = 0.02), and KO (*p = 0.03). Two-way ANOVA with repeated measures, graphs show mean ± SEM with individual values. (Barti et al., 2024)

4.3. Nanodomain-specific assessment of CB_1R distribution at CB_1BC – PC connections

4.3.1. Nanoscale CB_1R/effector stoichiometry determines tonic cannabinoid signaling

It was previously shown that whole boutonal CB_1R levels cannot predict the magnitude of tonic cannabinoid signaling (Lenkey et al., 2015). However, GPCRs exist in both active and inactive conformational states. As neutral CB_1R antagonist did not affect perisomatic GABAergic synapses (Lee et al., 2015), CB_1Rs also have constitutive activity at these synapses. Because there is a pre existing equilibrium between constitutively active and inactive receptor conformations (Weis and Kobilka, 2018), we reasoned that if constitutive CB_1R activity contributes to the synaptic cannabinoid tone, then the molecular abundance of CB_1Rs within the close proximity of the synaptic area should predict the magnitude of the cannabinoid tone.

Therefore, to test this hypothesis more directly, we developed a workflow in which beside the measurement of physiological parameters from unitary synaptic connections, correlative morphological data, and nanoscale-level molecular distribution of receptors were also available within complex brain tissue (Figure 15/a). We carried out paired recordings from CB_1BCs and CA1 pyramidal neurons, and recorded IPSCs before and after AM251 application to measure the magnitude of the synaptic cannabinoid tone (Figure 15/b). The presynaptic basket cell and the postsynaptic PC were filled with biocytin and Cascade Blue, respectively. The neuronal processes were anatomically reconstructed at high magnification to determine all synaptic connections (Figure 15/c, d). Since previous variance-mean experiments revealed that even in a single bouton with a single active zone there might be multiple release sites (Biro et al., 2006), we focused on pairs that were connected with a single synapse and contained one confocal bassoon cluster (identified via neighboring bassoon positive voxels on the confocal image) located opposite to the postsynaptic neuron. After identification of the unitary synapses, 300 µm slices were resectioned to 10 µm thin sections and processed for immunostaining and subsequent STORM imaging. The z-stack image of the synaptic connection was acquired by volumetric 3D-STORM super-resolution imaging to visualize the synapse regardless of bouton orientation (Figure 15/e, f). CB_1R nanoscale density was calculated in relation to the active zone visualized by bassoon-immunolabeling (Figure 16/a).

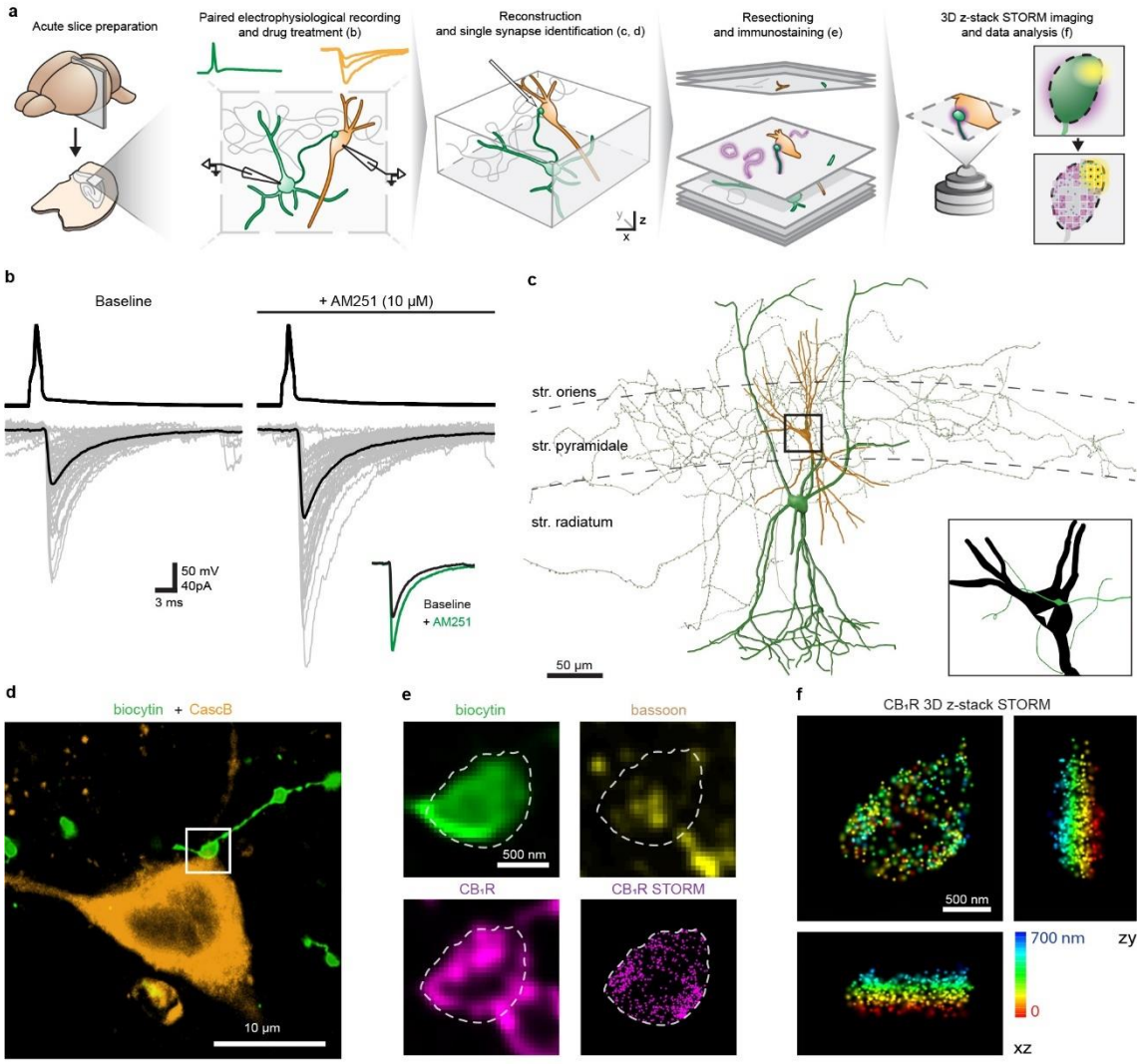

Figure 15. ***Correlated electrophysiological, anatomical and nanoscale molecular analysis of unitary CB1BC - PC synapses.*** **a)** Schematic workflow of the experimental procedure. **b)** Example traces of paired recording reveals baseline properties of synaptic transmission and tonic cannabinoid signaling. **c)** Morphological reconstruction of the recorded CB_1BC (biocytin, green) and PC (CascB, orange). **d)** Confocal microscopic image of single identified synaptic connection between recorded cells (arrowhead). **e)** Boxed region in d is shown at higher magnification after immunostaining. Correlated confocal and STORM super-resolution imaging of the biocytin-filled axon terminal (green) was used to identify the presynaptic active zone by bassoon-immunolabeling (yellow) and was exploited to quantify the nanoscale distribution of CB_1Rs (magenta). **f)** 3D z-stack STORM of the identified CB_1R-positive axon terminal. (Barti et al., 2024)

As variance-mean analysis predicted low baseline Pr under our experimental conditions, this parameter together with low connection numbers allowed us to estimate Pr values based on successes recorded during paired recordings (see Methods), therefore we calculated the estimated Pr values on our selected pairs. Pr value was estimated from the success ratio of IPSCs assuming 3 functional release sites per active zone (based on quantal analysis). Collectively, this correlative workflow enables direct quantification of the nanoscale abundance of CB_1Rs that directly underlie the effect of the synaptic cannabinoid tone on neurotransmitter release within a single synapse. Correlated measurements of the estimated Pr, the active zone size, and the number of CB_1Rs along the entire bouton surface revealed that the total CB_1R number on the axon terminal does not predict Pr (Figure 16/b). Bassoon voxel numbers also did not correlate with Pr (Figure 16/c). These observations suggest that instead of a single molecular or anatomical parameter, the stoichiometric relationship of the regulatory receptor and its effectors may better predict how constitutive CB_1R activity controls neurotransmitter release. This also implies that the nanoscale physical distance between the receptor and its effector strongly affects potency. Therefore, we next aimed to test the hypothesis that the nanoscale stoichiometric ratio may be the key determinant of the magnitude of the synaptic cannabinoid tone and its influence on GABA release.

When the nanoscale stoichiometry parameter was calculated by measuring the ratio of intra/perisynaptic CB_1Rs and bassoon-positive voxels, we found a strong inverse correlation with the estimated release probability suggesting that the more CB_1Rs are active in the nanoscale vicinity of the release machinery, the smaller the Pr is. Moreover, there was a steep decrease in the correlation coefficient value more than 200 nm away from the active zone, highlighting the specific importance of the nanoscale physical distance (Figure 16/d, e). Importantly, the correlative relationship depends on the persistent activity of intra/perisynaptic CB_1Rs, because AM251 administration on the same pairs eliminated the correlation between the receptor/effector ratio and the Pr (Figure 16/f). In addition, the nanoscale stoichiometry positively scales with the effect of AM251. In other words, the more intra/perisynaptic CB_1Rs control the release machinery, the larger the impact of synaptic cannabinoid tone on the release probability. Accordingly, low Pr unitary synaptic connections were associated with a stronger cannabinoid tone (Figure 16/g, h). These measurements together provide insights into the qualitative and

quantitative nature of how constitutively active metabotropic receptors control neurotransmitter release.

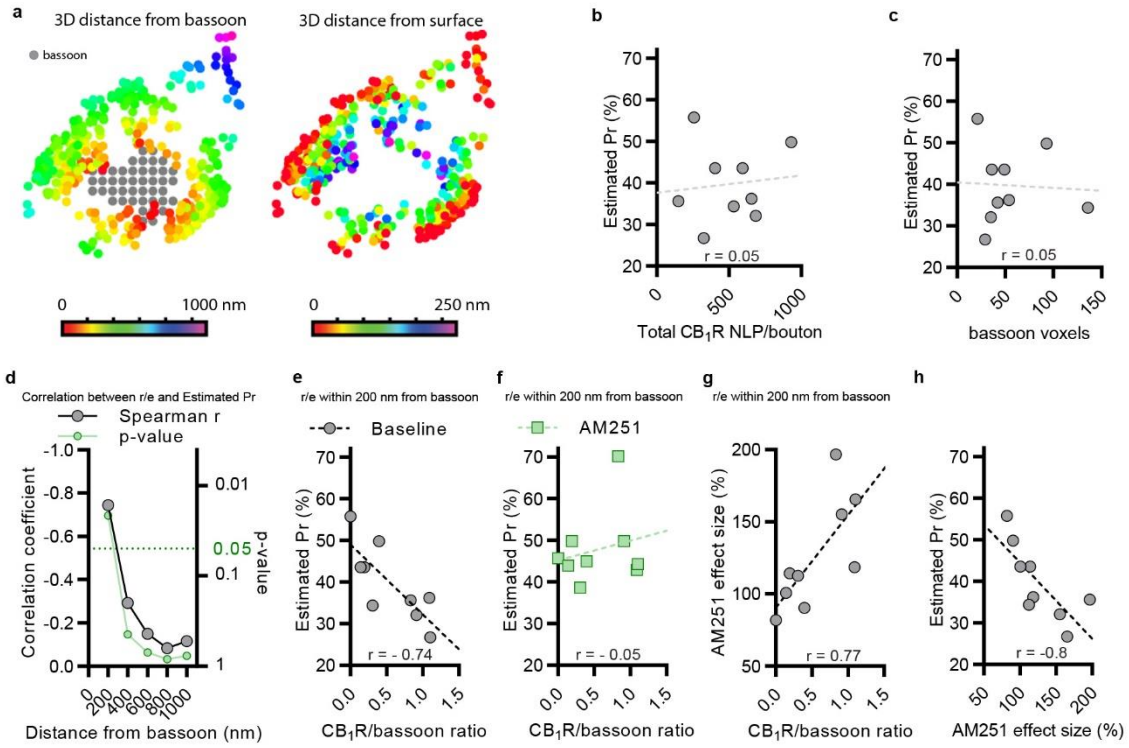

Figure 16. ***Nanoscale receptor/effector stoichiometry determines the synaptic cannabinoid tone.*** **a)** 3D z-stack STORM data was used to calculate the nanoscale distance of each individual CB_1R from the bassoon-positive voxels and from the surface of the axon terminal. **b)** The total number of CB_1Rs on the axon terminal does not predict the estimated Pr (n = 9 pairs, p_{ns} = 0.90, r = 0.05). **c)** The number of bassoon voxels does not co-vary with the estimated Pr (p_{ns} = 0.90, r = 0.05). **d)** Correlation coefficients of the CB_1R/bassoon stoichiometry calculated at various distances from bassoon labeling. The receptor/effector stoichiometry scales with the estimated Pr in a nanoscale distance-dependent manner. **e)** Correlation plot shows an inverse correlation between the estimated Pr and the nanoscale CB_1R/bassoon ratio measured within 200 nm distance from the active zone (*p = 0.03, r = -0.74). **f)** Application of AM251 impairs the inverse correlation between the estimated Pr and the nanoscale CB_1R/bassoon ratio at the same recorded pairs as shown at baseline on panel e (p_{ns} = 0.90, r = -0.05). **g)** Correlation plot shows positive correlation with the nanoscale CB_1R/bassoon ratio and the strength of the synaptic cannabinoid tone (*p = 0.02, r = 0.77). **h)** Plot shows negative correlation between the strength of the synaptic cannabinoid tone and the estimated Pr (*p = 0.01, r = -0.8, Spearman rank-order correlation). (Barti et al., 2024)

4.3.2. Selective reduction of extrasynaptic CB_1R abundance does not affect the cannabinoid tone

If nanodomain-specific CB_1R activity is indeed responsible for the synaptic cannabinoid tone, then selective perturbation of intra- vs extrasynaptic CB_1R abundance would differentially affect this synaptic phenomenon. Therefore, next, we investigated whether perturbations that change CB_1R density can affect tonic cannabinoid signaling. Previous studies have shown that CB_1R binding sites are reduced by half in membrane fractions from mice heterozygous for the CB_1R knockout allele (HET) compared to WT samples (Selley et al., 2001). By using western blot in electrophysiological slice preparations, we found that CB_1R HET mice have ~50% less CB_1R protein compared to littermate WT mice (Figure 17/a). Because CB_1Rs are present in many cell types and protein level changes can occur in a cell-type-specific manner, we measured CB_1R-immunolabeling on perisomatically-targeting GABAergic axon terminals by STORM imaging (Figure 17/b). While bouton size and active zone size were not affected by genotype (Figure 17/c, d), the number of localization points representing CB_1R proteins along the entire bouton surface was strongly reduced in HET mice (Figure 17/e). In contrast, CB_1R numbers in the nanoscale vicinity of bassoon clusters were similar in both genotypes, suggesting that axon terminals first fill up the intra/perisynaptic CB_1R population (Figure 17/g). Moreover, the nanoscale receptor/effector ratio was also comparable between WT and HET mice (Figure 17/f). Notably, paired recordings showed that neither phasic endocannabinoid signaling nor cannabinoid tone and its impact on synaptic variability were affected in HET mice despite the substantially lower extrasynaptic CB_1R density (Figure 18/a-f).

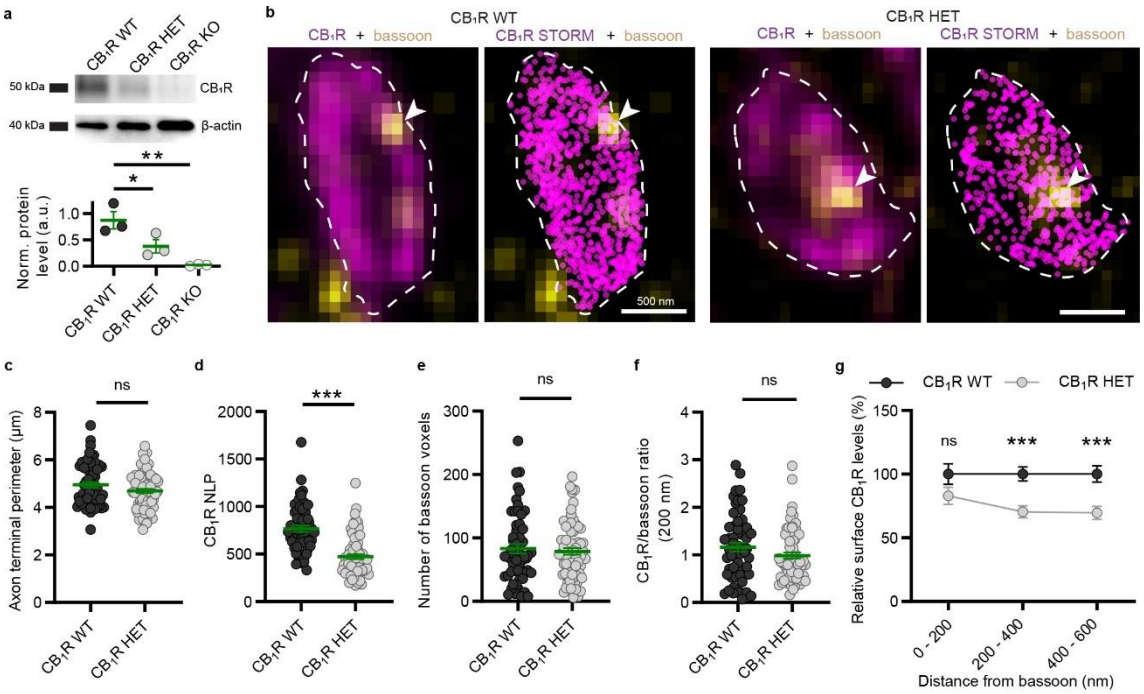

Figure 17. ***Selective reduction of extrasynaptic CB_1R numbers in CB_1R HET mice.*** **a)** Western blot of WT, CB_1R heterozygotes (HET) and CB_1R KO hippocampal lysates (n = 3 animals/ genotype, *p = 0.046 between WT and HET, **p = 0.04 between WT and KO, one-way ANOVA with Dunnett's multiple comparisons test). **b)** Confocal images show immunolabeling for CB_1R (magenta) and the active zone (arrowhead) labeled via bassoon protein (yellow), whereas the corresponding STORM super-resolution images display the nanoscale distribution CB_1Rs in axon terminals. **c)** Summary graph of the perimeter of axon terminals in WT and HET samples (WT: n = 57 boutons, HET: n = 71 boutons, p_{ns} = 0.18). **d)** Summary graph of the number of bassoon-positive voxels shows identical active zone size in the axon terminals of WT and HET mice (p_{ns} = 0.94). **e)** Summary graph of the total number of CB_1R localization points (NLP) on axon terminals measured with STORM (***p < 0.0001). **f)** Summary graph of nanoscale CB_1R/bassoon ratio in the vicinity (200 nm) of the active zone (p_{ns} = 0.17). **g)** Summary graph of distance-dependent decrease of CB1Rs on the surface of boutons in HET mice (0-200 nm: p_{ns} = 0.08, 200-400, 400-600 nm: ***p < 0.0001). Mann-Whitney U test. (Barti et al., 2024)

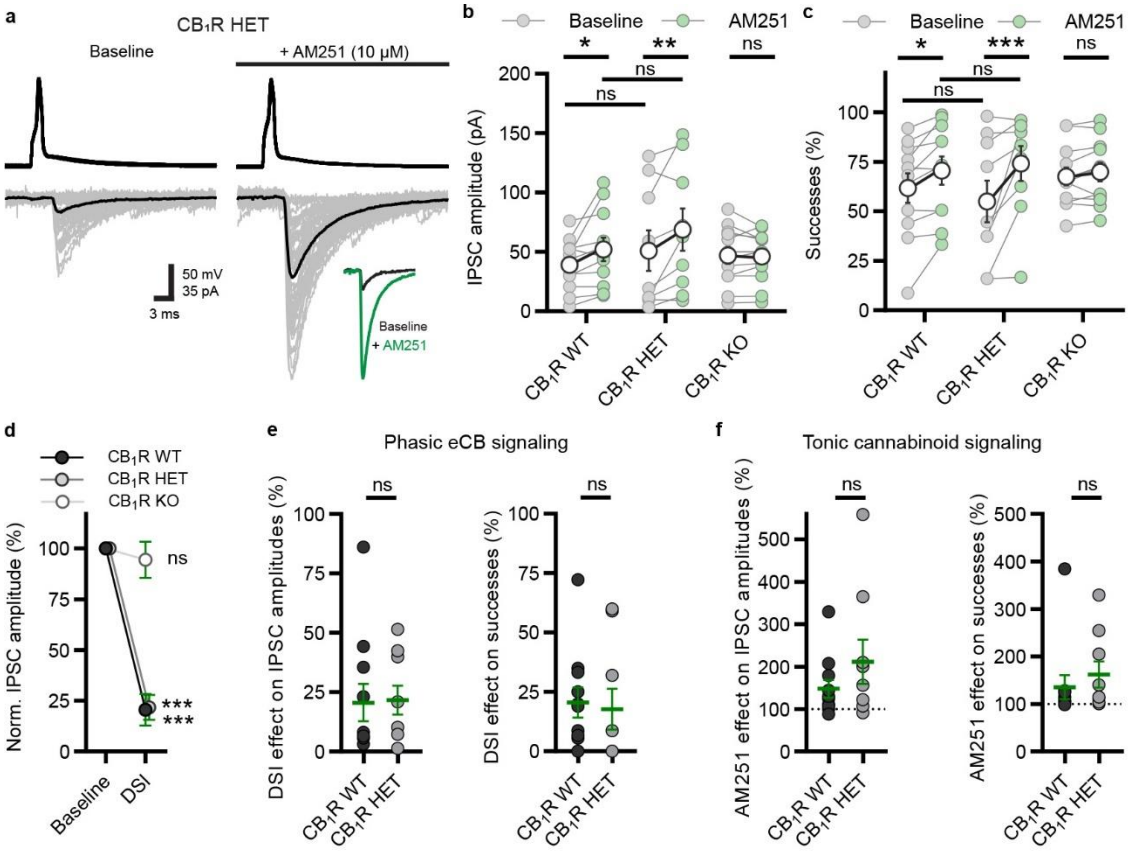

Figure 18. ***Selective reduction of extrasynaptic CB₁Rs in CB₁R HET mice does not affect the cannabinoid tone.*** **a)** Representative traces from paired recordings obtained from HET mice before and after the application of AM251. **b)** Graph of IPSC amplitudes before (baseline) and after application of AM251 in CB_1R WT (n = 11 pairs, *p = 0.01), HET (n = 9 pairs, **p = 0.003) and KO samples (n = 12 pairs, p_{ns} = 0.9). **c)** Graph of successes before and after application of AM251 in CB_1R WT (*p=0.02), HET (*** p < 0.0001) and KO samples (p_{ns} = 0.5). **d)** Summary graph of DSI effect on IPSC amplitudes during baseline and after AM251 application in CB_1R WT (n = 8 pairs, ***p < 0.001), HET (n = 6 pairs, *** p < 0.0001) and KO samples (n = 11 pairs, p_{ns} = 0.6). **e)** Effect of DSI (a form of phasic endocannabinoid release) on IPSC amplitudes and successes between CB_1R WT and HET genotypes (WT: n = 11, HET n = 9 pairs, IPSC: p_{ns} = 0.3702, successes: p_{ns} = 0.3696). **f)** Summary graphs of AM251 effect (unmasked tonic cannabinoid signaling) on baseline IPSC amplitudes and successes in CB_1R WT and HET animals (IPSC: p_{ns} = 0.5, successes: p_{ns} = 0.66). Graphs b-d shows mean ± SEM with individual values, Two-way ANOVA with repeated measures, e-f show median ± IQR with individual values, Mann-Whitney U test. (Barti et al., 2024)

4.3.3. *In vivo* THC administration disrupts presynaptic nanoscale stoichiometry and the synaptic cannabinoid tone

The complex behavioral effects of cannabis are largely due to the activation of CB_1Rs by THC, the psychoactive phytocannabinoid substance. By cell-type-specific STORM imaging, our colleagues previously found that *in vivo* THC administration causes strong dose-dependent reduction in the total CB_1R content of CB_1BC boutons (Dudok et al., 2015). However, our findings in HET mice revealed that a robust reduction of CB_1Rs in axon terminals measured at the microdomain level may not necessarily have functional consequences on synaptic transmission. Conversely, if THC exposure compromises the intrasynaptic nanoscale stoichiometry, then changes in the cannabinoid tone would be expected. To address this question, we repeated the THC administration paradigm that was optimized to study behavioral tolerance in mice. After *in vivo* THC treatment, *ex vivo* biocytin-filled CB_1BCs were processed for correlated confocal and STORM imaging (Figure 19/a, b). There was no change in the size of axon terminals and active zones (Figure 19/c, d). In contrast, THC administration caused a significant decrease in overall CB_1R numbers (Figure 19/e). The magnitude of reduction in total CB_1R abundance was comparable in HET mice and after THC treatment (38% vs 47%). In striking contrast to the observations in HET mice, we found a marked decrease in the intra/perisynaptic CB_1R population and in the nanoscale receptor/effector ratio after THC exposure (Figure 19/f, g). Paired patch-clamp recordings in hippocampal slices obtained from THC-treated mice revealed robust changes in the basic synaptic physiological properties (Figure 20/a). Remarkably, the synaptic cannabinoid tone was completely absent. AM251 application could not increase IPSC amplitudes and the number of successful events in line with the strong increase in baseline parameters (Figure 20/b-d). The decrease in CV and their insensitivity to AM251 revealed that THC also diminishes synaptic variability (Figure 20/e). In contrast, phasic endocannabinoid signaling (DSI) was only mildly affected and remained sensitive to AM251 (Figure 20/f, g).

These findings demonstrate that THC exposure impairs the precise nanoscale functional organization that underlies the synaptic cannabinoid tone and reduces the synapse-specific variability of CB_1BC output synapses. Our results also highlight the importance of nanodomain-specific measurements for providing physiologically and pathologically relevant insights into drug-induced molecular changes.

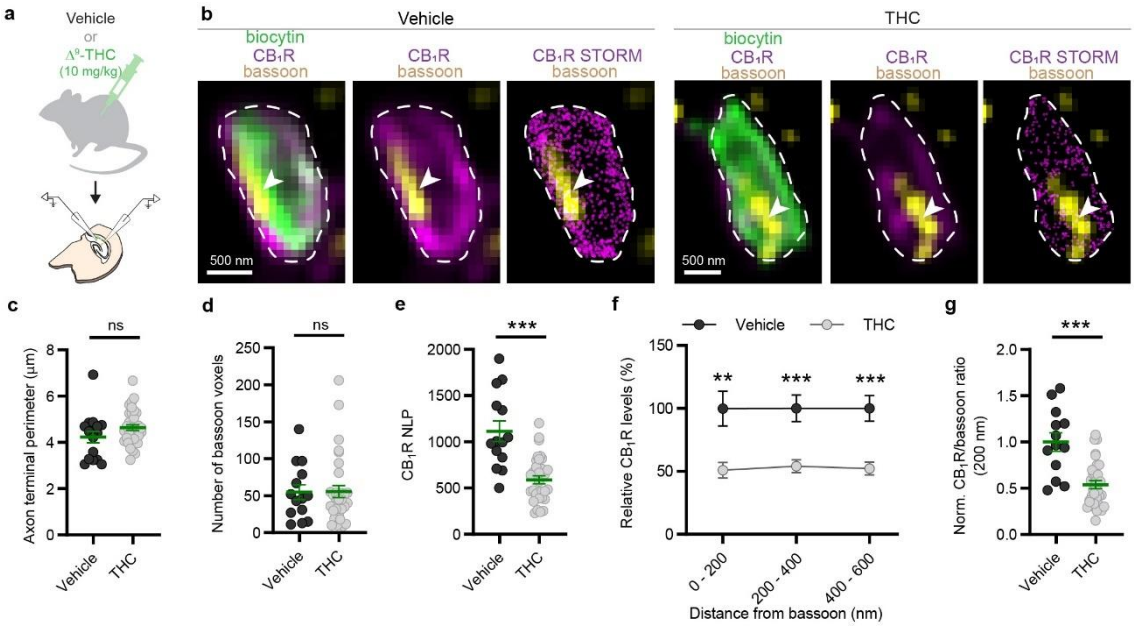

Figure 19. ***General reduction of peri- and extrasynaptic CB₁Rs after in vivo THC treatment.*** **a)** Schematic illustration of experimental design. **b)** Confocal- and combined STORM images of CB1R labeling (magenta) on biocytin-labeled (green) boutons from either vehicle or THC treated animals. Arrowhead marks bassoon labeled synaptic active zone (yellow). **c)** Summary graph of axon terminal perimeter in vehicle and THC treated samples (vehicle: n = 16 boutons, THC: n = 35 boutons, p_{ns} = 0.14). **d)** Summary graph of bassoon-positive voxel numbers (vehicle: n = 14 boutons, THC: n = 32 boutons, p_{ns} = 0.84). **e)** Summary graph of CB1R STORM localization point numbers (NLP) (***p < 0.0001). **f)** Summary graph of distance-independent decrease of CB1Rs on the bouton surface in THC treated mice. (0-200 nm: **p = 0.002, 200-400, 400-600 nm: ***p < 0.0001). **g)** Summary graph of CB_1R/bassoon ratio in vehicle and THC treated boutons (***p = 0.0001). Graphs show mean ± SEM with individual values, Mann-Whitney U test. (Barti et al., 2024)

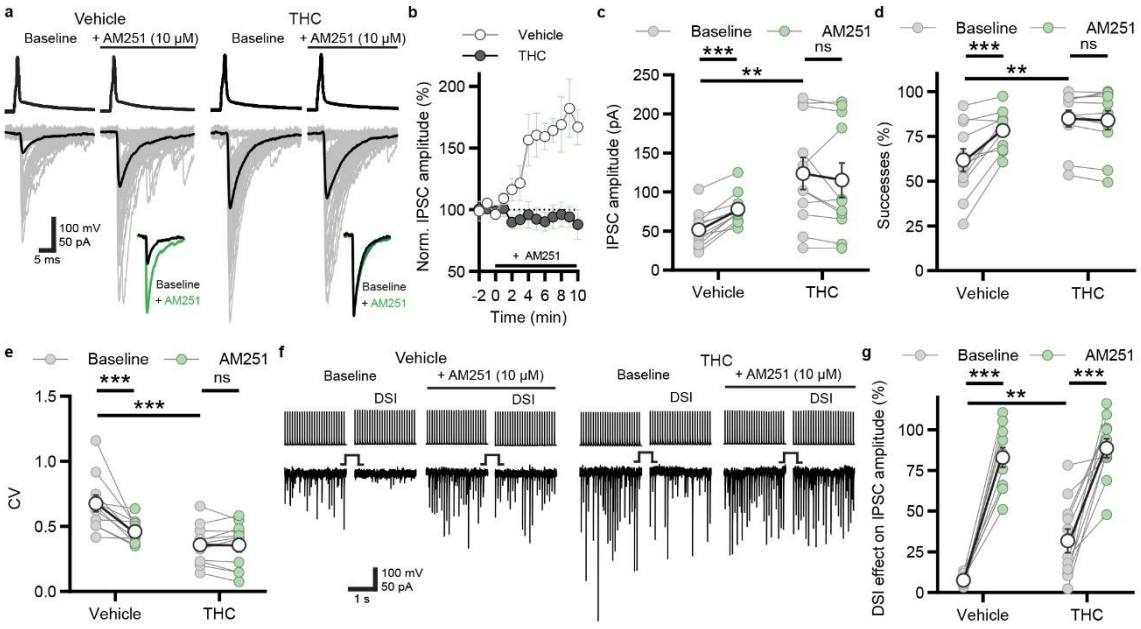

Figure 20. ***THC disrupts the intrasynaptic nanoscale stoichiometry and the cannabinoid tone.*** **a)** Example traces of paired recordings before and after AM251 application from slices of in vivo vehicle or THC treated mice. **b)** Summary plots of IPSC amplitudes during the whole experiment. **c)** Summary graph of IPSC amplitudes during baseline and after application of AM251 in vehicle- or THC treated groups (n = 11 pairs/ group, ***p = 0.0004, p_{ns} = 0.18, baseline difference: **p = 0.002). **d)** Summary graph of successes (***p < 0.0001, p_{ns} = 0.74, baseline difference: **p = 0.002). **e)** Summary graph of IPSC CV values (***p < 0.0001, pns = 0.96, baseline difference: ***p < 0.0001). **f)** Representative IPSC responses on DSI before and after AM251 application on vehicle- or THC treated slices. **g)** Summary graph of DSI effect on IPSC amplitudes (***p < 0.0001, baseline difference: **p = 0.004). Graphs show mean ± SEM with individual values, Two-way ANOVA with repeated measures. (Barti et al., 2024)

5. Discussion

In the present study, we identified NAPE-PLD and DAGLα independent tonic cannabinoid signaling that contribute to baseline synaptic variability in a postsynaptic cell-specific manner at CB_1BC – PC synapses in the hippocampal CA1 region. In order to investigate the underlying molecular principles of this signaling modality, we developed and applied a methodology, in which we combined cell- and synapse-specific *in vitro* electrophysiological investigation of neurotransmitter release with the analysis of anatomical features – visualized via confocal microscopy, and examination of nanoscale molecular distributions of CB_1R – detected via STORM super-resolution microscopy in acute brain slices. The joint electrophysiological and nanoscale molecular data of single identified synapses revealed correlations between the estimated Pr, the magnitude of tonic cannabinoid signaling and the molecular ratio of active zone adjacent CB_1Rs with bassoon. Importantly, perturbations of CB_1R numbers that did not affect the active zone adjacent receptor pool also did not affect tonic cannabinoid signaling, while THC treatment altered intra/perisynaptic CB_1R numbers and impaired tonic cannabinoid signaling. Overall, our current study reveals a previously unknown high-level nanoscale organization principle of CB_1Rs at presynaptic active zones in the mouse hippocampal inhibitory synapses, which can contribute to the understanding of general GPCR-modulation of neurotransmitter release.

5.1 Variability of CB_1BC – PC synaptic transmission is regulated by multiple cell domain-specific anatomical and molecular properties

The qualitative and quantitative properties of neurotransmitter release are established by numerous physical, chemical, and biological parameters that together determine intricate synapse-specific differences. Our results showed that at CB_1BC – PC synapses, a certain variability of synaptic transmission is arising from purely anatomical parameters, like the number of established connections between cells. Variance-mean analysis revealed that these synapses contain multiple functional release sites, which serves as another potential platform of increasing variability in neurotransmission. However, as the number of boutons between cell pairs does not show clear correlation with the measured IPSC amplitudes or successes, there are likely other mechanisms that

fine-tune synaptic transmission at these connections. Our results also showed that beside anatomical parameters, the synaptic cannabinoid tone, that can be set at each synapse postsynaptic target-specifically also contributes to synaptic variability.

As the tight spatial and temporal regulation of Ca^{2+}-signaling is pivotal in most neuronal physiological processes (Schwaller, 2020), the local intracellular Ca^{2+}-buffering capabilities might also influence synaptic functions. The EF-hand calcium binding proteins serve as well-established markers of certain neuron types for decades (Alpár et al., 2012). Therefore, there is a general view that each GABAergic interneuron type expresses characteristic and functionally relevant Ca^{2+}-buffers. Although NECAB proteins have been cloned more than 20 years ago (Bernier et al., 2001; Sugita et al., 2002), our knowledge about their cell physiological functions is still very limited. Our i*n silico* data revealed consistently high levels of both NECAB1-2 mRNA levels in every highly CB_1R-expressing GABAergic interneuron, while it was completely lacking from PV-expressing ones (Miczán et al., 2021). Detailed investigations via utilization of the most sensitive RNAscope and confocal imaging approaches verified the high-level colocalization of NECAB1-2 mRNA and protein predominantly with CB_1R-positive interneurons (Miczán et al., 2021). Direct measurement of Ca^{2+}-transients by two-photon laser microscopy in CB_1R-positive interneurons provided compelling evidence for striking differences in dendritic and boutonal Ca^{2+}-dynamics (Kisfali et al., 2013). Our findings, which show that the two NECAB proteins are localized at different subcellular domains of individually labeled interneurons suggests a distinct contribution of NECAB1 and NECAB2 to somatodendritic and boutonal Ca^{2+}- dynamics. As these molecular differences in Ca^{2+}-buffering could define specific features of the CB_1R-expressing cell population during *in vivo* network oscillations (Dudok et al., 2024; Klausberger et al., 2005), our present anatomical subcellular domain-specific investigations of the NECAB proteins will hopefully help to orient future studies that aim to uncover unknown physiological roles of NECABs by using loss-of-function approaches.

These observations together suggest that besides morphological and anatomical properties, cell domain-specific molecular differences may underlie the distinctive neurotransmitter release properties of CB_1BCs.

5.2. DAGLα- and NAPE-PLD-independent tonic cannabinoid signaling regulates synaptic variability at hippocampal inhibitory synapses

A long-time pending question in endocannabinoid research is whether 2-AG or AEA is the major lipid messenger underlying persistent cannabinoid signaling. Evidence support AEA as a major regulator of tonic eCB signaling in the basolateral amygdala (Hill et al., 2009; Morena et al., 2016). Other studies found continuous release of 2-AG in the dorsal raphe nucleus, in the hippocampus, in the subiculum and in the prelimbic prefrontal cortex (Anderson et al., 2015; Haj-Dahmane et al., 2018; Lee et al., 2015; Marcus et al., 2020). A likely explanation of this controversy is the brain area specific nature of the phenomenon. Unexpectedly, we found that neither of the two main endocannabinoid-producing enzymes are involved in this form of tonic cannabinoid signaling. While the existence of an unknown lipid, peptide or gaseous retrograde messenger can never be fully excluded, it is likely that the two traditional endocannabinoid messengers are not involved in this phenomenon.

Due to the lipid nature of eCBs, precise control over their synthesis is essential to generate ligand-dependent tonic cannabinoid signaling. Two isoforms of diacylglycerol lipase (DAGLα and β) are considered as the major serine hydrolases which are able to generate 2-AG (Bisogno et al., 2003). Moreover, surprising observations pinpointed ABHD6, a 2-AG hydrolase can also act as an enzyme that possesses diacylglycerol lipase activity in certain brain states, therefore can be also participate in the generation of 2-AG (Van Esbroeck et al., 2019). Therefore, there is a possibility that DAGLβ and ABHD6 generate 2-AG in our knockout model in the absence of DAGLα. Indeed, our lipid measurements showed a remaining ~23% of 2-AG in the hippocampus of DAGLα KO animals. However, while DAGLα expression in the hippocampus is mainly associated with neurons (Jung et al., 2007; Katona et al., 2006), DAGLβ is detected solely in microglia in cortical samples (Viader et al., 2016). Although the specific role of neuronal DAGLβ in other brain regions cannot be excluded (Liu et al., 2022), these findings support the notion that the two isoforms of DAGLs potentially generate different pools of 2-AG, from which DAGLα-dependent 2-AG pool regulates synaptic function in the hippocampus (Gao et al., 2010; Tanimura et al., 2010; Yoshino et al., 2011). The second potential 2-AG source in DAGLα KO animals is generated by ABHD6, however, studies utilizing light- and electron microscopy showed that this enzyme is expressed by principal

glutamatergic neurons at postsynaptic dendritic spines (Marrs et al., 2010; Straiker et al., 2009). Moreover, ABHD6 is also associated with glutamatergic AMPA receptors and forms macromolecular complexes by which it regulates AMPA receptor function (Schwenk et al., 2012; Wei et al., 2016), therefore the ABHD6-dependent 2-AG generation presumably does not present at inhibitory synapses on pyramidal cell somata investigated by this study. Electrophysiological experiments, showing that pharmacological blockade of ABHD6 does not affect neither eCB mediated DSI nor DSE further strengthen this assumption (Straiker et al., 2009; Straiker and Mackie, 2009). The lipid 2-AG also has critical functions that does not involve endocannabinoid signaling (Baggelaar et al., 2018). Thus DAGLα generated 2-AG potentially influences neuronal synaptic transmission, while the remaining levels of 2-AG in the DAGLα KO animals could serve as a precursor for arachidonic acid, prostaglandin and other general lipid signaling pathways (Reisenberg et al., 2012).

AEA can be synthetized through more complex enzymatic pathways (Hussain et al., 2017), however, NAPE-PLD is described as the primary enzyme responsible for the synthesis of AEA (Okamoto et al., 2004; Ueda et al., 2013). Moreover, recent evidence also suggests that this enzyme generates an endogenous anandamide tone (Mock et al., 2020). In this study, we focused on the role of NAPE-PLD generated AEA, which based on our findings does not influence inhibitory CB_1BC synapses. Therefore, while there are still eCB ligands present in our samples, it is likely that this form of cannabinoid signaling functions in a ligand-independent manner, potentially in cooperation with specific cell-adhesion molecules (Anderson et al., 2015; Földy et al., 2013). Although the fine molecular mechanistic details of the phenomenon are still concealed, our current results show that 2-AG and AEA generated by DAGLα and NAPE-PLD respectively, are not necessary for tonic cannabinoid signaling.

5.3. Nanoscale receptor/effector stoichiometry controls neurotransmitter release by setting the cannabinoid tone

The significance of the cannabinoid tone in adjusting target cell-dependent synaptic strength represents the existence of a synapse-specific retrograde mechanism. First, we identified the intrasynaptic nanoscale stoichiometry parameter that is sufficient

to predict the magnitude of the synaptic cannabinoid tone and its influence on GABA release. The observation that the CB_1R inverse agonist/antagonist AM251 disrupts the correlation between the estimated Pr and the nanoscale receptor/effector ratio suggests that the high correlation coefficient requires persistent CB_1R activity. This is further supported by the strong positive correlation between the effect of AM251 and the nanoscale receptor/effector ratio. It is conceivable that CB_1Rs immobilized in the nanoscale vicinity of the release site have a more robust functional impact on basal synaptic transmission because the synaptic cannabinoid tone relies on membrane-delimited beta/gamma subunit signaling and inhibition of presynaptic N-type calcium channels (Jensen et al., 2021; Szabó et al., 2014). This suggests that synapses may be capable of regulating the size of their intrasynaptic CB_1R population by specific mechanisms. For example, cannabinoid tone requires intact postsynaptic neuroligin-3 function (Földy et al., 2013). Thus, trans-synaptic protein-protein interactions that are known to regulate constitutive GPCR activity (Dunn et al., 2019) may be ideal synapse-specific candidate mechanisms to determine how many tonically active intrasynaptic CB_1Rs control the release machinery.

What could be the physiological role of tonic cannabinoid signaling? Synapses formed by either PV- or CB_1BCs in the hippocampus have markedly distinct roles in circuit functions. While PV-containing basket cells work as a clockwork to precisely regulate network oscillations, CB_1BCs operate at complementary time windows *in vivo*, in a more asynchronous and imprecise manner (Dudok et al., 2021; Hefft and Jonas, 2005). Phasic cannabinoid signaling at CB_1BCs has been shown to modulate place cell tuning *in vivo* and therefore potentially influence spatial memory (Dudok et al., 2024). As presented in the introduction, multiple studies also support that hippocampal CB_1R-expressing interneurons have important roles in memory discrimination and engram formation. At these synapses, the ability for fast, energy efficient learning is likely crucial in order to effectively participate in both short- and long term memory-related processes (Aitchison et al., 2021). As synapses with a larger presynaptic variance possess enhanced learning rates, tonic cannabinoid signaling can potentially contribute to these mechanisms as it can add to the synaptic variability via modifying Pr, therefore making these synapses more- or less susceptible for synaptic learning depending on physiological states and activation of intra/perisynaptic CB_1Rs.

The presented results also pinpoint the possibility that different CB_1R pools on the boutonal surface might have distinct roles. While intra/perisynaptic CB_1Rs contribute to synapse-specific tuning of neurotransmitter release, extrasynaptic CB_1Rs can potentially mediate phasic eCB signaling. Moreover, extrasynaptic CB_1Rs can also act either as a reservoir pool that contributes to rapid recycling of active receptors (Jullié et al., 2020) or it can have distinct cell physiological and signaling role, such as regulating the actomyosin cytoskeleton (Roland et al., 2014), regulate the size of the vesicle pool (Patzke et al., 2021) or to initiate receptor tyrosine kinases transactivation and signaling (Zhou et al., 2019). Although, contribution of intra/perisynaptic CB_1Rs in the above-mentioned processes cannot be excluded, detailed investigations are still needed in the future to elucidate these hypotheses.

5.4. Marijuana consumption alters intra/perisynaptic CB_1R levels in synaptic active zones

Cannabis use disorder is now becoming a major social-economic burden as due to constant rise in cannabis utilization in the population diagnosis rate increases (Ferland and Hurd, 2020). As not only the use continues to grow, but the consumed THC concentrations also show prominent increase (Chandra et al., 2019), a detailed neurobiological investigation of high dose drug effects are needed. Since *in vivo* THC treatment decreases CB_1R numbers on inhibitory bouton surfaces in dose-dependent manner (Dudok et al., 2015), we studied whether there is a nanodomain-specific alteration in the synaptic active zone after THC administration. In principle, this observation is an appealing example of a maladaptive molecular tolerance phenomenon, and the hypothesized concomitant synaptic defects could readily contribute to the behavioral tolerance associated with cannabis use disorder. However, in the present study, we found that a strong reduction in the total CB_1R levels on axon terminals is not necessarily accompanied by impaired phasic endocannabinoid signaling or abnormal synaptic cannabinoid tone. Considering the nanoscale organization of intrasynaptic CB_1R signaling is a central determinant of retrograde synaptic signaling, and that it remained unaffected in CB_1R HET mice despite the substantial reduction in total CB_1R levels, we reasoned that it is important to determine whether THC administration affects the nanodomain-specific CB_1R activity in the active zone. Notably, we observed a strong

decrease in the intra/perisynaptic CB_1R population and in the nanoscale stoichiometry parameter after THC treatment. Consequently, the synaptic cannabinoid tone was completely absent and synaptic variability was strongly reduced. As genetic deletion of CB_1Rs specifically from inhibitory neurons can reduce hippocampal long-term potentiation and rescue the memory impairment effects caused by acute and chronic THC administration (Monory et al., 2015; Puighermanal et al., 2009, 2013), it would be interesting to test in further studies how precise receptor stoichiometries contribute to these memory-related maladaptive processes that arise after marijuana consumption. Overall, our results highlight the importance of not only cell-type, but also cellular nanodomain specific investigations to reveal clinically and physiologically relevant functional consequences of substance abuse and drug use.

6. Conclusions

In this thesis, we examined the quantitative organizational principle of retrograde cannabinoid signaling in a specific hippocampal inhibitory synapse between CB_1BC and PCs. Our main conclusions are the following:

At CB_1BC – PC synapses, synaptic variability is set by multiple factors, including target cell-specific anatomical properties, presynaptic molecular features (expression of specific calcium-binding proteins) and retrograde signaling pathways.

Tonic cannabinoid signaling at these synapses is independently regulated from the two main endocannabinoid ligand-synthesizing enzymes, DAGLα and NAPE-PLD.

We developed an approach for the direct measurement of synaptic physiological signals, morphological parameters, and nanoscale receptor distributions within a single identified synapse in complex mammalian brain circuit. Using this approach, we demonstrated that the precise nanoscale stoichiometry of CB_1R/effector ratio controls neurotransmitter release probability and synaptic variability (Figure 21/a).

We found that CB_1R levels are reduced in CB_1R HET mice, however, the reduction primarily affects the extrasynaptic nanodomains of CB_1BC boutons, hence, not disrupting intrasynaptic nanoscale receptor stoichiometry (Figure 21/b).

In vivo drug administration animal models provide evidence that THC, the psychoactive substance of marijuana, dismantles the presynaptic nanoscale architecture and cancels the synaptic cannabinoid tone, but only mildly affect phasic endocannabinoid signaling (Figure 21/b).

Altogether, these findings indicate a striking versatility of the retrograde cannabinoid signaling and contribute to further understanding of how synapses are regulated by GPCRs, not only cell type-specifically, but also in a synapse and synaptic nanodomain specific manner.

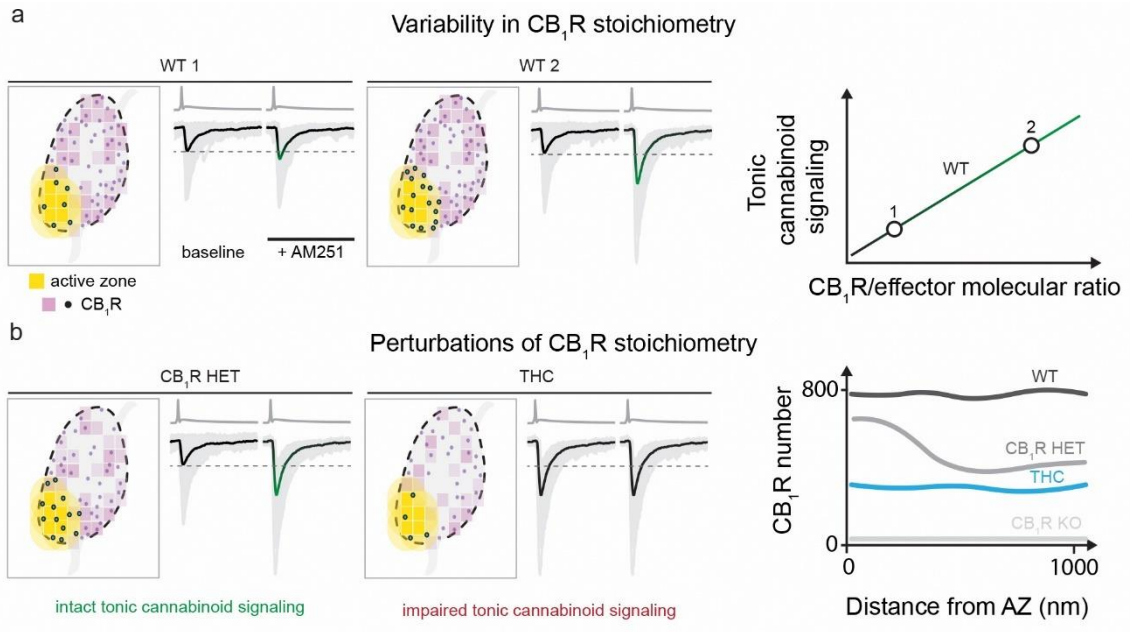

Figure 21. ***Summary about the proposed molecular logic of tonic cannabinoid signaling at CB$_1$BC – PC synapses.*** **a)** Under physiological conditions, variations in the number of CB$_1$Rs in the close vicinity of the synaptic active zone and their stoichiometric relation to the effector molecules (VGCCs) determine the magnitude of tonic cannabinoid signaling. **b)** Genetic and pharmacological perturbations can alter CB$_1$R numbers. In CB$_1$R HET mice receptor numbers are reduced compared to WT littermates, however, the reduction primarily affects regions further away from the active zone. Since CB$_1$Rs around the synapse remained intact, tonic cannabinoid signaling is not affected. On the contrary, chronic administration of THC in mice reduces receptor levels both on synaptic and extrasynaptic areas of the bouton. Electrophysiological experiments showed impaired tonic cannabinoid signaling in samples derived from these mice.

7. Summary

Neurotransmission in the brain is achieved through delicate cooperation between distinct molecular machineries, which are segregated into functionally different, spatially aligned nanodomains at both excitatory and inhibitory synapses. Precise and specific arrangement of these molecular complexes allows the fine regulation of the neurotransmitter release probability, which defines the strength of the synapse. While our quantitative understanding of the molecular architecture that determines anterograde synaptic transmission is rapidly expanding, the nanoscale functional organization of retrograde synaptic communication remains elusive.

In this study, we show that a specific form of retrograde cannabinoid signaling is essential for setting target cell-dependent synaptic variability at hippocampal inhibitory synapses. Importantly, it does not require the activity of the two major endocannabinoid-producing enzymes diacylglycerol lipase-α (DAGLα) and N-acyl phosphatidylethanolamine phospholipase D (NAPE-PLD). By developing a workflow for the measurement of physiological, anatomical, and molecular parameters at the same unitary synapse, we demonstrate that the nanoscale stoichiometric ratio of CB_1 receptors (CB_1R) to the release machinery is sufficient to predict synapse-specific release probability. Accordingly, selective extrasynaptic CB_1R reduction does not affect synaptic transmission, whereas *in vivo* treatment by the psychoactive phytocannabinoid Δ^9-tetrahydrocannabinol (THC) disrupts the intrasynaptic nanoscale stoichiometry and reduces synaptic variability. Our results imply that synapses leverage the nanoscale stoichiometry of presynaptic receptor coupling to the release machinery to establish synaptic strength in a target cell-dependent manner. These findings provide insights into the molecular tolerance mechanisms underlying cannabis use disorder and highlight that nanodomain-specific molecular imaging is essential to understand the physiological consequences of drug effects.

8. Összefoglalás

Az idegsejtek között végbemenő neurotranszmisszió egy rendkívül precíz és összetett molekuláris szerveződés eredménye. A folyamatot szabályozó különböző fehérjék térben és időben is nanoskálán mérhető összehangolt munkával képesek kivitelezni az információtovábbítást serkentő és gátló szinapszisoknál egyaránt. Ezen molekuláris komplexek precíz és specifikus elrendeződése teszi lehetővé a neurotranszmitter felszabadulás finomhangolását, amely meghatározza az adott szinapszis erősségét. Bár az anterográd szinaptikus transzmissziót meghatározó kvantitatív szabályszerűségekre egyre nagyobb rálátást nyertünk az utóbbi időben, a retrográd szinaptikus kommunikáció nanoskálájú funkcionális szerveződési elvei még ismeretlenek.

Ebben a tanulmányban megmutatjuk, hogy a retrográd kannabinoid jelátvitel egy speciális formája nélkülözhetetlen a posztszinaptikus sejt-specifikus szinaptikus variancia beállításához a hippokampális gátló szinapszisoknál. Meglepő módon ez a jelátvitel független a két főbb endokannabinoid ligand szintetizáló enzim (diacilglicerin lipáz-α (DAGLα) és N-acil foszfatidiletanolamin foszfolipáz D (NAPE-PLD)) aktivitásától. Egy olyan módszer kifejlesztésével, amely lehetővé tette a fiziológiai, anatómiai és molekuláris paraméterek vizsgálatát a kompakt agyszövetben található egyedi szinapszisokon, megmutattuk, hogy a CB_1 receptorok (CB_1R) és a vezikulafelszabadulást szabályozó molekulák nanoskálájú sztöchiometrikus aránya meghatározza az adott szinapszisban a vezikulafelszabadulás valószínűségét. Ezzel megegyezően, szelektív extraszinaptikus csökkenés a CB_1R szintben nem befolyásolja a szinaptikus transzmissziót, míg a marihuána pszichoaktív összetevőjének (Δ^9-tetrahidrokannabinol, THC) *in vivo* alkalmazása rombolja az intraszinaptikus receptor sztöchiometriát, ezáltal csökkenti a szinaptikus variabilitást. Az eredmények alapján a szinapszisok egyedileg szabályozzák a preszinaptikus receptorok nanoskálájú elrendeződését a vezikulafelszabadulást szabályozó molekulák helyzetéhez képest, hogy sejt-specifikusan beállíthassák ezáltal a szinaptikus erősséget. Emellett az eredmények továbbá rámutatnak a kannabisz használat következtében kialakuló molekuláris tolerancia mechanizmusára hangsúlyozva, hogy az idegsejteknél a nanodomén-specifikus molekuláris képalkotás nélkülözhetetlen ahhoz, hogy pontos képet kapjunk a gyógyszerek hatásainak fiziológiai következményeiről az agyban.

9. References

Acsády, L., and Káli, S. (2007). Models, structure, function: the transformation of cortical signals in the dentate gyrus. *Prog. Brain Res.*, *163*, 577–599. https://doi.org/10.1016/S0079-6123(07)63031-3

Acsády, L., Kamondi, A., Sík, A., Freund, T., and Buzsáki, G. (1998). GABAergic cells are the major postsynaptic targets of mossy fibers in the rat hippocampus. *J. Neurosci.*, *18*(9), 3386–3403. http://www.ncbi.nlm.nih.gov/pubmed/9547246

Ahn, K., McKinney, M. K., and Cravatt, B. F. (2008). Enzymatic pathways that regulate endocannabinoid signaling in the nervous system. *Chem. Rev.*, *108*(5), 1687–1707. https://doi.org/10.1021/cr0782067

Aitchison, L., Jegminat, J., Menendez, J. A., Pfister, J.-P., Pouget, A., and Latham, P. E. (2021). Synaptic plasticity as Bayesian inference. *Nat. Neurosci.*, *24*(4), 565–571. https://doi.org/10.1038/s41593-021-00809-5

Alger, B. E. (2012). Endocannabinoids at the synapse a decade after the dies mirabilis (29 March 2001): What we still do not know. *J. Physiol.*, *590*(10), 2203–2212. https://doi.org/10.1113/jphysiol.2011.220855

Alger, B. E., and Kim, J. (2011). Supply and demand for endocannabinoids. *Trends Neurosci.*, *34*(6), 304–315. https://doi.org/10.1016/j.tins.2011.03.003

Ali, A. B., and Todorova, M. (2010). Asynchronous release of GABA via tonic cannabinoid receptor activation at identified interneuron synapses in rat CA1. *Eur. J. Neurosci.*, *31*(7), 1196–1207. https://doi.org/10.1111/j.1460-9568.2010.07165.x

Alkaitis, M. S., Solorzano, C., Landry, R. P., Piomelli, D., Deleo, J. A., and Romero-Sandoval, E. A. (2010). Evidence for a role of endocannabinoids, astrocytes and p38 phosphorylation in the resolution of postoperative pain. *PLoS One*, *5*(5). https://doi.org/10.1371/journal.pone.0010891

Allen, N. J., and Lyons, D. A. (2018). Glia as architects of central nervous system formation and function. *Science (80-.).*, *362*(6411), 181–185.

Alpár, A., Attems, J., Mulder, J., Hökfelt, T., and Harkany, T. (2012). The renaissance of Ca 2+-binding proteins in the nervous system: Secretagogin takes center stage. *Cell. Signal.*, *24*(2), 378–387. https://doi.org/10.1016/j.cellsig.2011.09.028

Andersen, P., Morris, R., Amaral, D., Bliss, T., and O'Keefe, J. (2007). *The hippocampus book*. Oxford University Press, USA.

Anderson, G. R., Aoto, J., Tabuchi, K., Földy, C., Covy, J., Yee, A. X., Wu, D., Lee, S.-J. J., Chen, L., Malenka, R. C., and Südhof, T. C. (2015). β-Neurexins Control Neural Circuits by Regulating Synaptic Endocannabinoid Signaling. *Cell*, *162*(3), 593–606. https://doi.org/10.1016/j.cell.2015.06.056

Augustin, I., Rosenmund, C., Südhof, T. C., and Brose, N. (1999). Munc13-1 is essential for fusion competence of glutamatergic synaptic vesicles. *Nature*, *400*(6743), 457–461. https://doi.org/10.1038/22768

Bacaj, T., Wu, D., Yang, X., Morishita, W., Zhou, P., Xu, W., Malenka, R. C., and Südhof, T. C. (2013). Synaptotagmin-1 and Synaptotagmin-7 Trigger Synchronous and Asynchronous Phases of Neurotransmitter Release. *Neuron*, *80*(4), 947–959. https://doi.org/10.1016/j.neuron.2013.10.026

Baggelaar, M. P., Maccarrone, M., and van der Stelt, M. (2018). 2-Arachidonoylglycerol: A signaling lipid with manifold actions in the brain. *Prog. Lipid Res.*, *71*, 1–17. https://doi.org/10.1016/j.plipres.2018.05.002

Barna, L., Dudok, B., Miczán, V., Horváth, A., László, Z. I., and Katona, I. (2016). Correlated confocal and super-resolution imaging by VividSTORM. *Nat. Protoc.*, *11*(1), 163–183. https://doi.org/10.1038/nprot.2016.002

Barti, B., Dudok, B., Kenesei, K., Zöldi, M., Miczán, V., Balla, G. Y., Zala, D., Tasso, M., Sagheddu, C., Kisfali, M., Tóth, B., Ledri, M., Vizi, E. S., Melis, M., Barna, L., Lenkei, Z., Soltész, I., and Katona, I. (2024). Presynaptic nanoscale components of retrograde synaptic signaling. *Sci. Adv.*, *10*(22). https://doi.org/10.1126/sciadv.ado0077

Baur, R., Gertsch, J., and Sigel, E. (2012). The cannabinoid CB1 receptor antagonists rimonabant (SR141716) and AM251 directly potentiate GABAA receptors. *Br. J. Pharmacol.*, *165*(8), 2479–2484. https://doi.org/10.1111/j.1476-5381.2011.01405.x

Benito, C., Tolón, R. M., Pazos, M. R., Núñez, E., Castillo, A. I., and Romero, J. (2008). Cannabinoid CB 2 receptors in human brain inflammation. *Br. J. Pharmacol.*, *153*(2), 277–285. https://doi.org/10.1038/sj.bjp.0707505

Bernier, G., Vukovich, W., Neidhardt, L., Herrmann, B. G., and Gruss, P. (2001). Isolation and characterization of a downstream target of Pax6 in the mammalian retinal primordium. *Development, 128*(20), 3987–3994.

Biederer, T., Kaeser, P. S., and Blanpied, T. A. (2017). Transcellular Nanoalignment of Synaptic Function. *Neuron, 96*(3), 680–696. https://doi.org/10.1016/j.neuron.2017.10.006

Biro, A. A., Holderith, N. B., and Nusser, Z. (2006). Release Probability-Dependent Scaling of the Postsynaptic Responses at Single Hippocampal GABAergic Synapses. *J. Neurosci., 26*(48), 12487–12496. https://doi.org/10.1523/JNEUROSCI.3106-06.2006

Bisogno, T., Howell, F., Williams, G., Minassi, A., Cascio, M. G., Ligresti, A., Matias, I., Schiano-Moriello, A., Paul, P., Williams, E.-J., Gangadharan, U., Hobbs, C., Di Marzo, V., and Doherty, P. (2003). Cloning of the first sn1-DAG lipases points to the spatial and temporal regulation of endocannabinoid signaling in the brain. *J. Cell Biol., 163*(3), 463–468. https://doi.org/10.1083/jcb.200305129

Blankman, J. L., Simon, G. M., and Cravatt, B. F. (2007). A Comprehensive Profile of Brain Enzymes that Hydrolyze the Endocannabinoid 2-Arachidonoylglycerol. *Chem. Biol., 14*(12), 1347–1356. https://doi.org/10.1016/j.chembiol.2007.11.006

Bloodgood, B. L., Sharma, N., Browne, H. A., Trepman, A. Z., and Greenberg, M. E. (2013). The activity-dependent transcription factor NPAS4 regulates domain-specific inhibition. *Nature, 503*(7474), 121–125. https://doi.org/10.1038/nature12743

Booker, S. A., Althof, D., Degro, C. E., Watanabe, M., Kulik, Á., and Vida, I. (2017). Differential surface density and modulatory effects of presynaptic GABAB receptors in hippocampal cholecystokinin and parvalbumin basket cells. *Brain Struct. Funct., 222*(8), 3677–3690. https://doi.org/10.1007/s00429-017-1427-x

Branco, T., and Staras, K. (2009). The probability of neurotransmitter release: variability and feedback control at single synapses. *Nat. Rev. Neurosci., 10*(5), 373–383. https://doi.org/10.1038/nrn2634

Branco, T., Staras, K., Darcy, K. J., and Goda, Y. (2008). Local Dendritic Activity Sets

Release Probability at Hippocampal Synapses. *Neuron*, *59*(3), 475–485. https://doi.org/10.1016/j.neuron.2008.07.006

Bugeon, S., Duffield, J., Dipoppa, M., Ritoux, A., Prankerd, I., Nicoloutsopoulos, D., Orme, D., Shinn, M., Peng, H., Forrest, H., Viduolyte, A., Reddy, C. B., Isogai, Y., Carandini, M., and Harris, K. D. (2022). A transcriptomic axis predicts state modulation of cortical interneurons. *Nature*, *607*(7918), 330–338. https://doi.org/10.1038/s41586-022-04915-7

Busquets-Garcia, A., Desprez, T., Metna-Laurent, M., Bellocchio, L., Marsicano, G., and Soria-Gomez, E. (2015). Dissecting the cannabinergic control of behavior: The where matters. *BioEssays*, *37*(11), 1215–1225. https://doi.org/10.1002/bies.201500046

Busquets-Garcia, A., Oliveira da Cruz, J. F., Terral, G., Zottola, A. C. P., Soria-Gómez, E., Contini, A., Martin, H., Redon, B., Varilh, M., Ioannidou, C., Drago, F., Massa, F., Fioramonti, X., Trifilieff, P., Ferreira, G., and Marsicano, G. (2018). Hippocampal CB1 Receptors Control Incidental Associations. *Neuron*, *99*(6), 1247-1259.e7. https://doi.org/10.1016/j.neuron.2018.08.014

Buzsáki, G., and Moser, E. I. (2013). Memory, navigation and theta rhythm in the hippocampal-entorhinal system. *Nat. Neurosci.*, *16*(2), 130–138. https://doi.org/10.1038/nn.3304

Castillo, P., Schoch, S., Schmitz, F., Südhof, T. C., and Malenka, R. C. (2002). RIM1 α is required for presynaptic long-term potentiation. *Nature*, *415*(6869), 327–330. https://doi.org/Doi 10.1038/415327a

Cembrowski, M. S., Bachman, J. L., Wang, L., Sugino, K., Shields, B. C., Cembrowski, M. S., Bachman, J. L., Wang, L., Sugino, K., Shields, B. C., and Spruston, N. (2016). Spatial Gene-Expression Gradients Underlie Prominent Heterogeneity of CA1 Pyramidal Neurons Article Spatial Gene-Expression Gradients Underlie Prominent Heterogeneity of CA1 Pyramidal Neurons. *Neuron*, *89*(2), 351–368. https://doi.org/10.1016/j.neuron.2015.12.013

Chandra, S., Radwan, M. M., Majumdar, C. G., Church, J. C., Freeman, T. P., and ElSohly, M. A. (2019). New trends in cannabis potency in USA and Europe during

the last decade (2008–2017). *Eur. Arch. Psychiatry Clin. Neurosci.*, *269*(1), 5–15. https://doi.org/10.1007/s00406-019-00983-5

Chen, C., Arai, I., Satterfield, R., Young, S. M., and Jonas, P. (2017). Synaptotagmin 2 Is the Fast Ca 2+ Sensor at a Central Inhibitory Synapse. *Cell Rep.*, *18*(3), 723–736. https://doi.org/10.1016/j.celrep.2016.12.067

Chen, K., Ratzliff, A., Hilgenberg, L., Gulyás, A., Freund, T. F., Smith, M., Dinh, T. P., Piomelli, D., Mackie, K., and Soltesz, I. (2003). Long-Term Plasticity of Endocannabinoid Signaling Induced by Developmental Febrile Seizures. *Neuron*, *39*(4), 599–611. https://doi.org/10.1016/S0896-6273(03)00499-9

Chevaleyre, V., and Castillo, P. E. (2003). Heterosynaptic LTD of hippocampal GABAergic synapses: A novel role of endocannabinoids in regulating excitability. *Neuron*, *38*(3), 461–472. https://doi.org/10.1016/S0896-6273(03)00235-6

Chevaleyre, V., Heifets, B. D., Kaeser, P. S., Südhof, T. C., Purpura, D. P., and Castillo, P. E. (2007). Endocannabinoid-Mediated Long-Term Plasticity Requires cAMP/PKA Signaling and RIM1α. *Neuron*, *54*(5), 801–812. https://doi.org/10.1016/j.neuron.2007.05.020

Chevaleyre, V., Takahashi, K. A., and Castillo, P. E. (2006). Endocannabinoid-Mediated Synaptic Plasticity in the Cns. *Annu. Rev. Neurosci.*, *29*(1), 37–76. https://doi.org/10.1146/annurev.neuro.29.051605.112834

Choquet, D., and Triller, A. (2013). The dynamic synapse. *Neuron*, *80*(3), 691–703. https://doi.org/10.1016/j.neuron.2013.10.013

Clements, J. D., and Silver, R. A. (2000). Unveiling synaptic plasticity: A new graphical and analytical approach. *Trends Neurosci.*, *23*(3), 105–113. https://doi.org/10.1016/S0166-2236(99)01520-9

Cobb, S. R., Buhl, E. H., Halasy, K., Paulsen, O., and Somogyi, P. (1995). Synchronization of neuronal activity in hippocampus by individual GABAergic interneurons. *Nature*, *378*(6552), 75–78. https://doi.org/10.1038/378075a0

Cravatt, B. F., Giang, D. K., Mayfield, S. P., Boger, D. L., Lerner, R. A., and Gilula, N. B. (1996). Molecular characterization of an enzyme that degrades neuromodulatory fatty-acid amides. *Nature*, *384*(7), 83–87. https://doi.org/10.1038/384083a0

Cristino, L., Starowicz, K., De Petrocellis, L., Morishita, J., Ueda, N., Guglielmotti, V., and Di Marzo, V. (2008). Immunohistochemical localization of anabolic and catabolic enzymes for anandamide and other putative endovanilloids in the hippocampus and cerebellar cortex of the mouse brain. *Neuroscience*, *151*(4), 955–968. https://doi.org/10.1016/j.neuroscience.2007.11.047

Dani, A., Huang, B., Bergan, J., Dulac, C., and Zhuang, X. (2010). Superresolution Imaging of Chemical Synapses in the Brain. *Neuron*, *68*(5), 843–856. https://doi.org/10.1016/j.neuron.2010.11.021

Davydova, D., Marini, C., King, C., Klueva, J., Bischof, F., Romorini, S., Montenegro-Venegas, C., Heine, M., Schneider, R., Schröder, M. S., Altrock, W. D., Henneberger, C., Rusakov, D. A., Gundelfinger, E. D., and Fejtova, A. (2014). Bassoon specifically controls presynaptic P/Q-type Ca2+ channels via RIM-binding protein. *Neuron*, *82*(1), 181–194. https://doi.org/10.1016/j.neuron.2014.02.012

De Robertis, E. D., and Bennett, H. S. (1955). Some features of the submicroscopic morphology of synapses in frog and earthworm. *J. Biophys. Biochem. Cytol.*, *1*(1), 47–58. https://doi.org/10.1083/jcb.1.1.47

Del Castillo, J., and Katz, B. (1954). Quantal Components of the End-Plate Potential. *J. Physiol*, *124*(3), 560–573. https://doi.org/10.1016/j.neuron.2009.06.014

del Pino, I., Brotons-Mas, J. R., Marques-Smith, A., Marighetto, A., Frick, A., Marín, O., and Rico, B. (2017). Abnormal wiring of CCK+ basket cells disrupts spatial information coding. *Nat. Neurosci.*, *20*(6), 784–792. https://doi.org/10.1038/nn.4544

Devane, W. A., Hanuš, L., Breuer, A., Pertwee, R. G., Lesley, A., Griffin, G., Gibson, D., Mandelbaum, A., and Etinger, A. (1992). Isolation and Structure of a Brain Constituent That Binds to the Cannabinoid Receptor. *Science (80-.).*, *258*(5090), 1946–1949.

Di Marzo, V. (2018). New approaches and challenges to targeting the endocannabinoid system. *Nat. Rev. Drug Discov.* https://doi.org/10.1038/nrd.2018.115

Diering, G. H., and Huganir, R. L. (2018). The AMPA Receptor Code of Synaptic

Plasticity. *Neuron*, *100*(2), 314–329. https://doi.org/10.1016/j.neuron.2018.10.018

Dittman, J. S., and Ryan, T. A. (2019). The control of release probability at nerve terminals. *Nat. Rev. Neurosci.*, *20*(3), 177–186. https://doi.org/10.1038/s41583-018-0111-3

Doischer, D., Hosp, J. A., Yanagawa, Y., Obata, K., Jonas, P., Vida, I., and Bartos, M. (2008). Postnatal differentiation of basket cells from slow to fast signaling devices. *J. Neurosci.*, *28*(48), 12956–12968. https://doi.org/10.1523/JNEUROSCI.2890-08.2008

Dudok, B., Barna, L., Ledri, M., Szabó, S. I., Szabadits, E., Pintér, B., Woodhams, S. G., Henstridge, C. M., Balla, G. Y., Nyilas, R., Varga, C., Lee, S.-H., Matolcsi, M., Cervenak, J., Kacskovics, I., Watanabe, M., Sagheddu, C., Melis, M., Pistis, M., … Katona, I. (2015). Cell-specific STORM super-resolution imaging reveals nanoscale organization of cannabinoid signaling. *Nat. Neurosci.*, *18*(1), 75–86. https://doi.org/10.1038/nn.3892

Dudok, B., Fan, L. Z., Farrell, J. S., Malhotra, S., Homidan, J., Kim, D. K., Wenardy, C., Ramakrishnan, C., Li, Y., Deisseroth, K., and Soltesz, I. (2024). Retrograde endocannabinoid signaling at inhibitory synapses in vivo. *Science (80-.).*, *383*(6686), 967–970. https://doi.org/10.1126/science.adk3863

Dudok, B., Klein, P. M., Hwaun, E., Lee, B. R., Yao, Z., Fong, O., Bowler, J. C., Terada, S., Sparks, F. T., Szabo, G. G., Farrell, J. S., Berg, J., Daigle, T. L., Tasic, B., Dimidschstein, J., Fishell, G., Losonczy, A., Zeng, H., and Soltesz, I. (2021). Alternating sources of perisomatic inhibition during behavior. *Neuron*, *109*(6), 997-1012.e9. https://doi.org/10.1016/j.neuron.2021.01.003

Dunn, H. A., Orlandi, C., and Martemyanov, K. A. (2019). Beyond the Ligand: Extracellular and Transcellular G Protein–Coupled Receptor Complexes in Physiology and Pharmacology. *Pharmacol. Rev.*, *71*(4), 503–519. https://doi.org/10.1124/pr.119.018044

Durkee, C. A., and Araque, A. (2019). Diversity and Specificity of Astrocyte–neuron Communication. *Neuroscience*, *396*(612), 73–78. https://doi.org/10.1016/j.neuroscience.2018.11.010

Dvorzhak, A., Semtner, M., Faber, D. S., and Grantyn, R. (2013). Tonic mGluR5/CB1-dependent suppression of inhibition as a pathophysiological hallmark in the striatum of mice carrying a mutant form of huntingtin. *J. Physiol.*, *591*(4), 1145–1166. https://doi.org/10.1113/jphysiol.2012.241018

Eggermann, E., Bucurenciu, I., Goswami, S. P., and Jonas, P. (2012). Nanodomain coupling between Ca2+ channels and sensors of exocytosis at fast mammalian synapses. *Nat. Rev. Neurosci.*, *13*(1), 7–21. https://doi.org/10.1038/nrn3125

Eggermann, E., and Jonas, P. (2012). How the "slow" Ca 2+ buffer parvalbumin affects transmitter release in nanodomain-coupling regimes. *Nat. Neurosci.*, *15*(1), 20–22. https://doi.org/10.1038/nn.3002

Evstratova, A., and Tóth, K. (2014). Information processing and synaptic plasticity at hippocampal mossy fiber terminals. *Front. Cell. Neurosci.*, *8*(FEB), 7–12. https://doi.org/10.3389/fncel.2014.00028

Falenski, K. W., Carter, D. S., Harrison, A. J., Martin, B. R., Blair, R. E., and DeLorenzo, R. J. (2009). Temporal characterization of changes in hippocampal cannabinoid CB1 receptor expression following pilocarpine-induced status epilepticus. *Brain Res.*, *1262*, 64–72. https://doi.org/10.1016/j.brainres.2009.01.036

Fanselow, M. S., and Dong, H. W. (2010). Are the Dorsal and Ventral Hippocampus Functionally Distinct Structures? *Neuron*, *65*(1), 7–19. https://doi.org/10.1016/j.neuron.2009.11.031

Farrell, J. S., Colangeli, R., Dong, A., George, A. G., Addo-Osafo, K., Kingsley, P. J., Morena, M., Wolff, M. D., Dudok, B., He, K., Patrick, T. A., Sharkey, K. A., Patel, S., Marnett, L. J., Hill, M. N., Li, Y., Teskey, G. C., and Soltesz, I. (2021). In vivo endocannabinoid dynamics at the timescale of physiological and pathological neural activity. *Neuron*, *109*(15), 2398-2403.e4. https://doi.org/10.1016/j.neuron.2021.05.026

Fatt, P., and Katz, B. (1952). Spontaneous subthreshold activity at motor nerve endings. *J. Physiol.*, *117*(1), 109–128. https://doi.org/10.1007/978-4-431-55750-0_3

Fauth, M., and Tetzlaff, C. (2016). Opposing effects of neuronal activity on structural

plasticity. *Front. Neuroanat.*, *10*(JUNE), 1–18. https://doi.org/10.3389/fnana.2016.00075

Ferland, J. M. N., and Hurd, Y. L. (2020). Deconstructing the neurobiology of cannabis use disorder. *Nat. Neurosci.*, *23*(5), 600–610. https://doi.org/10.1038/s41593-020-0611-0

Fernández-Chacón, R., Königstorfer, A., Gerber, S. H., García, J., Matos, M. F., Stevens, C. F., Brose, N., Rizo, J., Rosenmund, C., and Südhof, T. C. (2001). Synaptotagmin I functions as a calcium regulator of release probability. *Nature*, *410*(6824), 41–49. https://doi.org/10.1038/35065004

Földy, C., Malenka, R. C., and Südhof, T. C. (2013). Autism-associated neuroligin-3 mutations commonly disrupt tonic endocannabinoid signaling. *Neuron*, *78*(3), 498–509. https://doi.org/10.1016/j.neuron.2013.02.036

Földy, C., Neu, A., Jones, M. V., and Soltesz, I. (2006). Presynaptic, Activity-Dependent Modulation of Cannabinoid Type 1 Receptor-Mediated Inhibition of GABA Release. *J. Neurosci.*, *26*(5), 1465–1469. https://doi.org/10.1523/JNEUROSCI.4587-05.2006

Frau, R., Miczán, V., Traccis, F., Aroni, S., Pongor, C. I., Saba, P., Serra, V., Sagheddu, C., Fanni, S., Congiu, M., Devoto, P., Cheer, J. F., Katona, I., and Melis, M. (2019). Prenatal THC exposure produces a hyperdopaminergic phenotype rescued by pregnenolone. *Nat. Neurosci.*, *22*(12), 1975–1985. https://doi.org/10.1038/s41593-019-0512-2

Freund, T. F., and Buzsáki, G. (1996). Interneurons of the Hippocampus. *Hippocampus*. https://doi.org/10.1002/(SICI)1098-1063(1996)6:43.0.CO;2-I

Freund, T. F., and Katona, I. (2007). Perisomatic Inhibition. *Neuron*, *56*(1), 33–42. https://doi.org/10.1016/j.neuron.2007.09.012

Fukaya, M., Uchigashima, M., Nomura, S., Hasegawa, Y., Kikuchi, H., and Watanabe, M. (2008). Predominant expression of phospholipase Cβ1 in telencephalic principal neurons and cerebellar interneurons, and its close association with related signaling molecules in somatodendritic neuronal elements. *Eur. J. Neurosci.*, *28*(9), 1744–1759. https://doi.org/10.1111/j.1460-9568.2008.06495.x

Fukudome, Y., Ohno-Shosaku, T., Matsui, M., Omori, Y., Fukaya, M., Tsubokawa, H., Taketo, M. M., Watanabe, M., Manabe, T., and Kano, M. (2004). Two distinct classes of muscarinic action on hippocampal inhibitory synapses: M2-mediated direct suppression and M1/M3-mediated indirect suppression through endocannabinoid signalling. *Eur. J. Neurosci.*, *19*(10), 2682–2692. https://doi.org/10.1111/j.0953-816X.2004.03384.x

Gaffuri, A.-L., Ladarre, D., and Lenkei, Z. (2012). Type-1 Cannabinoid Receptor Signaling in Neuronal Development. *Pharmacology*, *90*(1–2), 19–39. https://doi.org/10.1159/000339075

Gao, Y., Vasilyev, D. V., Goncalves, M. B., Howell, F. V., Hobbs, C., Reisenberg, M., Shen, R., Zhang, M.-Y., Strassle, B. W., Lu, P., Mark, L., Piesla, M. J., Deng, K., Kouranova, E. V., Ring, R. H., Whiteside, G. T., Bates, B., Walsh, F. S., Williams, G., … Doherty, P. (2010). Loss of Retrograde Endocannabinoid Signaling and Reduced Adult Neurogenesis in Diacylglycerol Lipase Knock-out Mice. *J. Neurosci.*, *30*(6), 2017–2024. https://doi.org/10.1523/JNEUROSCI.5693-09.2010

Gaston, T. E., and Friedman, D. (2017). Pharmacology of cannabinoids in the treatment of epilepsy. *Epilepsy Behav.*, *70*, 313–318. https://doi.org/10.1016/j.yebeh.2016.11.016

Glebov, O. O., Jackson, R. E., Winterflood, C. M., Owen, D. M., Barker, E. A., Doherty, P., Ewers, H., and Burrone, J. (2017). Nanoscale Structural Plasticity of the Active Zone Matrix Modulates Presynaptic Function. *Cell Rep.*, *18*(11), 2715–2728. https://doi.org/10.1016/j.celrep.2017.02.064

Glickfeld, L. L., and Scanziani, M. (2006). Distinct timing in the activity of cannabinoid-sensitive and cannabinoid-insensitive basket cells. *Nat. Neurosci.*, *9*(6), 807–815. https://doi.org/10.1038/nn1688

Gray, E. G. (1959). Axo-somatic and axo-dendritic synapses of the cerebral cortex: an electron microscope study. *J. Anat.*, *93*(4), 420–433. https://doi.org/10.1016/B978-0-12-801426-4.05001-X

Gulyas, A. I., Cravatt, B. F., Bracey, M. H., Dinh, T. P., Piomelli, D., Boscia, F., and Freund, T. F. (2004). Segregation of two endocannabinoid-hydrolyzing enzymes

into pre- and postsynaptic compartments in the rat hippocampus, cerebellum and amygdala. *Eur. J. Neurosci.*, *20*(2), 441–458. https://doi.org/10.1111/j.1460-9568.2004.03428.x

Haj-Dahmane, S., Shen, R.-Y. Y., Elmes, M. W., Studholme, K., Kanjiya, M. P., Bogdan, D., Thanos, P. K., Miyauchi, J. T., Tsirka, S. E., Deutsch, D. G., Kaczocha, M., Fauzan, M., Oubraim, S., Yu, M., Glaser, S. T., Kaczocha, M., and Haj-Dahmane, S. (2018). Fatty-acid–binding protein 5 controls retrograde endocannabinoid signaling at central glutamate synapses. *Proc. Natl. Acad. Sci.*, *115*(13), 3482–3487. https://doi.org/10.1073/pnas.1721339115

Hallermann, S., Fejtova, A., Schmidt, H., Weyhersmüller, A., Silver, R. A., Gundelfinger, E. D., and Eilers, J. (2010). Bassoon speeds vesicle reloading at a central excitatory synapse. *Neuron*, *68*(4), 710–723. https://doi.org/10.1016/j.neuron.2010.10.026

Hänggi, P. (2002). Stochastic resonance in biology: How noise can enhance detection of weak signals and help improve biological information processing. *ChemPhysChem*, *3*(3), 285–290. https://doi.org/10.1002/1439-7641(20020315)3:3<285::AID-CPHC285>3.0.CO;2-A

Harkany, T., Guzmán, M., Galve-Roperh, I., Berghuis, P., Devi, L. A., and Mackie, K. (2007). The emerging functions of endocannabinoid signaling during CNS development. *Trends Pharmacol. Sci.*, *28*(2), 83–92. https://doi.org/10.1016/j.tips.2006.12.004

Harris, K. D., Hochgerner, H., Skene, N. G., Magno, L., Katona, L., Bengtsson Gonzales, C., Somogyi, P., Kessaris, N., Linnarsson, S., and Hjerling-Leffler, J. (2018). Classes and continua of hippocampal CA1 inhibitory neurons revealed by single-cell transcriptomics. *PLOS Biol.*, *16*(6), e2006387. https://doi.org/10.1371/journal.pbio.2006387

Harris, K. M., and Weinberg, R. J. (2012). Ultrastructure of synapses in the mammalian brain. *Cold Spring Harb. Perspect. Biol.*, *4*(5), 7. https://doi.org/10.1101/cshperspect.a005587

Hartzell, A. L., Martyniuk, K. M., Brigidi, G. S., Heinz, D. A., Djaja, N. A., Payne, A.,

and Bloodgood, B. L. (2018). NPAS4 recruits CCK basket cell synapses and enhances cannabinoid-sensitive inhibition in the mouse hippocampus. *Elife*, *7*, 1–24. https://doi.org/10.7554/eLife.35927.001

Hashimotodani, Y., Ohno-Shosaku, T., and Kano, M. (2007). Presynaptic Monoacylglycerol Lipase Activity Determines Basal Endocannabinoid Tone and Terminates Retrograde Endocannabinoid Signaling in the Hippocampus. *J. Neurosci.*, *27*(5), 1211–1219. https://doi.org/10.1523/JNEUROSCI.4159-06.2007

Hashimotodani, Y., Ohno-Shosaku, T., Tsubokawa, H., Ogata, H., Emoto, K., Maejima, T., Araishi, K., Shin, H. S., and Kano, M. (2005). Phospholipase Cβ serves as a coincidence detector through its Ca 2+ dependency for triggering retrograde endocannabinoid signal. *Neuron*, *45*(2), 257–268. https://doi.org/10.1016/j.neuron.2005.01.004

Hefft, S., and Jonas, P. (2005). Asynchronous GABA release generates long-lasting inhibition at a hippocampal interneuron–principal neuron synapse. *Nat. Neurosci.*, *8*(10), 1319–1328. https://doi.org/10.1038/nn1542

Heifets, B. D., and Castillo, P. E. (2009). Endocannabinoid Signaling and Long-Term Synaptic Plasticity. *Annu. Rev. Physiol.*, *71*(1), 283–306. https://doi.org/10.1146/annurev.physiol.010908.163149

Herlitze, S., Garcla, D. E., Mackle, K., Hille, B., Scheuer, T., and Catterall, W. A. (1996). Modulation of Ca2+ channels by G-protein βγ subunits. In *Nature* (Vol. 380, Issue 6571, pp. 258–262). https://doi.org/10.1038/380258a0

Hill, M. N., McLaughlin, R. J., Morrish, A. C., Viau, V., Floresco, S. B., Hillard, C. J., and Gorzalka, B. B. (2009). Suppression of amygdalar endocannabinoid signaling by stress contributes to activation of the hypothalamic-pituitary-adrenal axis. *Neuropsychopharmacology*, *34*(13), 2733–2745. https://doi.org/10.1038/npp.2009.114

Holderith, N., Lorincz, A., Katona, G., Rózsa, B., Kulik, A., Watanabe, M., and Nusser, Z. (2012). Release probability of hippocampal glutamatergic terminals scales with the size of the active zone. *Nat. Neurosci.*, *15*(7), 988–997. https://doi.org/10.1038/nn.3137

Holehouse, A. S., and Kragelund, B. B. (2024). The molecular basis for cellular function of intrinsically disordered protein regions. *Nat. Rev. Mol. Cell Biol.*, *25*(3), 187–211. https://doi.org/10.1038/s41580-023-00673-0

Howlett, A. C., Bidaut-Russell, M., Devane, W. A., Melvin, L. S., Johnson, M. R., and Herkenham, M. (1990). The cannabinoid receptor: biochemical, anatomical and behavioral characterization. *Trends Neurosci.*, *13*(10), 420–423. https://doi.org/10.1016/0166-2236(90)90124-S

Høydal, Ø. A., Skytøen, E. R., Andersson, S. O., Moser, M. B., and Moser, E. I. (2019). Object-vector coding in the medial entorhinal cortex. *Nature*, *568*(7752), 400–404. https://doi.org/10.1038/s41586-019-1077-7

Hsu, K. L., Tsuboi, K., Adibekian, A., Pugh, H., Masuda, K., and Cravatt, B. F. (2012). DAGLβ inhibition perturbs a lipid network involved in macrophage inflammatory responses. *Nat. Chem. Biol.*, *8*(12), 999–1007. https://doi.org/10.1038/nchembio.1105

Hu, S. S.-J., and Mackie, K. (2015). Distribution of the endocannabinoid system in the central nervous system. In *Endocannabinoids*. Springer International Publishing, Switzerland. https://doi.org/10.1007/978-3-319-20825-1

Hua, T., Vemuri, K., Nikas, S. P., Laprairie, R. B., Wu, Y., Qu, L., Pu, M., Korde, A., Jiang, S., Ho, J. H., Han, G. W., Ding, K., Li, X., Liu, H., Hanson, M. A., Zhao, S., Bohn, L. M., Makriyannis, A., Stevens, R. C., and Liu, Z. J. (2017). Crystal structures of agonist-bound human cannabinoid receptor CB 1. *Nature*, *547*(7664), 468–471. https://doi.org/10.1038/nature23272

Hua, T., Vemuri, K., Pu, M., Qu, L., Han, G. W., Wu, Y., Zhao, S., Shui, W., Li, S., Korde, A., Laprairie, R. B., Stahl, E. L., Ho, J.-H., Zvonok, N., Zhou, H., Kufareva, I., Wu, B., Zhao, Q., Hanson, M. A., … Liu, Z.-J. (2016). Crystal Structure of the Human Cannabinoid Receptor CB 1. *Cell*, *167*(3), 750–762. https://doi.org/10.1016/j.cell.2016.10.004

Huang, G. Z., and Woolley, C. S. (2012). Estradiol Acutely Suppresses Inhibition in the Hippocampus through a Sex-Specific Endocannabinoid and mGluR-Dependent Mechanism. *Neuron*, *74*(5), 801–808. https://doi.org/10.1016/j.neuron.2012.03.035

Hussain, Z., Uyama, T., Tsuboi, K., and Ueda, N. (2017). Mammalian enzymes responsible for the biosynthesis of N-acylethanolamines. *Biochim. Biophys. Acta - Mol. Cell Biol. Lipids*, *1862*(12), 1546–1561. https://doi.org/10.1016/j.bbalip.2017.08.006

Jensen, K. R., Berthoux, C., Nasrallah, K., and Castillo, P. E. (2021). Multiple cannabinoid signaling cascades powerfully suppress recurrent excitation in the hippocampus. *Proc. Natl. Acad. Sci.*, *118*(11). https://doi.org/10.1073/pnas.2102334118

Jhaveri, M. D., Richardson, D., Kendall, D. A., Barrett, D. A., and Chapman, V. (2006). Analgesic effects of fatty acid amide hydrolase inhibition in a rat model of neuropathic pain. *J. Neurosci.*, *26*(51), 13318–13327. https://doi.org/10.1523/JNEUROSCI.3326-06.2006

Jonas, P., Bischofberger, J., Fricker, D., and Miles, R. (2004). Interneuron Diversity series: Fast in, fast out - Temporal and spatial signal processing in hippocampal interneurons. *Trends Neurosci.*, *27*(1), 30–40. https://doi.org/10.1016/j.tins.2003.10.010

Josselyn, S. A., and Tonegawa, S. (2020). Memory engrams: Recalling the past and imagining the future. *Science (80-.).*, *367*(6473), eaaw4325. https://doi.org/10.1126/science.aaw4325

Jullié, D., Stoeber, M., Sibarita, J. B., Zieger, H. L., Bartol, T. M., Arttamangkul, S., Sejnowski, T. J., Hosy, E., and von Zastrow, M. (2020). A Discrete Presynaptic Vesicle Cycle for Neuromodulator Receptors. *Neuron*, *105*(4), 663-677.e8. https://doi.org/10.1016/j.neuron.2019.11.016

Jung, K.-M., Astarita, G., Zhu, C., Wallace, M., Mackie, K., and Piomelli, D. (2007). A Key Role for Diacylglycerol Lipase- in Metabotropic Glutamate Receptor-Dependent Endocannabinoid Mobilization. *Mol. Pharmacol.*, *72*(3), 612–621. https://doi.org/10.1124/mol.107.037796

Jung, K. M., Sepers, M., Henstridge, C. M., Lassalle, O., Neuhofer, D., Martin, H., Ginger, M., Frick, A., Dipatrizio, N. V., MacKie, K., Katona, I., Piomelli, D., and Manzoni, O. J. (2012). Uncoupling of the endocannabinoid signalling complex in a

mouse model of fragile X syndrome. *Nat. Commun.*, *3*. https://doi.org/10.1038/ncomms2045

Kaeser, P. S., Deng, L., Wang, Y., Dulubova, I., Liu, X., Rizo, J., and Südhof, T. C. (2011). RIM proteins tether Ca2+ channels to presynaptic active zones via a direct PDZ-domain interaction. *Cell*, *144*(2), 282–295. https://doi.org/10.1016/j.cell.2010.12.029

Kano, M. (2014). Control of synaptic function by endocannabinoid-mediated retrograde signaling. *Proc. Japan Acad. Ser. B Phys. Biol. Sci.*, *90*(7), 235–250. https://doi.org/10.2183/pjab.90.235

Kano, M., Ohno-Shosaku, T., Hashimotodani, Y., Uchigashima, M., and Watanabe, M. (2009). Endocannabinoid-Mediated Control of Synaptic Transmission. *Physiol. Rev.*, *89*(1), 309–380. https://doi.org/10.1152/physrev.00019.2008

Katona, I. (2015). Cannabis and endocannabinoid signaling in epilepsy. In Endocannabinoids. In *Handbook of Experimental Pharmoacology*. Springer International Publishing, Switzerland. https://doi.org/10.1007/978-3-319-20825-1_8

Katona, I., and Freund, T. F. (2008). Endocannabinoid signaling as a synaptic circuit breaker in neurological disease. *Nat. Med.*, *14*(9), 923–930. https://doi.org/10.1038/nm.f.1869

Katona, I., and Freund, T. F. (2012). Multiple Functions of Endocannabinoid Signaling in the Brain. *Annu. Rev. Neurosci.*, *35*(1), 529–558. https://doi.org/10.1146/annurev-neuro-062111-150420

Katona, I., Sperlágh, B., Sík, A., Käfalvi, A., Vizi, E. S., Mackie, K., and Freund, T. F. (1999). Presynaptically located CB1 cannabinoid receptors regulate GABA release from axon terminals of specific hippocampal interneurons. *J. Neurosci.*, *19*(11), 4544–4558.

Katona, I., Urbán, G. M., Wallace, M., Ledent, C., Jung, K.-M., Piomelli, D., Mackie, K., and Freund, T. F. (2006). Molecular Composition of the Endocannabinoid System at Glutamatergic Synapses. *J. Neurosci.*, *26*(21), 5628–5637. https://doi.org/10.1523/JNEUROSCI.0309-06.2006

Kawamura, Y., Fukaya, M., Maejima, T., Yoshida, T., Miura, E., Watanabe, M., Ohno-Shosaku, T., and Kano, M. (2006). The CB1 cannabinoid receptor is the major cannabinoid receptor at excitatory presynaptic sites in the hippocampus and cerebellum. *J. Neurosci.*, *26*(11), 2991–3001. https://doi.org/10.1523/JNEUROSCI.4872-05.2006

Kesner, R. P., and Rolls, E. T. (2015). A computational theory of hippocampal function, and tests of the theory: New developments. *Neurosci. Biobehav. Rev.*, *48*, 92–147. https://doi.org/10.1016/j.neubiorev.2014.11.009

Kim, J., and Alger, B. E. (2010). Reduction in endocannabinoid tone is a homeostatic mechanism for specific inhibitory synapses. *Nat. Neurosci.*, *13*(5), 592–600. https://doi.org/10.1038/nn.2517

Kisfali, M., Lorincz, T., and Vizi, E. S. (2013). Comparison of Ca2+ transients and [Ca2+]i in the dendrites and boutons of non-fast-spiking GABAergic hippocampal interneurons using two-photon laser microscopy and high- and low-affinity dyes. *J. Physiol.*, *591*(22), 5541–5553. https://doi.org/10.1113/jphysiol.2013.258863

Klausberger, T., Marton, L. F., O'Neill, J., Huck, J. H. J., Dalezios, Y., Fuentealba, P., Wai Yee Suen, E. P., Kaneko, T., Watanabe, M., Jozsef Csicsvari, and Somogyi, P. (2005). Complementary Roles of Cholecystokinin- and Parvalbumin-Expressing GABAergic Neurons in Hippocampal Network Oscillations. *J. Neurosci.*, *25*(42), 9782–9793. https://doi.org/10.1523/JNEUROSCI.3269-05.2005

Klausberger, T., and Somogyi, P. (2008). Neuronal diversity and temporal dynamics: The unity of hippocampal circuit operations. *Science (80-.).*, *321*(5885), 53–57. https://doi.org/10.1126/science.1149381

Kohara, K., Pignatelli, M., Rivest, A. J., Jung, H., Kitamura, T., Suh, J., Frank, D., Kajikawa, K., Mise, N., Obata, Y., Wickersham, I. R., and Tonegawa, S. (2013). Cell type – specific genetic and optogenetic tools reveal hippocampal CA2 circuits. *Nat. Publ. Gr.*, *17*(2), 269–279. https://doi.org/10.1038/nn.3614

Kreitzer, A. C., and Regehr, W. G. (2001). Retrograde inhibition of presynaptic calcium influx by endogenous cannabinoids at excitatory synapses onto Purkinje cells. *Neuron*, *29*(3), 717–727. https://doi.org/10.1016/S0896-6273(01)00246-X

Ladarre, D., Roland, A. B., Roland, A. B., Ricobaraza, A., and Lenkei, Z. (2015). Polarized cellular patterns of endocannabinoid production and detection shape cannabinoid signaling in neurons. *Front. Cell. Neurosci.*, *8*(JAN), 1–14. https://doi.org/10.3389/fncel.2014.00426

Laprairie, R. B., Kulkarni, P. M., Deschamps, J. R., Kelly, M. E. M., Janero, D. R., Cascio, M. G., Stevenson, L. A., Pertwee, R. G., Kenakin, T. P., Denovan-Wright, E. M., and Thakur, G. A. (2017). Enantiospecific Allosteric Modulation of Cannabinoid 1 Receptor. *ACS Chem. Neurosci.*, *8*(6), 1188–1203. https://doi.org/10.1021/acschemneuro.6b00310

Lee, S.-H., Foldy, C., and Soltesz, I. (2010). Distinct Endocannabinoid Control of GABA Release at Perisomatic and Dendritic Synapses in the Hippocampus. *J. Neurosci.*, *30*(23), 7993–8000. https://doi.org/10.1523/JNEUROSCI.6238-09.2010

Lee, S.-H., Ledri, M., Tóth, B., Marchionni, I., Henstridge, C. M., Dudok, B., Kenesei, K., Barna, L., Szabó, S. I., Renkecz, T., Oberoi, M., Watanabe, M., Limoli, C. L., Horvai, G., Soltesz, I., and Katona, I. (2015). Multiple Forms of Endocannabinoid and Endovanilloid Signaling Regulate the Tonic Control of GABA Release. *J. Neurosci.*, *35*(27), 10039–10057. https://doi.org/10.1523/JNEUROSCI.4112-14.2015

Lee, S.-H., Marchionni, I., Bezaire, M., Varga, C., Danielson, N., Lovett-Barron, M., Losonczy, A., and Soltesz, I. (2014). Parvalbumin-Positive Basket Cells Differentiate among Hippocampal Pyramidal Cells. *Neuron*, *82*(5), 1129–1144. https://doi.org/10.1016/j.neuron.2014.03.034

Lenkey, N., Kirizs, T., Holderith, N., Máté, Z., Szabó, G., Vizi, E. S., Hájos, N., and Nusser, Z. (2015). Tonic endocannabinoid-mediated modulation of GABA release is independent of the CB1 content of axon terminals. *Nat. Commun.*, *6*(1), 6557. https://doi.org/10.1038/ncomms7557

Li, X., Hua, T., Vemuri, K., Ho, J. H., Wu, Y., Wu, L., Popov, P., Benchama, O., Zvonok, N., Locke, K., Qu, L., Han, G. W., Iyer, M. R., Cinar, R., Coffey, N. J., Wang, J., Wu, M., Katritch, V., Zhao, S., … Liu, Z. J. (2019). Crystal Structure of the Human Cannabinoid Receptor CB2. *Cell*, *176*(3), 459-467.e13. https://doi.org/10.1016/j.cell.2018.12.011

Li, Y., Xu, J., Liu, Y., Zhu, J., Liu, N., Zeng, W., Huang, N., Rasch, M. J., Jiang, H., Gu, X., Li, X., Luo, M., Li, C., Teng, J., Chen, J., Zeng, S., Lin, L., and Zhang, X. (2017). A distinct entorhinal cortex to hippocampal CA1 direct circuit for olfactory associative learning. *Nat. Neurosci.*, *20*(4), 559–570. https://doi.org/10.1038/nn.4517

Lisman, J., Buzsáki, G., Eichenbaum, H., Nadel, L., Rangananth, C., and Redish, A. D. (2017). Viewpoints: How the hippocampus contributes to memory, navigation and cognition. *Nat. Neurosci.*, *20*(11), 1434–1447. https://doi.org/10.1038/nn.4661

Liu, Z., Yang, N., Dong, J., Tian, W., Chang, L., Ma, J., Guo, J., Tan, J., Dong, A., He, K., Zhou, J., Cinar, R., Wu, J., Salinas, A. G., Sun, L., Kumar, M., Sullivan, B. T., Oldham, B. B., Pitz, V., … Tang, B. (2022). Deficiency in endocannabinoid synthase DAGLB contributes to early onset Parkinsonism and murine nigral dopaminergic neuron dysfunction. *Nat. Commun.*, *13*(1), 3490. https://doi.org/10.1038/s41467-022-31168-9

Losonczy, A., Biró, Á. A., and Nusser, Z. (2004). Persistently active cannabinoid receptors mute a subpopulation of hippocampal interneurons. *Proc. Natl. Acad. Sci. U. S. A.*, *101*(5), 1362–1367. https://doi.org/10.1073/pnas.0304752101

Ludanyi, A., Eross, L., Czirjak, S., Vajda, J., Halasz, P., Watanabe, M., Palkovits, M., Magloczky, Z., Freund, T. F., and Katona, I. (2008). Downregulation of the CB1 Cannabinoid Receptor and Related Molecular Elements of the Endocannabinoid System in Epileptic Human Hippocampus. *J. Neurosci.*, *28*(12), 2976–2990. https://doi.org/10.1523/JNEUROSCI.4465-07.2008

Maccarrone, M. (2017). Metabolism of the endocannabinoid anandamide: Open questions after 25 years. *Front. Mol. Neurosci.*, *10*(May), 1–10. https://doi.org/10.3389/fnmol.2017.00166

Maccarrone, M., Dainese, E., and Oddi, S. (2010). Intracellular trafficking of anandamide: new concepts for signaling. *Trends Biochem. Sci.*, *35*(11), 601–608. https://doi.org/10.1016/j.tibs.2010.05.008

Maglóczky, Z., Tóth, K., Karlócai, R., Nagy, S., Erocombining Double Acute Accentss, L., Czirják, S., Vajda, J., Rásonyi, G., Kelemen, A., Juhos, V., Halász, P., Mackie,

K., and Freund, T. F. (2010). Dynamic changes of CB1-receptor expression in hippocampi of epileptic mice and humans. *Epilepsia*, *51*(SUPPL. 3), 115–120. https://doi.org/10.1111/j.1528-1167.2010.02624.x

Malagon, G., Miki, T., Tran, V., Gomez, L., and Marty, A. (2020). Incomplete vesicular docking limits synaptic strength under high release probability conditions. *Elife*, *9*, e52137.

Mallory, C. S., and Giocomo, L. M. (2018). Heterogeneity in hippocampal place coding. *Curr. Opin. Neurobiol.*, *49*, 158–167. https://doi.org/10.1016/j.conb.2018.02.014

Marcus, D. J., Bedse, G., Gaulden, A. D., Ryan, J. D., Kondev, V., Winters, N. D., Rosas-Vidal, L. E., Altemus, M., Mackie, K., Lee, F. S., Delpire, E., and Patel, S. (2020). Endocannabinoid Signaling Collapse Mediates Stress-Induced Amygdalo-Cortical Strengthening. *Neuron*, *105*(6), 1062-1076.e6. https://doi.org/10.1016/j.neuron.2019.12.024

Maroso, M., Szabo, G. G., Kim, H. K., Alexander, A., Bui, A. D., Lee, S.-H., Lutz, B., and Soltesz, I. (2016). Cannabinoid Control of Learning and Memory through HCN Channels. *Neuron*, *89*(5), 1059–1073. https://doi.org/10.1016/j.neuron.2016.01.023

Marr, D. (1971). Simple memory: a theory for archicortex. *Philos. Trans. R. Soc. Lond. B. Biol. Sci.* https://doi.org/10.1098/rstb.1971.0078

Marrs, W. R., Blankman, J. L., Horne, E. A., Thomazeau, A., Lin, Y. H., Coy, J., Bodor, A. L., Muccioli, G. G., Hu, S. S. J., Woodruff, G., Fung, S., Lafourcade, M., Alexander, J. P., Long, J. Z., Li, W., Xu, C., Möller, T., MacKie, K., Manzoni, O. J., … Stella, N. (2010). The serine hydrolase ABHD6 controls the accumulation and efficacy of 2-AG at cannabinoid receptors. *Nat. Neurosci.*, *13*(8), 951–957. https://doi.org/10.1038/nn.2601

Marsicano, G., Wotjak, C. T., Azad, S. C., Bisogno, T., Rammes, G., Cascioll, M. G., Hermann, H., Tang, J., Hofmann, C., Zieglgänsberger, W., Di Marzo, V., and Lutz, B. (2002). The endogenous cannabinoid system controls extinction of aversive memories. *Nature*, *418*(6897), 530–534. https://doi.org/10.1038/nature00839

Masurkar, A. V, Srinivas, K. V, Brann, D. H., Warren, R., Lowes, D. C., and Siegelbaum, S. A. (2017). Medial and Lateral Entorhinal Cortex Differentially Excite Deep versus Superficial CA1 Pyramidal Neurons. *Cell Rep.*, *18*(1), 148–160. https://doi.org/10.1016/j.celrep.2016.12.012

Matsuda, L. A., Lolait, S. J., Brownstein, M. J., Young, A. C., and Bonner, T. I. (1990). Structure of a cannabinoid receptor and functional expression of the cloned cDNA. *Nature*, *346*(6284), 561–564. https://doi.org/10.1038/346561a0

Maus, L., Lee, C. K., Altas, B., Sertel, S. M., Weyand, K., Rizzoli, S. O., Rhee, J. S., Brose, N., Imig, C., and Cooper, B. H. (2020). Ultrastructural Correlates of Presynaptic Functional Heterogeneity in Hippocampal Synapses. *Cell Rep.*, *30*(11), 3632-3643.e8. https://doi.org/10.1016/j.celrep.2020.02.083

McFadden, M. H., Xu, H., Cui, Y., Piskorowski, R. A., Leterrier, C., Zala, D., Venance, L., Chevaleyre, V., and Lenkei, Z. (2018). Actomyosin-mediated nanostructural remodeling of the presynaptic vesicle pool by cannabinoids induces long-term depression. *BioRxiv*, 1–18. https://doi.org/10.1101/444950

Mechoulam, R., Ben-Shabat, S., Hanus, L., Ligumsky, M., Kaminski, N. E., Schatz, A. R., Gopher, A., Almog, S., Martin, B. R., Compton, D. R., Pertwee, R. G., Griffin, G., Bayewitch, M., Barg, J., and Vogel, Z. (1995). Identification of an endogenous 2-monoglyceride, present in canine gut, that binds to cannabinoid receptors. *Biochem. Pharmacol.*, *50*(1), 83–90. https://doi.org/10.1016/0006-2952(95)00109-D

Miczán, V., Kelemen, K., Glavinics, J. R., László, Z. I., Barti, B., Kenesei, K., Kisfali, M., and Katona, I. (2021). NECAB1 and NECAB2 are Prevalent Calcium-Binding Proteins of CB1/CCK-Positive GABAergic Interneurons. *Cereb. Cortex*, *31*(3), 1786–1806. https://doi.org/10.1093/cercor/bhaa326

Miki, T., Kaufmann, W. A., Malagon, G., Gomez, L., Tabuchi, K., Watanabe, M., Shigemoto, R., and Marty, A. (2017). Numbers of presynaptic Ca^{2+} channel clusters match those of functionally defined vesicular docking sites in single central synapses. *Proc. Natl. Acad. Sci.*, 201704470. https://doi.org/10.1073/pnas.1704470114

Mizuseki, K., Diba, K., Pastalkova, E., and Buzsáki, G. (2011). Hippocampal CA1 pyramidal cells form functionally distinct sublayers. *Nat. Publ. Gr.*, *14*(9), 1174–1181. https://doi.org/10.1038/nn.2894

Mock, E. D., Mustafa, M., Gunduz-Cinar, O., Cinar, R., Petrie, G. N., Kantae, V., Di, X., Ogasawara, D., Varga, Z. V., Paloczi, J., Miliano, C., Donvito, G., van Esbroeck, A. C. M., van der Gracht, A. M. F., Kotsogianni, I., Park, J. K., Martella, A., van der Wel, T., Soethoudt, M., … van der Stelt, M. (2020). Discovery of a NAPE-PLD inhibitor that modulates emotional behavior in mice. *Nat. Chem. Biol.*, *16*(6), 667–675. https://doi.org/10.1038/s41589-020-0528-7

Monory, K., Polack, M., Remus, A., Lutz, B., and Korte, M. (2015). Cannabinoid CB1 Receptor Calibrates Excitatory Synaptic Balance in the Mouse Hippocampus. *J. Neurosci.*, *35*(9), 3842–3850. https://doi.org/10.1523/JNEUROSCI.3167-14.2015

Morena, M., Patel, S., Bains, J. S., and Hill, M. N. (2016). Neurobiological Interactions Between Stress and the Endocannabinoid System. *Neuropsychopharmacology*, *41*(1), 80–102. https://doi.org/10.1038/npp.2015.166

Morozov, Y. M., Torii, M., and Rakic, P. (2009). Origin, early commitment, migratory routes, and destination of cannabinoid type 1 receptor-containing interneurons. *Cereb. Cortex*, *19*(SUPPL. 1). https://doi.org/10.1093/cercor/bhp028

Moser, E. I., Kropff, E., and Moser, M.-B. (2008). Place Cells, Grid Cells, and the Brain's Spatial Representation System. *Annu. Rev. Neurosci.*, *31*(1), 69–89. https://doi.org/10.1146/annurev.neuro.31.061307.090723

Moser, M.-B., Moser, E. I., Forrest, E., Andersen, P., and Morris, R. G. M. (1995). Spatial learning with a minislab in the dorsal hippocampus. *Proc. Natl. Acad. Sci.*, *92*(21), 9697–9701. https://doi.org/10.1073/pnas.92.21.9697

Moser, M. B., and Moser, E. I. (1998). Functional differentiation in the hippocampus. *Hippocampus*, *8*(6), 608–619. https://doi.org/10.1002/(SICI)1098-1063(1998)8:6<608::AID-HIPO3>3.0.CO;2-7

Munro, S., Thomas, K. L., and Abu-Shaar, M. (1993). Molecular characterization of a peripheral receptor for cannabinoids. *Nature*, *365*(6441), 61–65. https://doi.org/10.1038/365061a0

Nair, D., Hosy, E., Petersen, J. D., Constals, A., Giannone, G., Choquet, D., and Sibarita, J. (2013). *Super-Resolution Imaging Reveals That AMPA Receptors Inside Synapses Are Dynamically Organized in Nanodomains Regulated by PSD95*. *33*(32), 13204–13224. https://doi.org/10.1523/JNEUROSCI.2381-12.2013

Navarrete, M., and Araque, A. (2008). Endocannabinoids Mediate Neuron-Astrocyte Communication. *Neuron*, *57*(6), 883–893. https://doi.org/10.1016/j.neuron.2008.01.029

Neu, A., Földy, C., and Soltesz, I. (2007). Postsynaptic origin of CB1-dependent tonic inhibition of GABA release at cholecystokinin-positive basket cell to pyramidal cell synapses in the CA1 region of the rat hippocampus. *J. Physiol.*, *578*(1), 233–247. https://doi.org/10.1113/jphysiol.2006.115691

Núñez, E., Benito, C., Pazos, M. R., Barbachano, A., Fajardo, O., González, S., Tolón, R. M., and Romero, J. (2004). Cannabinoid CB2 receptors are expressed by perivascular microglial cells in the human brain: An Immunohistochemical Study. *Synapse*, *53*(4), 208–213. https://doi.org/10.1002/syn.20050

Nusser, Z. (2018). Creating diverse synapses from the same molecules. *Curr. Opin. Neurobiol.*, *51*, 8–15. https://doi.org/10.1016/j.conb.2018.01.001

Nyilas, R., Dudok, B., Urban, G. M., Mackie, K., Watanabe, M., Cravatt, B. F., Freund, T. F., and Katona, I. (2008). Enzymatic Machinery for Endocannabinoid Biosynthesis Associated with Calcium Stores in Glutamatergic Axon Terminals. *J. Neurosci.*, *28*(5), 1058–1063. https://doi.org/10.1523/JNEUROSCI.5102-07.2008

O'Keefe, J., Dostrovsky, J., and J. O'Keefe, J. D. (1971). Short Communications The hippocampus as a spatial map . Preliminary evidence from unit activity in the freely-moving rat. *Brain Res.*, *34*(1), 171–175. http://www.ncbi.nlm.nih.gov/pubmed/5124915

Ohno-Shosaku, T., and Kano, M. (2014). Endocannabinoid-mediated retrograde modulation of synaptic transmission. *Curr. Opin. Neurobiol.*, *29*, 1–8. https://doi.org/10.1016/j.conb.2014.03.017

Okamoto, Y., Morishita, J., Tsuboi, K., Tonai, T., and Ueda, N. (2004). Molecular Characterization of a Phospholipase D Generating Anandamide and Its Congeners.

J. Biol. Chem., *279*(7), 5298–5305. https://doi.org/10.1074/jbc.M306642200

Palade, G. E., and Palay, S. L. (1954). Electron microscope observations of interneuronal and neuromuscular synapses. *Anat Rec*, *118*, 335–336.

Pamplona, F. A., Ferreira, J., De Lima, O. M., Duarte, F. S., Bento, A. F., Forner, S., Villarinho, J. G., Bellochio, L., Wotjak, C. T., Lerner, R., Monory, K., Lutz, B., Canetti, C., Matias, I., Calixto, J. B., Marsicano, G., Guimarães, M. Z. P., and Takahashi, R. N. (2012). Anti-inflammatory lipoxin A4 is an endogenous allosteric enhancer of CB1 cannabinoid receptor. *Proc. Natl. Acad. Sci. U. S. A.*, *109*(51), 21134–21139. https://doi.org/10.1073/pnas.1202906109

Pan, B., Wang, W., Zhong, P., Blankman, J. L., Cravatt, B. F., and Liu, Q. -s. (2011). Alterations of Endocannabinoid Signaling, Synaptic Plasticity, Learning, and Memory in Monoacylglycerol Lipase Knock-out Mice. *J. Neurosci.*, *31*(38), 13420–13430. https://doi.org/10.1523/JNEUROSCI.2075-11.2011

Patzke, C., Dai, J., Brockmann, M. M., Sun, Z., Fenske, P., Rosenmund, C., and Südhof, T. C. (2021). Cannabinoid receptor activation acutely increases synaptic vesicle numbers by activating synapsins in human synapses. *Mol. Psychiatry*, *26*(11), 6253–6268. https://doi.org/10.1038/s41380-021-01095-0

Pelkey, K. A., Chittajallu, R., Craig, M. T., Tricoire, L., Wester, J. C., and McBain, C. J. (2017). Hippocampal gabaergic inhibitory interneurons. *Physiol. Rev.*, *97*(4), 1619–1747. https://doi.org/10.1152/physrev.00007.2017

Pertwee, R G, Howlett, A. C., Abood, M. E., Alexander, S. P. H., Marzo, V. Di, Elphick, M. R., Greasley, P. J., Hansen, H. S., and Kunos, G. (2010). Cannabinoid Receptors and Their Ligands : Beyond CB 1 and CB 2. *Pharmacol. Rev.*, *62*(4), 588–631. https://doi.org/10.1124/pr.110.003004.588

Pertwee, Roger G. (1997). Pharmacology of cannabinoid CB1 and CB2 receptors. *Pharmacol. Ther.*, *74*(2), 129–180. https://doi.org/10.1016/S0163-7258(97)82001-3

Petrie, G. N., Balsevich, G., Füzesi, T., Aukema, R. J., Driever, W. P. F., van der Stelt, M., Bains, J. S., and Hill, M. N. (2023). Disruption of tonic endocannabinoid signalling triggers cellular, behavioural and neuroendocrine responses consistent

with a stress response. *Br. J. Pharmacol.* https://doi.org/10.1111/bph.16198

Piomelli, D. (2003). The molecular logic of endocannabinoid signalling. *Nat. Rev. Neurosci.*, *4*(11), 873–884. https://doi.org/10.1038/nrn1247

Pitler, T. A., and Alger, B. E. (1992). Postsynaptic spike firing reduces synaptic GABAA responses in hippocampal pyramidal cells. *J. Neurosci.*, *12*(10), 4122–4132. https://doi.org/10.1523/JNEUROSCI.12-10-04122.1992

Porcu, A., Melis, M., Turecek, R., Ullrich, C., Mocci, I., Bettler, B., Gessa, G. L., and Castelli, M. P. (2018). Rimonabant, a potent CB1 cannabinoid receptor antagonist, is a Gαi/o protein inhibitor. *Neuropharmacology*, *133*, 107–120. https://doi.org/10.1016/j.neuropharm.2018.01.024

Pothuizen, H. H. J., Zhang, W. N., Jongen-Rêlo, A. L., Feldon, J., and Yee, B. K. (2004). Dissociation of function between the dorsal and the ventral hippocampus in spatial learning abilities of the rat: A within-subject, within-task comparison of reference and working spatial memory. *Eur. J. Neurosci.*, *19*(3), 705–712. https://doi.org/10.1111/j.0953-816X.2004.03170.x

Poulin, J. F., Tasic, B., Hjerling-Leffler, J., Trimarchi, J. M., and Awatramani, R. (2016). Disentangling neural cell diversity using single-cell transcriptomics. *Nat. Neurosci.*, *19*(9), 1131–1141. https://doi.org/10.1038/nn.4366

Puighermanal, E., Busquets-Garcia, A., Gomis-González, M., Marsicano, G., Maldonado, R., and Ozaita, A. (2013). Dissociation of the Pharmacological Effects of THC by mTOR Blockade. *Neuropsychopharmacology*, *38*(7), 1334–1343. https://doi.org/10.1038/npp.2013.31

Puighermanal, E., Marsicano, G., Busquets-Garcia, A., Lutz, B., Maldonado, R., and Ozaita, A. (2009). Cannabinoid modulation of hippocampal long-term memory is mediated by mTOR signaling. *Nat. Neurosci.*, *12*(9), 1152–1158. https://doi.org/10.1038/nn.2369

Pulido, C., and Marty, A. (2017). Quantal Fluctuations in Central Mammalian Synapses: Functional Role of Vesicular Docking Sites. *Physiol. Rev.*, *97*(4), 1403–1430. https://doi.org/10.1152/physrev.00032.2016

Pulido, C., Trigo, F. F., Marty, A., Pulido, C., Trigo, F. F., Llano, I., and Marty, A.

(2015). Vesicular release statistics and unitary postsynaptic current at single GABAergic synapses. *Neuron*, *85*(1), 159–172. https://doi.org/10.1016/j.neuron.2014.12.006

Raffa, R. B., and Ward, S. J. (2012). CB 1-independent mechanisms of Δ 9-THCV, AM251 and SR141716 (rimonabant). *J. Clin. Pharm. Ther.*, *37*(3), 260–265. https://doi.org/10.1111/j.1365-2710.2011.01284.x

Reisenberg, M., Singh, P. K., Williams, G., and Doherty, P. (2012). The diacylglycerol lipases: Structure, regulation and roles in and beyond endocannabinoid signalling. *Philos. Trans. R. Soc. B Biol. Sci.*, *367*(1607), 3264–3275. https://doi.org/10.1098/rstb.2011.0387

Ribrault, C., Sekimoto, K., and Triller, A. (2011). From the stochasticity of molecular processes to the variability of synaptic transmission. *Nat. Rev. Neurosci.*, *12*(7), 375–387. https://doi.org/10.1038/nrn3025

Roland, A. B., Ricobaraza, A., Carrel, D., Jordan, B. M., Rico, F., Simon, A., Humbert-Claude, M., Ferrier, J., McFadden, M. H., Scheuring, S., and Lenkei, Z. (2014). Cannabinoid-induced actomyosin contractility shapes neuronal morphology and growth. *Elife*, *3*, 1–23. https://doi.org/10.7554/elife.03159

Ronesi, J., Gerdeman, G. L., and Lovinger, D. M. (2004). Disruption of Endocannabinoid Release and Striatal Long-Term Depression by Postsynaptic Blockade of Endocannabinoid Membrane Transport. *J. Neurosci.*, *24*(7), 1673–1679. https://doi.org/10.1523/JNEUROSCI.5214-03.2004

Rozov, A., Burnashev, N., Sakmann, B., and Neher, E. (2001). Transmitter release modulation by intracellular Ca 2+ buffers in facilitating and depressing nerve terminals of pyramidal cells in layer 2/3 of the rat neocortex indicates a target cell-specific difference in presynaptic calcium dynamics. *J. Physiol.*, *531*(3), 807–826. https://doi.org/10.1111/j.1469-7793.2001.0807h.x

Sabatini, B. L., and Regehr, W. G. (1996). Timing of neurotransmission at fast synapses in the mammalian brain. *Nature*, *384*(6605), 170–172. https://doi.org/10.1038/384170a0

Sagar, D. R., Burston, J. J., Woodhams, S. G., and Chapman, V. (2012). Dynamic

changes to the endocannabinoid system in models of chronic pain. *Philos. Trans. R. Soc. B Biol. Sci.*, *367*(1607), 3300–3311. https://doi.org/10.1098/rstb.2011.0390

Sakamoto, H., Ariyoshi, T., Kimpara, N., Sugao, K., Taiko, I., Takikawa, K., Asanuma, D., Namiki, S., and Hirose, K. (2018). Synaptic weight set by Munc13-1 supramolecular assemblies. *Nat. Neurosci.*, *21*(1), 41–55. https://doi.org/10.1038/s41593-017-0041-9

Schlosburg, J. E., Carlson, B. L. A., Ramesh, D., Abdullah, R. A., Long, J. Z., Cravatt, B. F., and Lichtman, A. H. (2009). Inhibitors of endocannabinoid-metabolizing enzymes reduce precipitated withdrawal responses in THC-dependent mice. *AAPS J.*, *11*(2), 342–352. https://doi.org/10.1208/s12248-009-9110-7

Schoch, S., Castillo, P. E., Jo, T., Mukherjee, K., Geppert, M., Wang, Y., Schmitz, F., Malenka, R. C., Su, T. C., and Südhof, T. C. (2002). RIM1alpha forms a protein scaffold for regulating neurotransmitter release at the active zone. *Nature*, *415*(6869), 321–326. https://doi.org/10.1038/415321a

Schug, S., Benzing, F., and Steger, A. (2021). Presynaptic stochasticity improves energy efficiency and helps alleviate the stability-plasticity dilemma. *Elife*, *10*, 1–23. https://doi.org/10.7554/eLife.69884

Schwaller, B. (2020). Cytosolic Ca 2+ Buffers Are Inherently Ca 2+ Signal Modulators. *Cold Spring Harb. Perspect. Biol.*, *12*(1), a035543. https://doi.org/10.1101/cshperspect.a035543

Schwenk, J., Harmel, N., Brechet, A., Zolles, G., Berkefeld, H., Müller, C. S., Bildl, W., Baehrens, D., Hüber, B., Kulik, A., Klöcker, N., Schulte, U., and Fakler, B. (2012). High-Resolution Proteomics Unravel Architecture and Molecular Diversity of Native AMPA Receptor Complexes. *Neuron*, *74*(4), 621–633. https://doi.org/10.1016/j.neuron.2012.03.034

Selley, D. E., Rorrer, W. K., Breivogel, C. S., Zimmer, A. M., Zimmer, A., Martin, B. R., and Sim-Selley, L. J. (2001). Agonist efficacy and receptor efficiency in heterozygous CB1 knockout mice: Relationship of reduced CB1 receptor density to G-protein activation. *J. Neurochem.*, *77*(4), 1048–1057. https://doi.org/10.1046/j.1471-4159.2001.00308.x

Sigal, Y. M., Zhou, R., and Zhuang, X. (2018). Visualizing and discovering cellular structures with super-resolution microscopy. *Science (80-.).*, *361*(6405), 880–887. https://doi.org/10.1126/science.aau1044

Silver, R. A. (2003). Estimation of nonuniform quantal parameters with multiple-probability fluctuation analysis: Theory, application and limitations. *J. Neurosci. Methods*, *130*(2), 127–141. https://doi.org/10.1016/j.jneumeth.2003.09.030

Silver, R. A., Momiyama, A., and Cull-Candy, S. G. (1998). Locus of frequency-dependent depression identified with multiple-probability fluctuation analysis at rat climbing fibre - Purkinje cell synapses. *J. Physiol.*, *510*(3), 881–902. https://doi.org/10.1111/j.1469-7793.1998.881bj.x

Sjöström, P. J., Turrigiano, G. G., and Nelson, S. B. (2003). Neocortical LTD via Coincident Activation of Presynaptic NMDA and Cannabinoid Receptors. *Neuron*, *39*(4), 641–654. https://doi.org/10.1016/S0896-6273(03)00476-8

Solstad, T., Boccara, C. N., Kropff, E., Moser, M.-B., and Moser, E. I. (2008). Representation of Geometric Borders in the Entorhinal Cortex. *Science (80-.).*, *322*(5909), 1865–1868. https://doi.org/10.1126/science.1166466

Soltesz, I., Alger, B. E., Kano, M., and Lee, S. (2015). Weeding out bad waves : towards selective cannabinoid circuit control in epilepsy. *Nat. Rev. Neurosci.*, *16*(5), 264–277. https://doi.org/10.1038/nrn3937

Soltesz, I., and Losonczy, A. (2018). CA1 pyramidal cell diversity enabling parallel information processing in the hippocampus. *Nat. Neurosci. 2018 214*, *21*(4), 484. https://doi.org/10.1038/s41593-018-0118-0

Somogyi, P., and Klausberger, T. (2005). *Defined types of cortical interneurone structure space and spike timing in the hippocampus*. *1*, 9–26. https://doi.org/10.1113/jphysiol.2004.078915

Somogyi, P., Nunzi, M. G., Gorio, A., and Smith, A. D. (1983). A new type of specific interneuron in the monkey hippocampus forming synapses exclusively with the axon initial segments of pyramidal cells. *Brain Res.*, *259*(1), 137–142. https://doi.org/10.1016/0006-8993(83)91076-4

Specht, C. G., Izeddin, I., Rodriguez, P. C., Beheiry, M. El, Rostaing, P., Darzacq, X.,

Dahan, M., Triller, A., and Supe, N. (2013). Article Quantitative Nanoscopy of Inhibitory Synapses : Counting Gephyrin Molecules and Receptor Binding Sites. *Neuron*, *79*(2), 308–321. https://doi.org/10.1016/j.neuron.2013.05.013

Speed, H. E., Kouser, M., Xuan, Z., Reimers, J. M., Ochoa, C. F., Gupta, N., Liu, S., and Powell, C. M. (2015). Autism-Associated Insertion Mutation (InsG) of Shank3 Exon 21 Causes Impaired Synaptic Transmission and Behavioral Deficits. *J. Neurosci.*, *35*(26), 9648–9665. https://doi.org/10.1523/JNEUROSCI.3125-14.2015

Stella, N. (2010). Cannabinoid and cannabinoid-like receptors in microglia, astrocytes, and astrocytomas. *Glia*, *58*(9), 1017–1030. https://doi.org/10.1002/glia.20983

Stella, N., Schweitzer, P., and Piomelli, D. (1997). A second endogenous' cannabinoid that modulates long-term potentiation. *Nature*, *388*(6644), 773–778. https://doi.org/10.1038/42015

Stempel, A. V., Stumpf, A., Zhang, H. Y., Özdoğan, T., Pannasch, U., Theis, A.-K. K., Otte, D.-M. M., Wojtalla, A., Rácz, I., Ponomarenko, A., Xi, Z. X., Zimmer, A., and Schmitz, D. (2016). Cannabinoid Type 2 Receptors Mediate a Cell Type-Specific Plasticity in the Hippocampus. *Neuron*, *90*(4), 795–809. https://doi.org/10.1016/j.neuron.2016.03.034

Stogsdill, J. A., and Eroglu, C. (2017). The interplay between neurons and glia in synapse development and plasticity. *Curr. Opin. Neurobiol.*, *42*, 1–8. https://doi.org/10.1016/j.conb.2016.09.016

Straiker, A., Hu, S. S. J., Long, J. Z., Arnold, A., Wager-Miller, J., Cravatt, B. F., and Mackie, K. (2009). Monoacylglycerol lipase limits the duration of endocannabinoid-mediated depolarization-induced suppression of excitation in autaptic hippocampal neurons. *Mol. Pharmacol.*, *76*(6), 1220–1227. https://doi.org/10.1124/mol.109.059030

Straiker, A., and Mackie, K. (2009). Cannabinoid signaling in inhibitory autaptic hippocampal neurons. *Neuroscience*, *163*(1), 190–201. https://doi.org/10.1016/j.neuroscience.2009.06.004

Strange, B. A., Witter, M. P., Lein, E. S., and Moser, E. I. (2014). Functional organization of the hippocampal longitudinal axis. *Nat. Rev. Neurosci.*, *15*(10),

655–669. https://doi.org/10.1038/nrn3785

Strüber, M., Jonas, P., and Bartos, M. (2015). Strength and duration of perisomatic GABAergic inhibition depend on distance between synaptically connected cells. *Proc. Natl. Acad. Sci.*, *112*(4), 1220–1225. https://doi.org/10.1073/pnas.1412996112

Südhof, T. C. (2012). The Presynaptic Active Zone. *Neuron*, *75*(1), 11–25. https://doi.org/10.1016/j.neuron.2012.06.012

Südhof, T. C. (2013). Neurotransmitter release: The last millisecond in the life of a synaptic vesicle. *Neuron*, *80*(3), 675–690. https://doi.org/10.1016/j.neuron.2013.10.022

Südhof, T. C., and Rothman, J. E. (2009). Membrane Fusion: Grappling with SNARE and SM Proteins. *Science (80-.).*, *323*(5913), 474–477. http://www.sciencemag.org/content/323/5913/474.full.pdf

Sugita, S., Ho, A., and Südhof, T. C. (2002). NECABs: A family of neuronal Ca2+-binding proteins with an unusual domain structure and a restricted expression pattern. *Neuroscience*, *112*(1), 51–63. https://doi.org/10.1016/S0306-4522(02)00063-5

Sun, X., Bernstein, M. J., Meng, M., Rao, S., Sørensen, A. T., Yao, L., Zhang, X., Anikeeva, P. O., and Lin, Y. (2020). Functionally Distinct Neuronal Ensembles within the Memory Engram. *Cell*, *181*(2), 410-423.e17. https://doi.org/10.1016/j.cell.2020.02.055

Szabadics, J., Varga, C., Molnár, G., Oláh, S., Barzó, P., and Tamás, G. (2006). Excitatory Effect of GABAergic Axo-Axonic Cells in Cortical Microcircuits. *Science (80-.).*, *311*(5758), 233–235. https://doi.org/10.1126/science.1121325

Szabó, G. G., Lenkey, N., Holderith, N., Andrási, T., Nusser, Z., and Hájos, N. (2014). Presynaptic calcium channel inhibition underlies CB1 cannabinoid receptor-mediated suppression of GABA release. *J. Neurosci.*, *34*(23), 7958–7963. https://doi.org/10.1523/JNEUROSCI.0247-14.2014

Tang, A.-H., Chen, H., Li, T. P., Metzbower, S. R., MacGillavry, H. D., and Blanpied, T. A. (2016). A trans-synaptic nanocolumn aligns neurotransmitter release to

receptors. *Nature*, *536*(7615), 210–214. https://doi.org/10.1038/nature19058

Tanimura, A., Yamazaki, M., Hashimotodani, Y., Uchigashima, M., Kawata, S., Abe, M., Kita, Y., Hashimoto, K., Shimizu, T., Watanabe, M., Sakimura, K., and Kano, M. (2010). The Endocannabinoid 2-Arachidonoylglycerol Produced by Diacylglycerol Lipase α Mediates Retrograde Suppression of Synaptic Transmission. *Neuron*, *65*(3), 320–327. https://doi.org/10.1016/j.neuron.2010.01.021

Tasic, B., Menon, V., Nguyen, T. N., Kim, T. K., Jarsky, T., Yao, Z., Levi, B., Gray, L. T., Sorensen, S. A., Dolbeare, T., Bertagnolli, D., Goldy, J., Shapovalova, N., Parry, S., Lee, C., Smith, K., Bernard, A., Madisen, L., Sunkin, S. M., … Zeng, H. (2016). *Adult mouse cortical cell taxonomy revealed by single cell transcriptomics*. *January*. https://doi.org/10.1038/nn.4216

Taube, J., Muller, R., and Ranck, J. (1990). Head-direction cells recorded from the postsubiculum in freely moving rats. I. Description and quantitative analysis. *J. Neurosci.*, *10*(2), 420–435. https://doi.org/10.1523/JNEUROSCI.10-02-00420.1990

Tomé, D. F., Zhang, Y., Aida, T., Mosto, O., Lu, Y., Chen, M., Sadeh, S., Roy, D. S., and Clopath, C. (2024). Dynamic and selective engrams emerge with memory consolidation. *Nat. Neurosci.*, 2022.03.13.484167. https://doi.org/10.1038/s41593-023-01551-w

Tricoire, L., Pelkey, K. A., Erkkila, B. E., Jeffries, B. W., Yuan, X., and McBain, C. J. (2011). A blueprint for the spatiotemporal origins of mouse hippocampal interneuron diversity. *J. Neurosci.*, *31*(30), 10948–10970. https://doi.org/10.1523/JNEUROSCI.0323-11.2011

Trotter, J. H., Hao, J., Maxeiner, S., Tsetsenis, T., Liu, Z., Zhuang, X., and Südhof, T. C. (2019). Synaptic neurexin-1 assembles into dynamically regulated active zone nanoclusters. *J. Cell Biol.*, *218*(8), 2677–2698. https://doi.org/10.1083/jcb.201812076

Tzakis, N., and Holahan, M. R. (2019). Social Memory and the Role of the Hippocampal CA2 Region. *Front. Behav. Neurosci.*, *13*(October), 1–15.

https://doi.org/10.3389/fnbeh.2019.00233

Ueda, N., Tsuboi, K., and Uyama, T. (2013). Metabolism of endocannabinoids and related N-acylethanolamines: Canonical and alternative pathways. *FEBS J.*, *280*(9), 1874–1894. https://doi.org/10.1111/febs.12152

Usoskin, D., Furlan, A., Islam, S., Abdo, H., Lönnerberg, P., Lou, D., Hjerling-Leffler, J., Haeggström, J., Kharchenko, O., Kharchenko, P. V., Linnarsson, S., and Ernfors, P. (2015). Unbiased classification of sensory neuron types by large-scale single-cell RNA sequencing. *Nat. Neurosci.*, *18*(1), 145–153. https://doi.org/10.1038/nn.3881

Van Esbroeck, A. C. M., Kantae, V., Di, X., van der Wel, T., den Dulk, H., Stevens, A. F., Singh, S., Bakker, A. T., Florea, B. I., Stella, N., Overkleeft, H. S., Hankemeier, T., and van der Stelt, M. (2019). Identification of α,β-Hydrolase Domain Containing Protein 6 as a Diacylglycerol Lipase in Neuro-2a Cells. *Front. Mol. Neurosci.*, *12*(November), 1–13. https://doi.org/10.3389/fnmol.2019.00286

Vancura, B., Geiller, T., Grosmark, A., Zhao, V., and Losonczy, A. (2023). Inhibitory control of sharp-wave ripple duration during learning in hippocampal recurrent networks. *Nat. Neurosci.*, *26*(5), 788–797. https://doi.org/10.1038/s41593-023-01306-7

Viader, A., Ogasawara, D., Joslyn, C. M., Sanchez-Alavez, M., Mori, S., Nguyen, W., Conti, B., and Cravatt, B. F. (2016). A chemical proteomic atlas of brain serine hydrolases identifies cell type-specific pathways regulating neuroinflammation. *Elife*, *5*(e12345), 1–24. https://doi.org/10.7554/eLife.12345

Voss, J. L., Bridge, D. J., Cohen, N. J., and Walker, J. A. (2017). A Closer Look at the Hippocampus and Memory. *Trends Cogn. Sci.*, *21*(8), 577–588. https://doi.org/10.1016/j.tics.2017.05.008

Wall, M. J., and Usowicz, M. M. (1998). Development of the quantal properties of evoked and spontaneous synaptic currents at a brain synapse. *Nat. Neurosci.*, *1*(8), 675–682.

Wei, M., Zhang, J., Jia, M., Yang, C., Pan, Y., Li, S., Luo, Y., Zheng, J., Ji, J., Chen, J., Hu, X., Xiong, J., Shi, Y., and Zhang, C. (2016). α/β-Hydrolase domain-containing

6 (ABHD6) negatively regulates the surface delivery and synaptic function of AMPA receptors. *Proc. Natl. Acad. Sci.*, *113*(19), E2695–E2704. https://doi.org/10.1073/pnas.1524589113

Weis, W. I., and Kobilka, B. K. (2018). The Molecular Basis of G Protein–Coupled Receptor Activation. *Annu. Rev. Biochem.*, *87*(1), 897–919. https://doi.org/10.1146/annurev-biochem-060614-033910

Wierenga, C. J., Müllner, F. E., Rinke, I., Keck, T., Stein, V., and Bonhoeffer, T. (2010). Molecular and electrophysiological characterization of GFP-expressing ca1 interneurons in GAD65-GFP mice. *PLoS One*, *5*(12), 1–11. https://doi.org/10.1371/journal.pone.0015915

Wilson, R. I., Kunos, G., and Nicoll, R. A. (2001). Presynaptic specificity of endocannabinoid signaling in the hippocampus. *Neuron*, *31*(3), 453–462. https://doi.org/10.1016/S0896-6273(01)00372-5

Wilson, R. I., and Nicoll, R. A. (2001). Endogenous cannabinoids mediate retrograde signalling at hippocampal synapses. *Nature*, *410*(6828), 588–592. https://doi.org/10.1038/35069076

Wilton, D. K., Dissing-Olesen, L., and Stevens, B. (2019). Neuron-Glia Signaling in Synapse Elimination. *Annu. Rev. Neurosci.*, *42*(1), 107–127. https://doi.org/10.1146/annurev-neuro-070918-050306

Woodhams, S. G., Chapman, V., Finn, D. P., Hohmann, A. G., and Neugebauer, V. (2017). The cannabinoid system and pain. *Neuropharmacology*, *124*, 105–120. https://doi.org/10.1016/j.neuropharm.2017.06.015

Yap, E. L., Pettit, N. L., Davis, C. P., Nagy, M. A., Harmin, D. A., Golden, E., Dagliyan, O., Lin, C., Rudolph, S., Sharma, N., Griffith, E. C., Harvey, C. D., and Greenberg, M. E. (2021). Bidirectional perisomatic inhibitory plasticity of a Fos neuronal network. *Nature*, *590*(7844), 115–121. https://doi.org/10.1038/s41586-020-3031-0

Yoshida, T., Fukaya, M., Uchigashima, M., Miura, E., Kamiya, H., Kano, M., and Watanabe, M. (2006). Localization of Diacylglycerol Lipase- around Postsynaptic Spine Suggests Close Proximity between Production Site of an Endocannabinoid,

2-Arachidonoyl-glycerol, and Presynaptic Cannabinoid CB1 Receptor. *J. Neurosci.*, *26*(18), 4740–4751. https://doi.org/10.1523/jneurosci.0054-06.2006

Yoshino, H., Miyamae, T., Hansen, G., Zambrowicz, B., Flynn, M., Pedicord, D., Blat, Y., Westphal, R. S., Zaczek, R., Lewis, D. A., and Gonzalez-Burgos, G. (2011). Postsynaptic diacylglycerol lipase α mediates retrograde endocannabinoid suppression of inhibition in mouse prefrontal cortex. *J. Physiol.*, *589*(20), 4857–4884. https://doi.org/10.1113/jphysiol.2011.212225

Younts, T. J., Monday, H. R., Dudok, B., Klein, M. E., Jordan, B. A., Katona, I., Castillo, P. E., Adermark, L., Talani, G., Lovinger, D. M., Akins, M. R., Leblanc, H. F., Stackpole, E. E., Chyung, E., Fallon, J. R., Alvarez, J., Giuditta, A., Koenig, E., Argaw, A., … Poo, M. M. (2016). Presynaptic Protein Synthesis Is Required for Long-Term Plasticity of GABA Release. *Neuron*, *92*(2), 479–492. https://doi.org/10.1016/j.neuron.2016.09.040

Zeisel, A., Manchado, A. B. M., Codeluppi, S., Lönnerberg, P., Manno, G. La, Juréus, A., and Marques, S. (2015). *Cell types in the mouse cortex and hippocampus revealed by single-cell RNA-seq*. *February*, 1–8.

Zhang, Y., Chen, K., Sloan, S. A., Bennett, M. L., Scholze, A. R., O'Keeffe, S., Phatnani, H. P., Guarnieri, P., Caneda, C., Ruderisch, N., Deng, S., Liddelow, S. A., Zhang, C., Daneman, R., Maniatis, T., Barres, B. A., and Wu, J. Q. (2014). An RNA-sequencing transcriptome and splicing database of glia, neurons, and vascular cells of the cerebral cortex. *J. Neurosci.*, *34*(36), 11929–11947. https://doi.org/10.1523/JNEUROSCI.1860-14.2014

Zhou, R., Han, B., Xia, C., and Zhuang, X. (2019). Membrane-associated periodic skeleton is a signaling platform for RTK transactivation in neurons. *Science (80-.).*, *365*(6456), 929–934. https://doi.org/10.1126/science.aaw5937

Zimmer, A., Zimmer, A. M., Hohmann, A. G., Herkenham, M., and Bonner, T. I. (1999). Increased mortality, hypoactivity, and hypoalgesia in cannabinoid CB1 receptor knockout mice. *Proc. Natl. Acad. Sci. U. S. A.*, *96*(10), 5780–5785. https://doi.org/10.1073/pnas.96.10.5780

Zou, S., and Kumar, U. (2018). Cannabinoid receptors and the endocannabinoid system:

Signaling and function in the central nervous system. *Int. J. Mol. Sci.*, *19*(3). https://doi.org/10.3390/ijms19030833

10. List of publications

Publications related to this thesis

Barti, B., Dudok, B., Kenesei, K., Zöldi, M., Miczán, V., Balla, G. Y., Zala, D., Tasso, M., Sagheddu, C., Kisfali, M., Tóth, B., Ledri, M., Vizi, E. S., Melis, M., Barna, L., Lenkei, Z., Soltész, I., and Katona, I. (2024). Presynaptic nanoscale components of retrograde synaptic signaling. *Sci. Adv.*, *10*(22). https://doi.org/10.1126/sciadv.ado0077

Miczán, V., Kelemen, K., Glavinics, J. R., László, Z. I., **Barti, B.**, Kenesei, K., Kisfali, M., and Katona, I. (2021). Necab1 and necab2 are prevalent calcium-binding proteins of cb1/cck-positive gabaergic interneurons. *Cereb. Cortex*, *31*(3), 1786–1806. https://doi.org/10.1093/cercor/bhaa326

Other publications

Kis, V., **Barti, B.**, Lippai, M., and Sass, M. (2015). Specialized cortex glial cells accumulate lipid droplets in Drosophila melanogaster. *PloS one*, *10*(7). https://doi.org/10.1371/journal.pone.0131250

Prokop, S., Ábrányi-Balogh, P., **Barti, B.**, Vámosi, M., Zöldi, M., Barna, L., Urbán, G. M., Tóth, A. D., Dudok, B., Egyed, A., Deng, H., Leggio, G. M., Hunyady, L., van der Stelt, M., Keserű, G. M., and Katona, I. (2021). PharmacoSTORM nanoscale pharmacology reveals cariprazine binding on Islands of Calleja granule cells. *Nat. Commun.*, *12*(1), 1–19. https://doi.org/10.1038/s41467-021-26757-z

11. Acknowledgements

I would like to thank my supervisor and PI, István Katona for the mentoring, guidance and that he gave me the opportunity to find and expand my scientific curiosity in both of his laboratories in Hungary and in the USA as well.

I am thankful for every former and current members of the Laboratory of Molecular Neurobiology and the Laboratory of Addiction and Neuroplasticity, especially to Barna Dudok, Miklós Zöldi, Gyula Balla, Vivien Miczán, Kata Kenesei, Máté Kisfali and László Barna who have contributed to the results presented here. The unique atmosphere of the labs where I found great friends and scientific partners contributed significantly to the preparation of this thesis. The many "science side-talks", hiking, sporting and social activities helped me to get through even the difficult periods.

I am also thankful for every advisor colleague from other laboratories who contributed to this project and to my scientific development as well, especially for János Szabadics, János Brunner, Norbert Hájos, Rita Karlócai, Zoltán Nusser and Noémi Holderith, who were always kind, helpful and taught me countless things about electrophysiology.

Last, but not least, I would like to express my greatest gratitude to my wife, my parents, and my whole family for supporting me throughout my entire life in every possible aspect, including the long years of studies that led me here. I feel fortunate that I had the possibility to grow up in such a warm and loving environment, therefore I dedicate this thesis to them.

I would also like to express my respect to those laboratory mice that were sacrificed in this study in order to understand the brain.